



MINISTÉRIO DA  
CIÊNCIA, TECNOLOGIA  
E INOVAÇÕES



sid.inpe.br/mtc-m21c/2020/04.01.21.50-TDI

**EVAPOTRANSPIRATION AND GROSS PRIMARY  
PRODUCTIVITY SEASONALITY IN A FLOODPLAIN  
FOREST AT THE BANANAL ISLAND REGION**

Leticia d'Agosto Miguel Fonseca

Doctorate Thesis of the Graduate  
Course in Terrestrial System  
Science, guided by Dra. Laura de  
Simone Borma, approved in March  
27, 2020.

URL of the original document:

<<http://urlib.net/8JMKD3MGP3W34R/428U3L5>>

INPE  
São José dos Campos  
2020

**PUBLISHED BY:**

Instituto Nacional de Pesquisas Espaciais - INPE  
Gabinete do Diretor (GBDIR)  
Serviço de Informação e Documentação (SESID)  
CEP 12.227-010  
São José dos Campos - SP - Brasil  
Tel.:(012) 3208-6923/7348  
E-mail: pubtc@inpe.br

**BOARD OF PUBLISHING AND PRESERVATION OF INPE  
INTELLECTUAL PRODUCTION - CEPPII (PORTARIA Nº  
176/2018/SEI-INPE):****Chairperson:**

Dra. Marley Cavalcante de Lima Moscati - Centro de Previsão de Tempo e Estudos  
Climáticos (CGCPT)

**Members:**

Dra. Carina Barros Mello - Coordenação de Laboratórios Associados (COCTE)  
Dr. Alisson Dal Lago - Coordenação-Geral de Ciências Espaciais e Atmosféricas  
(CGCEA)  
Dr. Evandro Albiach Branco - Centro de Ciência do Sistema Terrestre (COCST)  
Dr. Evandro Marconi Rocco - Coordenação-Geral de Engenharia e Tecnologia  
Espacial (CGETE)  
Dr. Hermann Johann Heinrich Kux - Coordenação-Geral de Observação da Terra  
(CGOBT)  
Dra. Ieda Del Arco Sanches - Conselho de Pós-Graduação - (CPG)  
Sílvia Castro Marcelino - Serviço de Informação e Documentação (SESID)

**DIGITAL LIBRARY:**

Dr. Gerald Jean Francis Banon  
Clayton Martins Pereira - Serviço de Informação e Documentação (SESID)

**DOCUMENT REVIEW:**

Simone Angélica Del Ducca Barbedo - Serviço de Informação e Documentação  
(SESID)  
André Luis Dias Fernandes - Serviço de Informação e Documentação (SESID)

**ELECTRONIC EDITING:**

Ivone Martins - Serviço de Informação e Documentação (SESID)  
Cauê Silva Fróes - Serviço de Informação e Documentação (SESID)



MINISTÉRIO DA  
CIÊNCIA, TECNOLOGIA  
E INOVAÇÕES



sid.inpe.br/mtc-m21c/2020/04.01.21.50-TDI

## EVAPOTRANSPIRATION AND GROSS PRIMARY PRODUCTIVITY SEASONALITY IN A FLOODPLAIN FOREST AT THE BANANAL ISLAND REGION

Leticia d'Agosto Miguel Fonseca

Doctorate Thesis of the Graduate  
Course in Terrestrial System  
Science, guided by Dra. Laura de  
Simone Borma, approved in March  
27, 2020.

URL of the original document:

<<http://urlib.net/8JMKD3MGP3W34R/428U3L5>>

INPE  
São José dos Campos  
2020

Cataloging in Publication Data

---

Fonseca, Leticia d'Agosto Miguel.

F733e Evapotranspiration and gross primary productivity seasonality in a floodplain forest at the bananal island region / Leticia d'Agosto Miguel Fonseca. – São José dos Campos : INPE, 2020. xxiv + 91 p. ; (sid.inpe.br/mtc-m21c/2020/04.01.21.50-TDI)

Thesis (Doctorate in Terrestrial System Science) – Instituto Nacional de Pesquisas Espaciais, São José dos Campos, 2020.

Guiding : Dra. Laura de Simone Borma.

1. Floodplain. 2. Amazon. 3. Bananal. 4. Gross Primary Productivity. 5. Evapotranspiration. I.Title.

CDU 551.435.12(811)

---



Esta obra foi licenciada sob uma Licença [Creative Commons Atribuição-NãoComercial 3.0 Não Adaptada](https://creativecommons.org/licenses/by-nc/3.0/).

This work is licensed under a [Creative Commons Attribution-NonCommercial 3.0 Unported License](https://creativecommons.org/licenses/by-nc/3.0/).

Aluno (a): **Letícia d' Agosto Miguel Fonseca**

Título: "EVAPOTRANSPIRATION AND GROSS PRIMARY PRODUCTIVITY SEASONALITY IN A FLOODPLAIN FOREST AT THE BANANAL ISLAND REGION"

Aprovado (a) pela Banca Examinadora  
em cumprimento ao requisito exigido para  
obtenção do Título de **Doutor(a)** em  
**Ciência do Sistema Terrestre**

Dr. Celso von Randow



---

**Presidente / INPE / São José dos Campos - SP**

**Participação por Vídeo - Conferência**

**Aprovado**       **Reprovado**

Dra. Laura De Simone Borma

p/



---


**Orientador(a) / INPE / São José dos Campos - SP**

**Participação por Vídeo - Conferência**

**Aprovado**       **Reprovado**

Dr. Camilo Daleles Rennó

p/



---

**Membro da Banca / INPE / SJC Campos - SP**

**Participação por Vídeo - Conferência**

**Aprovado**       **Reprovado**

Dr. Humberto Ribeiro da Rocha

p/



---

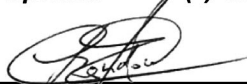
**Convidado(a) / IAG/USP / São Paulo - SP**

**Participação por Vídeo - Conferência**

**Aprovado**       **Reprovado**

Dr. Thiago Sanna Freire Silva

p/



---

**Convidado(a) / UNI. STIR / Inglaterra - UK**

**Participação por Vídeo - Conferência**

**Aprovado**       **Reprovado**

**Este trabalho foi aprovado por:**

**maioria simples**

**unanimidade**



*“O geógrafo é, antes de tudo, um filósofo, e os filósofos são otimistas, porque  
diante deles está a infinidade.”*

*Milton Santos*





*(In Portuguese)*

*Dedico este trabalho:*

*Aos meus pais, **Roselene (in memoriam)** e **Paulo**, por me incentivarem na  
busca constante do conhecimento.*

*Às minhas irmãs, **Mariana** e **Helena**, meus exemplos de força, dedicação e  
resiliência.*

*À minha sobrinha **Elaine**, por ser meu maior presente.*



## ACKNOWLEDGMENT

(In Portuguese)

Agradeço ao Instituto Nacional de Pesquisas Espaciais pelo importante papel que desempenha na sociedade brasileira, produzindo ciência e fornecendo informação de qualidade para a população. Tenho muito orgulho de fazer parte dessa história.

À Coordenação de Aperfeiçoamento Pessoal de nível superior – CAPES, por financiar minha bolsa de doutorado e do período sanduíche.

À Fundação de Amparo à Pesquisa do Estado de São Paulo – FAPESP, pelo financiamento do projeto GoAmazon (processo nº2013/50531-2), cujos recursos subsidiaram as campanhas de campo realizadas na Amazônia.

Ao programa LBA/Palmas Tocantins (Experimento de Grande Escala da Biosfera-Atmosfera da Amazônia) em parceria com a Fundação Universidade do Tocantins, pelo apoio logístico e institucional para a realização dos trabalhos de campo no sítio Javaesinho, em especial ao Anatálio Batista.

À professora Dra. Laura De Simone Borma, por abrir as portas da Amazônia para mim, me apaixonei e entendi a grandeza dessa floresta ao seu lado. Obrigada pelos ensinamentos, tempo, dedicação e confiança no meu trabalho.

Às minhas irmãs e ao meu pai, por acreditarem no meu potencial e me estimularem sempre, vocês são meus grandes amores.

À minha mãe Roselene e à minha tia Elaine, mulheres à frente do tempo, que me ensinaram o poder libertador da educação em todas as suas esferas.

À minha amada prima Ludmila Miguel Abramov, por ser meu exemplo de resiliência, além da ajuda direta na edição das figuras.

Às famílias Miguel e Fonseca, meus alicerces nessa vida, sem vocês eu não teria chegado tão longe.

Ao meu companheiro de todas as horas, Thiago Sailer, pelas intermináveis conversas, risadas, amor, e principalmente, pela amizade.

Aos amigos que caminharam ao meu lado, Talita Assis, Janaína Guidolini, Silvia Polizel, Duarte Costa, Priscila Vega, Iane Tavares e Ranieli Anjos, sejam nos trabalhos de disciplina, trabalhos de campo, interpretação de dados, saídas para espairar ou um simples cafezinho na copa, vocês foram essenciais nessa jornada, sou muito grata a vocês!

Ao amigo Ricardo Dal'Agnol, por fornecer os dados de sensoriamento remoto e me ajudar diretamente na análise deles. Obrigada pelas diversas discussões científicas e trocas de conhecimento, aprendi muito com você.

A todos os colegas do CST que compartilharam experiências nas disciplinas, e por vezes, nos corredores.

À Angela e à Mariana, por serem sempre muito solícitas e receptivas na secretaria do CST.

Ao professor Yadvinder Malhi, que me proporcionou a melhor experiência da minha vida ao me aceitar para o período sanduíche na Universidade de Oxford. A todos os pesquisadores com quem tiver a oportunidade de conviver nesse período, em especial ao Sami Rifai e às queridas Erika Berenguer e Marina Scalon, mulheres que me inspiram nessa caminhada como pesquisadora.

Aos amigos de longa data, os quais moram no meu coração e estão sempre na minha torcida, Tatiane Tagliatti, Fernanda Almeida, Tales Augusto, Bianca Lima, William Gesualdo e Marya Rabelo. Essa conquista foi trilhada passo a passo e vocês foram essenciais para que eu chegasse até aqui, obrigada por tudo!

Aos meus eternos orientadores Marcos Hott e João Luiz Lani, vocês me incentivaram a alcançar voos mais altos.

## ABSTRACT

The Amazon forest plays an important role in regulating the local, regional and global climate, due to the high potential for absorbing carbon in its biomass and transferring large amounts of water from the land surface to the atmosphere through evapotranspiration. Despite the several studies that have explored the mechanisms of seasonal vegetation control, a small number of them have focused on flooded forests. In the Amazon basin, it corresponds to c.a. 14% of the basin. This study was performed in a floodplain forest located at the transition area between the Amazon and *Cerrado* (Savana) biomes, near the Bananal (BAN) Island region seeking to understand the mechanisms of vegetation control during the dry and flooded periods. The seasonality of gross primary productivity (GPP) and evapotranspiration (ET) from eddy covariance measurements were assessed, along with environmental drivers and phenological patterns, obtained from the field (leaf litter mass) and satellite measurements (enhanced vegetation index (EVI) from the Moderate Resolution Imaging Spectroradiometer/multi-angle implementation correction (MODIS/MAIAC)). ET measurements presented many gaps, and a statistical model (the Generalized Additive Model - GAM) was used to reconstruct the records from 2004 to 2017, using the ERA5 reanalysis climate data. Moreover, the remote sensing product (MOD16A2) was acquired to analyze the reliability of this product in describing seasonal ET. The long-term change on the hydrological pattern at the BAN region was analyzed through the Gravity Recovery and Climate Experiment (GRACE) satellite product. The results revealed that Gross primary production is limited by soil moisture during the flooded period due to the excess water, while GPP is positively associated with soil moisture during non-flooded months. Besides, GPP is maximized when the accumulated water deficit (CWD) increases, indicating that it depends on the amount of water input in the environment. EVI was positively associated with leaf litter mass and GPP, suggesting the synchrony between leaf production and the photosynthetic capacity of the canopy, decreasing at the peak of the flooded period and at the end of the dry season. The EVI was also able to describe the interannual variations of the canopy in relation to environmental factors, such as during the extreme drought of the El Niño year (2015/2016). The main ET drivers were identified during the model calibration process, which are: vapour pressure deficit, radiation and soil moisture. The seasonal ecosystem productivity and evapotranspiration are not synchronized in this Southern Amazon forest during the flooded period, because the free water evaporation mainly drives ET. However, during non-flooded months ET is governed by forest transpiration, as indicated by the association with the carbon, phenological and meteorological seasonal patterns. The flood pulse regulates the soil volume water content, and consequently, the water availability for plants during non-flooded months. These findings highlighted the vulnerability of this forest facing extreme dry years, given the decreased flood pulse trend reported here, which consequently diminished the total water storage in this region during 2016, assessed through GRACE product.

Keywords: Floodplain. Amazon. Bananal. Gross Primary Productivity. Evapotranspiration. Phenology. EVI. Eddy-covariance. Generalized Additive Model.

# SAZONALIDADE DA EVAPOTRANSPIRAÇÃO E DA PRODUTIVIDADE PRIMÁRIA BRUTA EM UMA FLORESTA ALAGÁVEL NA REGIÃO DA ILHA DO BANANAL

## RESUMO

A floresta amazônica desempenha um importante papel na regulação do clima em escala local, regional e global, devido ao elevado potencial de absorção de carbono em sua biomassa e da transferência de água para a atmosfera através da evapotranspiração. Apesar dos inúmeros estudos que exploraram os mecanismos de controle sazonal da vegetação, poucos se concentraram nas florestas inundadas, as quais correspondem a aproximadamente 14% da bacia Amazônica. Em busca de compreender os mecanismos de controle da vegetação durante os períodos secos e inundados, o presente trabalho foi realizado em uma floresta sazonalmente alagada localizada na área de transição entre os biomas Amazônia e Cerrado, próximo à região da Ilha do Bananal (BAN). Foi realizada a análise da sazonalidade da produtividade primária bruta (PPB) e da evapotranspiração (ET) obtidas através da torre micrometeorológica, juntamente com variáveis climáticas e padrões fenológicos, estes, obtidos em campo (massa foliar) e através do índice de vegetação melhorado (EVI). O EVI foi calculado a partir de imagens com resolução moderada e correção angular e atmosférica (MODIS / MAIAC)). As medidas de ET apresentaram muitas lacunas e um modelo estatístico (*do inglês, Generalized Additive Model - GAM*) foi usado para reconstruir a série temporal desse dado de 2004 a 2017, dados climáticos de reanálise (ERA5) foram utilizados como variáveis preditoras nesse modelo. Além disso, o produto de sensoriamento remoto MOD16A2 foi adquirido para analisar a potencialidade do mesmo em representar a sazonalidade da ET. As mudanças no padrão hidrológico da região foram analisadas por meio do produto do satélite GRACE (*do inglês, Gravity Recovery and Climate Experiment*). Os resultados revelaram que a produtividade do ecossistema é limitada pela umidade do solo de duas maneiras, durante o período alagado, o excesso de água limita a PPB, enquanto a PPB está associada positivamente à umidade do solo durante os meses não alagados. Além disso, a PPB é maximizada quando o déficit acumulado de água (CWD) aumenta, indicando a dependência da quantidade de água que entra no sistema. O EVI associou-se positivamente à massa foliar e à PPB, sugerindo a sincronia entre a produção foliar e a capacidade fotossintética do dossel, diminuindo no pico do período de inundação e no final da estação seca. O EVI também foi capaz de descrever as variações interanuais do dossel em relação aos fatores ambientais, como durante a seca extrema do ano de El Niño (2015/2016). Os principais fatores climáticos que influenciam na sazonalidade da ET são: O déficit de pressão de vapor, a radiação e a umidade do solo, identificados durante o processo de calibração do modelo estatístico. A produtividade sazonal do ecossistema e a evapotranspiração são dissociadas nesta floresta, pois as altas taxas de ET estão relacionadas

principalmente com a evaporação de água livre durante o alagamento, enquanto durante os meses não inundados, a transpiração da floresta é o principal regulador da ET, como indicado pela sazonalidade do carbono, da fenologia e dos dados climáticos. O pulso de inundação regula o volume de água no solo e, conseqüentemente, a disponibilidade de água para as plantas durante os meses não inundados. Esses resultados evidenciam a vulnerabilidade dessa floresta em anos extremos de seca, dada à tendência de diminuição da amplitude do alagamento identificada nesse estudo, que conseqüentemente diminuiu o armazenamento total de água na região durante o ano de 2016, observado através do produto do satélite GRACE.

Palavras-chave: Planície de inundação. Amazônia. Bananal. Produtividade Primária Bruta. Evapotranspiração. Fenologia. EVI. Modelo Aditivo Generalizado.



## LIST OF FIGURES

	<u>Pág.</u>
Figure 2.1 - Tocantins Araguaia basin (grey polygon) in the context of the legal Amazon delimitation (yellow polygon) and the Amazon basin (beige polygon). .	7
Figure 3.1 - LBA eddy flux tower location. A) Tocantins State inside Legal Amazon delimitation (red line), B) Cantão State Park located in the transition area between the Amazon and Cerrado biomes (IBGE delimitation, green and beige), and C) LBA tower inside Cantão State Park (Sentinel-2 image, RGB composite of June 2018). .....	15
Figure 3.2 - Experimental plots (yellow squares; BAN1 and BAN2) and piezometers (blue dots, PZ1, PZ2, PZ3) location around the LBA flux tower (red triangle). .....	17
Figure 3.4 - Seasonal pattern of flood height measured at the BAN Tower (red line), river level measured at the ANA station (Blue line), and total water storage from satellite data (black line).....	19
Figure 4.1 - Monthly scatterplot of rainfall data from TRMM against flux tower data (a) and a monthly scatterplot of VPD from ERA5 against tower data (b). The fitted regression line (red).....	31
Figure 4.2 - Average annual cycle of ET (2004 to 2014; black line) and rainfall from TRMM (2004 to 2016; dark grey bar) (a), cumulative water deficit (2004 to 2016; CWD) (b), vapour pressure deficit (2004 to 2014; VPD) (c), soil moisture (2004 to 2016; SM) and flood height (2004 to 2016; dark blue line) (d), net radiation (2004 to 2016; dashed black line) and air temperature (2004 to 2014; brown solid line) (e), GPP (2011 to 2013; black solid line) (f), and EVI (2004 to 2016; long dashed black line) (g). The shaded blue area corresponds to the flooded period. The standard deviation of the monthly variables is indicated by either shading or error bars. ....	36
Figure 4.3 - Shuttle Radar Topographic Mission (SRTM) classified as areas below and above the tower level, which is located at 181 meters of altitude according to SRTM (red dot). Grey squares represent the Moderate Resolution	

Imaging Spectroradiometer (MODIS) pixels within the tower footprint (green circle, Borma et al. (2009)) selected to extract mean EVI and be analyzed. .... 37

Figure 4.4 - Scatterplots between the daily mean of eddy covariance GPP compared to climate drivers from 2011 to 2013: Net radiation (a), ET (b), VPD (c), Average soil moisture for layers up to 200 cm depth (d), Rainfall (e), Ta (f) and the monthly average of GPP compared to CWD (g) and EVI (h). Both lines represent the regression fit between variables during flooded (blue) and non-flooded (yellow) months. .... 39

Figure 4.5 - Monthly average leaf litter mass rate (solid black line) collected at the surrounding area of the tower from April 2004 to May 2005 (Moreira et al., 2005), and monthly average EVI-multi-angle implementation correction (MAIAC) (black dashed line) for the same period. The flooded period is represented by the blue shading area (a). Scatterplot between EVI and leaf litter mass with the fitted regression line (red) (b). .... 40

Figure 4.6 - a) Spatial and temporal correlation between tower EVI and pixels with less than 10% of permanent water channels [52] inside the Cantão State Park. b) LiDAR canopy height model (CHM) transect and gaps (< 2m height) in red. .... 41

Figure 4.7 - Monthly variation of CWD (a), temperature (b), VPD (c), river level (d), soil moisture (e) and EVI (f). The dashed line represents the average value (2004–2016), the standard deviation of the monthly variables is indicated by the grey shading, the blue line represents the wettest year (2009), the red line the driest year (2016) and grey lines represent remaining years (2004–2015). .... 42

Figure 5.1 - Flow chart describing the overview of this study. The gray squares are representing the main results. .... 51

Figure 5.2 - Daily scatterplot between tower (ordinate), and its correspondent variable from ERA5 and TRMM data (abscissa). The red line represents the fitted regression line. .... 54

Figure 5.3 - Interannual relationship between soil moisture measured at different depths from the BAN flux tower and soil moisture measurements from ERA5 products. The black line represents volumetric soil moisture layers from ERA5,

and the tower (FDR) lines are varying according to the depth, 20 cm is red, 80cm is blue, 220cm is purple and 293 cm is the dark yellow line. .... 55

Figure 5.4 – Correlation between soil moisture measured close to the BAN tower (UmidSol\_20cm, UmidSol\_80cm, UmidSol\_150cm, UmidSol\_220cm, UmidSol\_293cm), ERA5 reanalysis data (swvl1, swvl2, swvl3, swvl4) and GRACE product (TWS). .... 56

Figure 5.5 - Seasonal quarters of predicted and observed half-hourly ET with tower covariates (A) and with ERA5 covariates (B). Periods are divided into Rising-water (NOV-DEC-JAN), full flooding (FEB-MAR-APR), falling water (MAY-JUN-JUL) and drainage (AGO-SEP-OCT). The color ramp represent the number of observations (n° OBS)..... 60

Figure 5.6 - Scatterplot between ET and Net radiation in an hourly time step (colour ramp), divided in months (1 to 12) for the periods of good ET observation density from the BAN flux tower. .... 61

Figure 5.7 - Scatterplot between ET and global radiation in an hourly time step (colour ramp), divided in months (1 to 12) for the periods of good ET observation density from the BAN flux tower. .... 62

Figure 5.8 - Scatterplot between ET and VPD in an hourly time step (colour ramp), divided in months (1 to 12) for the periods of good ET observation density from the BAN flux tower. .... 62

Figure 5.9 - Scatterplot between ET and soil moisture content at 20 cm depth in a daily time step divided by months (1 to 12) for the periods of good ET observation density from the BAN flux tower..... 63

Figure 5.10 - Scatterplot between ET and soil moisture content at 80 cm depth in a daily time step divided by months (1 to 12) for the periods of good ET observation density from the BAN flux tower..... 63

Figure 5.11 - Scatterplot between ET and soil moisture content at 220 cm depth in a daily time step divided by months (1 to 12) for the periods of good ET observation density from the BAN flux tower..... 64

Figure 5.12 - Seasonal daily observed (black line), predicted (yellow line) and MODIS product ET (purple line) from 2004 to 2010 (considering days of good ET

observed records). The standard deviation of the monthly variables is indicated by the corresponding shading color.....	65
Figure 5.13 - Scatterplot between observed ET from the tower and MODIS (a) and scatterplot between predicted ET from GAM using ERA5 data and observed ET (tower data) in a 8 day time scale. ....	66
Figure 5.14 - Interannual ET (a), meteorological drivers (b,c,d,e,g), soil moisture (f), and the phenology pattern (h) represented by the EVI. The grey shaded area corresponds to the ENSO period (May 2015 to May 2016), and the yellow ones correspond to the annual dry season (June to September). Gray lines represent the ET (a) and the rainfall (b) seasonal average. ....	67
Figure 5.15 - Monthly variation of ET from 2004 to 2017. The standard deviation of the monthly variables is indicated by the grey shading. ....	68
Figure 5.16 - Javaés river level from 1980 to 2018 at Barreira da Cruz station..	69
Figure 5.17 - The standard anomaly of total water storage from GRACE product from January 2004 to December 2016. ....	70
Figure A.1 - Bing Virtual Earth image. MODIS MAIAC pixels (red squares) around the LBA tower (Yellow dot) and mapped water channels. ....	87
Figure A. 2 - Monthly GPP and EVI from May 2011 to September 2013.....	89
Figure B.1 - Monthly scatterplot of rainfall data from TRMM against flux tower data. The fitted regression line (red).....	90
Figure B. 2 - Hourly observed (red) and predicted (black) ET.....	90
Figure B.3 - Scatterplots between monthly EVI and ET from 2004 to 2017. Both lines represent the regression fit between variables during flooded (blue) and non-flooded (yellow) months. ....	91

## LIST OF TABLES

	<u>Pág.</u>
Table 3.1 - Equipments and measurements recorded on the flux tower .....	20
Table 4.1 - Availability and usage description of tower, satellite and field data.	33
Table 4.2 - Experimental plots and LiDAR statistics regarding tree height measurements.....	41
Table 5.1 - Tower data and availability, ERA5 and satellite correspondent variables and usage description.....	59
Table A.1 - Percentage of permanent water channels and forest cover in MODIS pixels as delineated with high-resolution Bing Virtual Earth image on QGIS.....	88



## LIST OF ABBREVIATIONS

d2m	2 Meter Dewpoint Temperature – ERA5 product
ECMWF	European Centre for Medium-Range Weather Forecasts
ERA5	The fifth generation ECMWF atmospheric reanalysis of the global climate
ET	Evapotranspiration
EVI	Enhanced Vegetation Index
GAM	Generalized Additive Model
GPP	Gross Primary Production
H	Sensible Heat
Ki	Global Radiation
LE	Latent Heat
MODIS	Moderate Resolution Imaging Spectroradiometer
NEE	Net Ecosystem Exchange
Net	Net Radiation
PAR	Photosynthetic Radiation
Press	Atmospheric Pressure
q	Specific Humidity
Rh	Relative Humidity
SRTM	Shuttle Radar Topography Mission
ssr	Surface Solar Net Radiation - ERA5 product
ssrd	Surface Solar Radiation Downwards - ERA5 product
swv1	Soil Water Volume Layer (0.7 m) - ERA5 product
swv2	Soil Water Volume Layer (0.7 m - 0.28 m) - ERA5 product
swv3	Soil Water Volume Layer (0.28 - 1.00 m) - ERA5 product

swvl4	Soil Water Volume Layer (1.0 - 2.89 m) - ERA5 product
Ta	Air Temperature - ERA5 product
Tar	Air Temperature
tp	Total Precipitation - ERA5 product
TRMM	Tropical Rainfall Measuring Mission
TWS	Total Water Storage
VPD	Vapour Pressure Deficit



## CONTENTS

	<u>Pág.</u>
1 INTRODUCTION .....	1
1.1 Goals.....	3
2 LITERATURE REVIEW .....	5
2.1 Wetlands and vegetation dynamics in the Amazon/Solimões and Araguaia floodplains.....	5
2.2 Floodplain forests adaptation strategies to drought and flood cycles .	8
2.3 Study of vegetation dynamics through remote sensing products.....	10
3 GENERAL METHODOLOGY .....	14
3.1 Study area.....	14
3.1.1 Experimental site .....	16
3.1.2 Micrometeorological tower.....	19
3.1.2.1 Net ecosystem exchange.....	21
3.1.2.2 Gap filling of CO <sub>2</sub> estimates .....	21
3.1.2.3 Energy balance .....	22
3.1.2.4 Evapotranspiration .....	23
4 PHENOLOGY AND SEASONAL ECOSYSTEM PRODUCTIVITY IN AN AMAZONIAN FLOODPLAIN FOREST .....	25
4.1 Introduction .....	25
4.2 Materials and methods.....	28
4.2.1 Flux tower and field data .....	28
4.2.2 Litterfall Collection .....	29
4.2.3 Remote-sensing data and products.....	29
4.2.4 Statistical analysis .....	32
4.3 Results.....	34
4.3.1 Seasonal meteorological, Gross Primary Productivity (GPP) and Enhanced Vegetation Index (EVI) patterns.....	34
4.3.2 Correlation between GPP, climatic variables and EVI.....	38

4.3.3	Seasonal phenology patterns and analysis of forest canopy gaps	39
4.3.4	Inter-annual variation of seasonal drivers and EVI-Multi-Angle Implementation Correction (MAIAC)	42
4.4	Discussion	43
4.5	Conclusions	45
5	ESTIMATION OF LONG-TERM EVAPOTRANSPIRATION OVER A TROPICAL FLOODPLAIN FOREST	47
5.1	Introduction	47
5.2	Methods	50
5.2.1	Gap filling and long-term ET prediction using the Generalized Additive Model (GAM)	51
5.2.2	Association between flux tower, reanalysis and remote sensing data	53
5.2.3	Seasonal analysis	56
5.2.4	Interannual ET analysis and the influence of extreme droughts over the Bananal forest	57
5.3	Results	59
5.3.1	Reconstructing ET measurements using GAMs	59
5.3.2	Do the meteorological and hydrological drivers of ET change throughout the year?	61
5.3.3	Seasonal ET variation	64
5.3.4	Interannual evapotranspiration variability and the ENSO drought	66
5.4	Discussion	70
5.5	Conclusion	73
6	GENERAL CONCLUSIONS	74
	REFERENCES	76
	APPENDIX A - COMPLEMENTARY MATERIAL OF CHAPTER 4	87
	APPENDIX B - COMPLEMENTARY MATERIAL OF CHAPTER 5	90



## 1 INTRODUCTION

The Amazon basin plays an essential role in the climate regulation services storing large amounts of carbon as biomass (PHILLIPS et al., 1998; MALHI et al., 2009; BRIENEN et al., 2015), and transferring water from the ground to the atmosphere through evapotranspiration (DA ROCHA et al., 2009; WRIGHT et al., 2017). These mechanisms are the main processes that influence regional and global climate.

Amazon forest accounts for more than 50% of tropical forests over the world (MALHI et al., 2006). In this context, it is expected that trees species may vary as an adaptation to geomorphological and climate conditions over this large region. In *terra firme* forests, water availability e.g. (MARKEWITZ et al., 2010; RESTREPO-COUBE et al., 2013), incident radiation and rainfall [e.g (SOMBROEK, 2001)] associated to plant traits and root depth e.g (BARROS et al., 2019; BRUM et al., 2019) modulates the forest functioning. In wetlands, these mechanisms are also associated with the flood pulse; thus, the vegetation established in floodplains responds to changes in the physical-chemical environment with morphological, anatomical, and physiological adaptations to flooding (JUNK; BAYLEY; SPARKS, 1989).

The wetlands areas covered by forests by large rivers as the Amazon and Araguaia ones are known as seasonally flooded forests (JUNK; BAYLEY; SPARKS, 1989). These areas are majority occupied by forests adapted to the seasonal flood pulse, which influences the distribution of plant communities according to the intensity and duration of flooding (JUNK et al., 2011). They play an essential ecological role as a source and sink of important elements of the biogeochemical cycles, habitat for endemic species of plants and animals, and timber and non-timber products to local populations (PIE DADE et al., 2013).

As these ecosystems are closely related to the flood pulse, they are susceptible to eventual changes that may occur in the hydrological regime (PIE DADE et al., 2013), as the ones that happen during extreme droughts in 2005 and 2010, which strongly diminished river levels over the Amazon (MARENGO et al., 2011). Some researches pointed to a greater resilience of these forests during seasonal

droughts, since the growth period occurs during the terrestrial phase, which represent the period when there is no flood (WORBES, 1997; SCHONGART et al., 2002, 2004; PAROLIN et al., 2004). However, recently reports have showed that the lack of water availability during the dry season could increase mortality (SCHEFFER et al., 2017; RESENDE et al., 2019).

On the other hand, several studies have sought to understand the forest response to seasonal climate variation at *terra firme* forest, coupling field and remote sensing multispectral vegetation indices. Some of them have pointed to the Amazon rainforest as resilient to seasonal droughts (HUETE et al., 2006) and also extreme droughts (SALESKA et al., 2007). Other studies, though, reported that an apparent greening of the forest could be attributed to the abnormal leaf flush or as an effect of sun position in relation to the sensor, increasing near-infrared reflectance, which did not reflect the resilience of the forest (ANDERSON et al., 2010; BRANDO et al., 2010; GALVÃO et al., 2011; XU et al., 2011; SOUDANI; FRANÇOIS, 2014; MORTON et al., 2016). However, given the reported uncertainties related to the sun-sensor geometry effects and atmospheric contamination, progress has been made with the development of more robust atmospheric correction methods and data normalization considering the Bidirectional Reflectance Distribution function (BRDF) for the MODIS data, such as the Multi-Angle Implementation Correction – MAIAC (LYAPUSTIN et al., 2012).

It is challenging to use optical images within flooded areas to investigate phenological patterns, given the possibility of free water interference on the vegetation indexes responses, due to the high absorption of the near infrared reflectance from free-standing water (HESS et al., 2009). Nonetheless, along the transition area between Amazon and Cerrado biomes, it is located the only flooded site within an LBA tower (Large Biosphere Atmosphere Program - LBA), which offers a unique opportunity to study the seasonal forest functioning coupling field, tower and satellite data.

Moreover, this forest imposes several complex analyses to understand how environmental changes regulate ET and how it is connected to the carbon cycle.

Thus, the main question that guided this study was: How does a seasonally flooded tropical forest respond to flood and drought cycles in terms of evaporative fluxes and gross primary productivity (GPP) associated to phenological patterns?

In order to answer this main question, eddy covariance, meteorological and soil moisture data obtained from the BAN tower were used to analyze the forest response to seasonal flood and drought cycles, comprising monthly records of these measurements from 2004 to 2014. Furthermore, the forest response to seasonal environmental changes was assessed through the phenological pattern using the enhanced vegetation index – EVI, meteorological data, and an interannual ET time series, comprising the El Niño period of 2015/2016.

Based on previous studies carried out at the Amazon forest and this site, it is expected that the enhanced vegetation index (EVI) will be able to describe the photosynthetic capacity of the canopy synchronized with the gross primary production (LOPES et al., 2016b; WU et al., 2016; MOURA et al., 2017), especially during the terrestrial phase, when GPP is maximized (COSTA, 2015). However, this site is located within an area with a prolonged dry season, which is expected to strongly affect the forest water availability (DA ROCHA et al., 2009), and consequently, the canopy phenology.

## **1.1 Goals**

The overall goal of this thesis is to evaluate the gross primary production and evapotranspiration seasonality associated with phenological patterns at the floodplain forest located in the Amazon-Cerrado transition, as well as its environmental controls, based on field observations and remote sensing data. Hence, the main goals to achieve these aims were:

- Analyzing the seasonal gross primary production and phenological patterns during flood and drought cycles, using flux tower and satellite data;
- Investigating the effects of hydroclimatic drivers upon evapotranspiration (ET) on a daily, monthly, and interannual basis.

This thesis is divided into six chapters. The first one briefly describes the theme, problem and main goals. The second Chapter exhibits the literature review and the third one describes the general methodology. The fourth Chapter investigates the seasonal ecosystem productivity coupling phenological and climatological drivers and the possible effects on forest functioning, given the environmental changes. The fifth Chapter focuses on reconstructing ET measurements from the eddy-covariance system using a statistical model (Generalized additive model). The results obtained from the reconstructed ET allowed accessing the daily, monthly, and yearly ET variations, regarding hydrological changes that took place over this region. Finally, the sixth Chapter summarizes the results obtained in both Chapters 4 and 5.

## 2 LITERATURE REVIEW

This section presents a literature review about the forest response to cycles of flood and drought, and its interaction with the atmosphere, focusing on floodplain areas of Central Amazon and in the Araguaia floodplain. This comparison is based on the similarities of the phytogeographical species domain located around the BAN tower and the ones located in the Amazon biome (TAVARES, 2019).

### 2.1 Wetlands and vegetation dynamics in the Amazon/Solimões and Araguaia floodplains

Wetlands are recognized as valuable ecosystems worldwide because they offer economic, social, and environmental benefits - recognized as ecosystem services (COSTANZA et al., 1997). The regulation of essential ecological processes, life support systems (e.g., climate regulation and the hydrological cycle) and flood prevention are examples of these services (MILLENNIUM ECOSYSTEM ASSESSMENT, 2005). Nonetheless, wetlands figure among the most threatened environments in the world, which had lost approximately 35% of the occupied area between 1970 and 2015, with accelerating rates of annual loss since the 2000s (WETLANDS, 2018).

The Amazon basin is estimated to comprise more than 400.000 km<sup>2</sup> of floodable areas in the Brazilian territory, along the Amazon/Solimões river and its large tributaries (MELACK and HESS, 2010). These areas are classified into two groups: *Várzeas* (white water river) and *Igapós* (black water river). *Várzeas* are predominant ecosystems comprising 300.000 km<sup>2</sup> of the floodplain areas in the Brazilian Amazon, which are fertile environments since the rivers associated with them cross geologically recent regions (Andean region). The water associated with *Igapós* regions (100.000 km<sup>2</sup>) is acidic, composed of diluted organic material (JUNK et al., 1989; WITTMAN et al., 2010).

The floristic composition of the Amazon floodplain forests along the topographic gradient was established according to the degree of species adaptation to flooding. Wittmann et al. (2002) divided the *Várzeas* into two groups, called *Low*



and high *Várzea* (*Várzea alta e Várzea baixa, in portuguese*), which are annually submitted to seasonal floods.

The structure and composition of tree species in the Low *Várzea* depend on the stage of succession, and their number is reduced by the impact caused by flooding (WORBES et al., 1992; WITTMANN et al., 2002). In response to prolonged flooding, trees in early succession stages often exhibit adaptations to anoxic conditions, such as reduced metabolic activity (PAROLIN et al., 2004). Many species in these environments present leaf flush during the flooded phase (SCHONGART et al., 2002), while at the high *Várzea*, the flushing occurs during the terrestrial phase (PAROLIN et al., 2010). As flooding in the high *Várzea* is reduced, species from adjacent *terra firme* forests can settle in this environment (WITTMANN; ANHUF; FUNK, 2002).

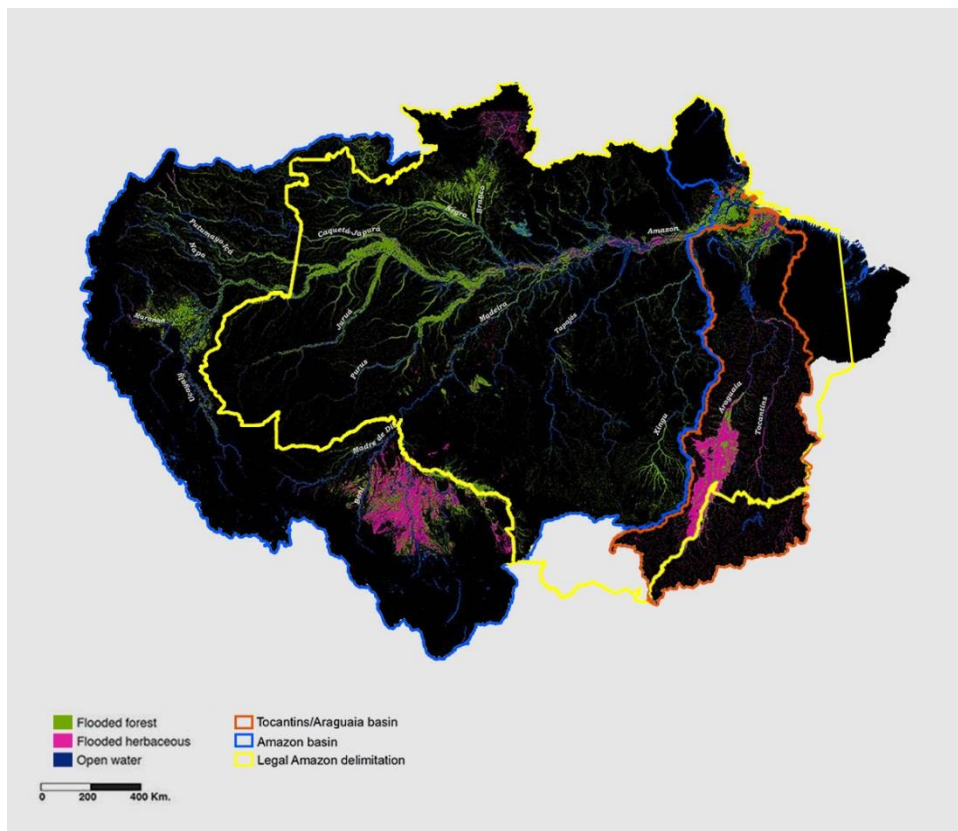
Regarding the trunk growth, Schongart et al. (2002) reported higher rates of biomass increment during the terrestrial phase, whereas a dormancy of 3 months was observed during the flooded period. Nonetheless, before the flooding ends, when the water level starts to decrease, trees produce new leaves, and the exchange rate activity immediately restarted (PIE DADE et al., 2013).

The amplitude of the water level considerably varies between regions of the Amazon basin, from 5 meters above the ground in the upper Negro river to 12 meters in the Solimões river, which could last more than seven months of flooding (JUNK; BAYLEY; SPARKS, 1989). This variation occurs due to geomorphological variability (LATUBERSSE, 2008; QUESADA et al., 2009), associated with hydrological and climatic gradients along the basin (SOMBROEK, 2001; MARENGO, 2005).

Another considerable wetland area is located in the Tocantins-Araguaia watershed, which is the fourth largest basin in South America (LATRUBESSE; STEVAUX, 2002). Part of this basin is located inside the legal Amazon delimitation within Mato Grosso, Tocantins, and Pará States, covering areas of the Amazon and the Cerrado (Savanna) biomes (Figure 2.1). The Araguaia River is the main system of the basin (AQUINO et al., 2008). The extension of its

medium river course is 1,160 km<sup>2</sup>, covering an extensive alluvial plain, which has 58,000 km<sup>2</sup> of wetlands. In this context, the Bananal Island covers an area of 21,000 km<sup>2</sup> and is the largest river island in the world covered mostly by savannas and pastures (AQUINO et al., 2008). Likely in the Amazon floodplain, the seasonal floodplain forest of Araguaia region is characterized by drought and flood cycles, however, the water amplitude level reaches a maximum of 4 m, lasting up to 5 months (BORMA et al., 2009).

Figure 2.1 - Tocantins Araguaia basin (grey polygon) in the context of the legal Amazon delimitation (yellow polygon) and the Amazon basin (beige polygon).



Source: Adapted from Hess et al. (2015).

The botanical family composition of the Araguaia floodplain is similar to the one found in the Amazon *Várzea forest* (KURZATKOWSKI et al., 2015). Moreover, the study carried out by Tavares (2019) reported that the phytogeographical domain of the species identified around the BAN tower occurs mainly in the

Amazon biome, followed by *Cerrado* and in a small number in *Mata Atlântica* biomes (TAVARES, 2019).

Approximately 44% from 46 tree species identified in the Araguaia floodplain are found in other seasonally flooded regions, such as in the riparian forests of the Amazon, *Cerrado*, *Mata Atlântica*, *Pantanal* forests, and in the *igapó* and *várzea* forests of the Amazon (TAVARES, 2019).

The species diversity did not vary much according to the topographic gradient as in *várzeas* forests (KURZATKOWSKI; LEUSCHNER; HOMEIER, 2015). Nonetheless, smaller wood density and tree height were observed in lowlands compared to trees located in higher terrain portions (KURZATKOWSKI; LEUSCHNER; HOMEIER, 2015).

The growth period occurs during the terrestrial phase in the Araguaia floodplain likewise in the Amazon flooded forests, however, some studies reported low rates of growth in this ecosystem due to the long dry season (Rocha et al., 2009) and low soil nutrient content (KURZATKOWSKI; LEUSCHNER; HOMEIER, 2015; TAVARES, 2019). Nonetheless, species located in these floodplains exhibit survival strategies to deal with drought and flood cycles as reported for central Amazon forests.

## **2.2 Floodplain forests adaptation strategies to drought and flood cycles**

The anaerobic condition of the roots during the flooded phase decreases the water conductance by the trunk and consequently reduces the canopy humidity, which leads to significant reductions in tree transpiration (PAROLIN et al., 2005) and vegetative dormancy (SCHONGART et al., 2002). Nonetheless, other studies have reported that the negative response that plants exhibit during the rising water phase is part of the acclimatization processes to undergo the flooded period (HERRERA, 2013). The production of new morpho-anatomical structures (adventitious roots) and the operation of physiological and biochemical processes, such as pressurized gas transport (which contributes to internal roots aeration) and aquaporin synthesis are part of the adaptation processes, which allow plants to reestablish their functioning during the flooded period, increasing

leaf-specific hydraulic conductivity, stomatal conductance and photosynthetic rates (HERRERA, 2013).

In this context, trees may present more than one mechanism of adaptation to flooding, such as: increase root porosity, aerenchyma formation in the root cortex, release organic substances into the atmosphere, enrichment of the rhizosphere with oxygen, photosynthesis reduction, anaerobic metabolism among others (DE SIMONE et al., 2002; DE SIMONE; JUNK; SCHMIDT, 2003; PAROLIN et al., 2004).

Floodplain root systems are shallow as an adaptation strategy to allow root aeration for a longer period during the terrestrial phase; however, the atmospheric demand at the onset of the dry season (when monthly evaporation usually exceed precipitation rates) might reduce the soil water availability, which could reach the permanent wilting point, causing drought stress in the floodable biota (PAROLIN et al., 2010). In this way, different forms of drought adaptation were observed in Amazonian floodplain forest, such as the reduction of leaf water potential, senescence, and xylem flow, which reduces the loss of water by transpiration during the dry phase (PAROLIN et al., 2010). Although literature has reported different strategies adopted by the forest to deal with drought, the flooded period seems to be more critical in this area (SCHONGART et al., 2004; ASSIS et al., 2019).

The Araguaia floodplain also presents the annual period of water stress due to flooding, becoming dormant as a survival strategy (TAVARES, 2019). Despite being subjected to flood, the forest behaved as a carbon sink during most of the year, which could be an assimilation period to anoxia-reduced stress (TANNUS, 2004; OLIVEIRA, 2006). The higher rates of CO<sub>2</sub> assimilation were recorded at the early dry season and during the rainy non-flooded period (COSTA, 2015), which also describes the higher biomass increment period, when the soil layer is not saturated or completely dry (TAVARES, 2019), characterizing the bimodal pattern of the forest function (COSTA, 2015).

The phenological canopy changes also occurs during the dry season, senescence and leaf flushing were reported from June to October (MOREIRA et al., 2005). The peaks of litterfall in June and October occur synchronized with peaks of GPP, suggesting that photosynthetic seasonality is explained by the interaction between leaf phenology and environmental drivers (e.g. RESTREPO-COUBE et al., 2013; WAGNER et al., 2017).

This floodplain forest exhibits a strong rainfall seasonality, since approximately 90% of annual precipitation occurs during the rainy season (ROCHA et al., 2009). During normal climatological years (2004 and 2006) soil moisture seemed to be sufficient to supply evapotranspiration throughout the dry season. However, low rates of evapotranspiration were reported during the extreme drought of 2005, given the low soil water retention capacity, associated with shallow clay layers (BORMA, et al., 2009). Moreover, decreased rates of biomass increment were also reported in this region for the same year (HOMEIER et al., 2017).

The drought vulnerability of this floodplain was highlighted in the study carried out by Tavares (2019), which reported the reduction of 50% in forest growth during the ENSO year of 2016, as a result of lower precipitation and soil water availability combined with higher temperature and VPD, compared to a typical climatological year.

### **2.3 Study of vegetation dynamics through remote sensing products**

Several optical sensors are providing free globally images to monitor forest dynamics, such as the Moderate Resolution Imaging Spectroradiometer (MODIS - Terra/Aqua), Thematic Mapper (TM - Landsat 5), Operational Land Imager (OLI - Landsat 8), Multispectral Image (MSI - Sentinel-2) among others (ESA, 2015; USGS, 2013). Vegetation dynamics (e. g. Photosynthetic capacity, leaf area index, and leaf flush) are widely analyzed using indices from these sensors, such as the Normalized difference vegetation index (NDVI), the Green chromatic coordinate (Gcc), the Enhanced vegetation index (EVI) among others. These indices are calculated using images from the visible and near-infrared reflectance spectrum, due to the ability of chlorophyll to absorb visible radiation (400 - 700

nm) and the leaf mesophyll to reflect infrared radiation (700 - 1100 nm) (JENSEN, 2009).

MODIS indices are widely used because of the characteristics that make this sensor suitable for monitoring large biomes, such as the data availability since the 2000s, and the revisit time from 1 to 2 days at the same location, which makes it possible to create composition images every 16 to 30 days, especially over tropical forests, that are often cloud covered. Moreover, progress has been made towards the development of more robust atmospheric correction methods and data normalization procedures for MODIS data, such as the multi-angle implementation correction (MAIAC) algorithm (LYAPUSTIN et al., 2012) implementation of the bidirectional reflectance distribution function (BRDF).

Regarding the correlation between vegetation dynamics with remote sensing products, several techniques have been developed in the study of the Amazon forest bottom-up phenology, using tower-based cameras (phenocams), which has optical principles similar to those used by spaceborne optical sensors, allowing the calculation of the same vegetation indices in a refine scale. Some of them have reported the synchronization between new leaves detected by the camera with litter production, obtained through litterfall collection, triggered by climatic drivers (MAEDA et al., 2016; WAGNER et al., 2017). It also provided improvements assigning spectral reflectances of leaves at different stages of maturation, which changes the canopy structure and the leaf area index (LOPES et al., 2016; WU et al., 2016; Wu et al., 2018). In this latter study, Wu et al. (2018) concluded that two phenological factors explain the reflectance seasonality observed by satellite data: (i) leafless crown fraction and (ii) leaf demography. These factors represent different ecophysiological strategies of trees to the seasonal / interannual variations of water availability or radiation. According to WU et al., (2018) the biophysical factors of the trees seasonality at the canopy level are observed through the EVI - MAIAC response (WU et al., 2018).

Enhanced vegetation index (EVI) values extracted from this improved MODIS product (MODIS-MAIAC) have shown a correlation between phenology and productivity of the Amazon forest occurring during the dry season, synchronized

with mature leaf area index (MOURA et al., 2015; LOPES et al., 2016; MAEDA et al., 2016; WU et al., 2016). These results have brought a major advance in the discussion of the response of the Amazon forest to seasonal or extreme droughts, supporting that the EVI corrected with MAIAC algorithm described the phenology of the forest, which also demonstrated their potential to identify anomalies in years of extreme drought (HILKER et al., 2014; MOURA et al., 2017; WAGNER et al., 2017; YANG et al., 2018).

The same indexes were used to study the relationship between seasonal phenology and meteorological drivers (precipitation) in the state of Tocantins, considering differences in vegetation cover. The EVI product showed a positive relationship with water availability and canopy changes. It decreased in the late dry season when the lowest leaf litter mass was recorded, while NDVI was more effective in identifying different land use and land cover classes (BECERRA; SHIMABUKURO; ALVALÁ, 2009).

Although the use of vegetation indices are widespread in monitoring the Amazon rainforest, few of them were used to investigate seasonal phenological changes in flooded areas, given the challenge to discriminate if low values of the index were representing the canopy changes (Senescence) or the high absorption of the near-infrared reflectance by the free standing water. In the central Amazonian floodplain forest, the EVI product demonstrated the flood pulse relationship with vegetation seasonality, the maximum peak corresponded to the period of maximum leaf area, and the lowest water table level (HESS et al., 2009).

The Pantanal biome is likewise characterized by the flood pulse as well as in the Amazon and Araguaia floodplains, extending for 160.000 km<sup>2</sup> in the middle of South America. The EVI product in this biome was used to map wetlands and non-flooded areas. The high absorption of the near-infrared reflectance by the water allowed mapping wetlands, which showed low values of EVI in the presence of free-standing water, given the sparse vegetation structure of this area (GOLTZ et al., 2007; VIANA; CÉLIA, 2011; LEIVAS; ANDRADE; BOLFE, 2012).

Nonetheless, microwave range data (synthetic aperture radar and emissivity data) are mainly used to map wetlands boundary and flood monitoring in dense forests like the Amazon, because of the ability to detect the presence of water under the canopy (HESS et al., 2003, 2016; ARNESEN et al., 2013; FURTADO; SILVA; NOVO, 2016).

Using vegetation indices as a *proxy* for photosynthetic capacity, leaf area, and leaf flush, combined with *in situ* data, can improve the biophysical understanding of forest dynamics in cycles of rainy, dry, and flooded periods.



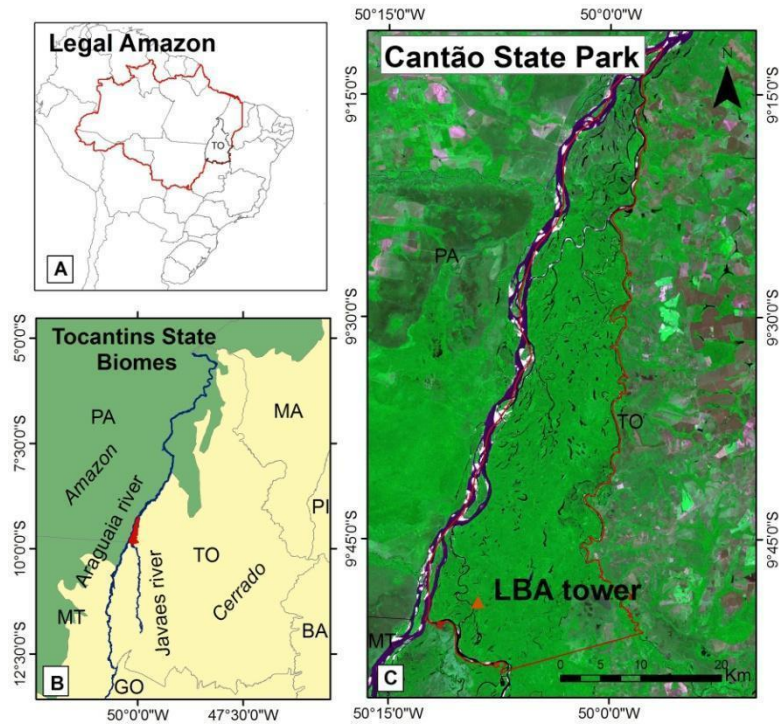
### **3 GENERAL METHODOLOGY**

This section briefly explains the site location, instruments, funding, data sources, and researches that have been carried out at the Bananal site.

#### **3.1 Study area**

The study site is located in a floodplain area of Cantão State Park (*Parque Estadual do Cantão, PEC*), which consists of approximately 90% natural vegetation and is located about 260 km west of Palmas, state of Tocantins, Brazil. The park is naturally limited by the Araguaia, Coco and Javaés river (Figure 3.1). The area is located at the transition between the Amazon and Cerrado (savanna) biomes, being characterized as a seasonally flooded Cerrado (JUNK et al., 2013), bounded in the southwest by the Bananal Island region, which is the largest river island in the world (BORMA et al., 2009). Because of this location, the site is also called within LBA program, Bananal site (BAN site). The LBA micrometeorological tower is located about 2 km east of Javaezinho river, a tributary of Javaes river. The annual average rainfall varies between 1300 to 1900 mm, and temperature varies from 22 °C in January to 31 °C in September (COSTA, 2015). Dry seasons occur between May and September, and wet seasons between October and April, concentrating approximately 90% of annual precipitation. The soils are hydromorphic sandy soil (BORMA et al., 2009). The local topography is flat, and the predominant soil type in this region is Gleysol (FAO classification) (DA ROCHA et al., 2009).

Figure 3.1 - LBA eddy flux tower location. A) Tocantins State inside Legal Amazon delimitation (red line), B) Cantão State Park located in the transition area between the Amazon and Cerrado biomes (IBGE delimitation, green and beige), and C) LBA tower inside Cantão State Park (Sentinel-2 image, RGB composite of June 2018).



Source: Adapted from Fonseca et al. (2019).

There are four vegetation types in the Cantão State Park: (1) Semideciduous seasonal forest (known as *Cerradão*), composed of trees with an average height of approximately 20 m and sparse shrubs that cover the highest terrain portions, which floods only during years of extreme flood; (2) *Cerrado stricto sensu*, composed of trees about 5 m height, on average, and dense understory, which cover the areas of intermediate terrain portions; (3) Seasonally flooded forests, occurring in the lower parts of the relief, where the water table level is shallow, and (4) swamps (known as *Varjão*), natural meadows with a high level of nutrients deposited mainly during flooding (ROCHA et al., 2009; TOCANTINS, 2016).

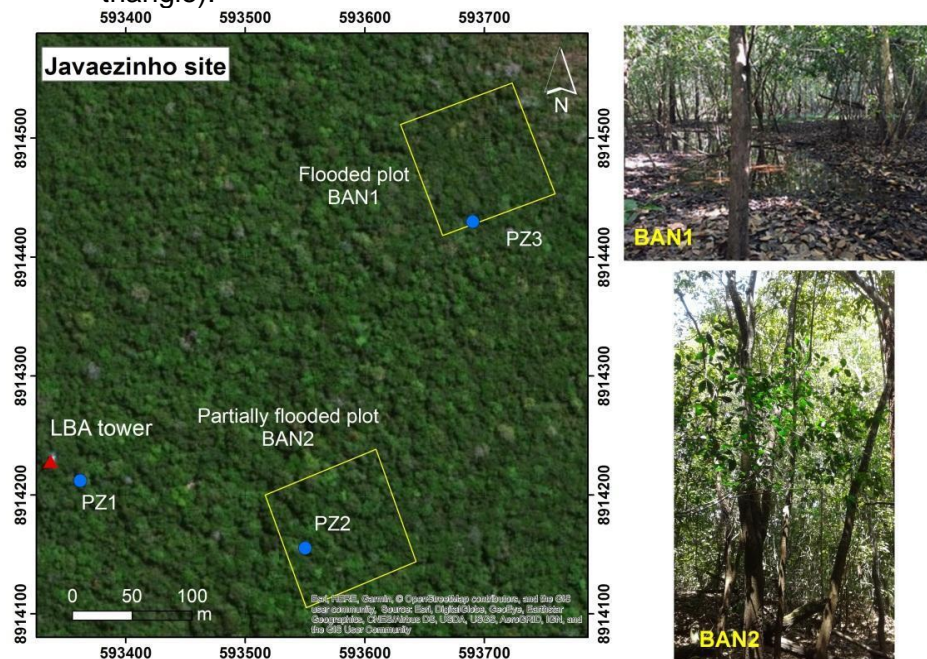
The local landscape around the BAN tower is not strictly ecotonal, but with distinct ecosystems that are associated with the water table (ROCHA et al., 2009). Thus,

the fetch area of the tower turbulent flux covers three types of physiognomy in different topographic level: (I) Cerradão and Semideciduous forests are located in the highest terrain portions (trees with an average height of approximately 18 m and sparse shrubs), (II) Cerrado ss is located in middle terrain portions and markedly to the east of the tower (dense scrub, with trees 5 m high and understory), and (III) areas of clean field and isolated lakes are located in the lower parts, where the water table is very shallow.

### **3.1.1 Experimental site**

Two plots of 1 ha each were delineated in 2013 close to the LBA tower. Plot 1 (BAN1) is located within a depression 380 m distant from the tower, being totally flooded during the flooded phase, which generally occurs from February to May. Plot 2 (BAN2) is located 180 m from the tower in a higher terrain portion, therefore 20% of its area floods annually (Figure 3.2). This site is part of collaborative research between the Foundation for Research Support of the State of São Paulo (FAPESP, grant: 2013 / 50531-2) and the LBA program managed and funded by the Ministry of Science, Technology, Innovation and Communication/ MCTIc, coordinated by the National Institute for Amazonian Research (INPA).

Figure 3.2 - Experimental plots (yellow squares; BAN1 and BAN2) and piezometers (blue dots, PZ1, PZ2, PZ3) location around the LBA flux tower (red triangle).



Source: Prepared by the author.

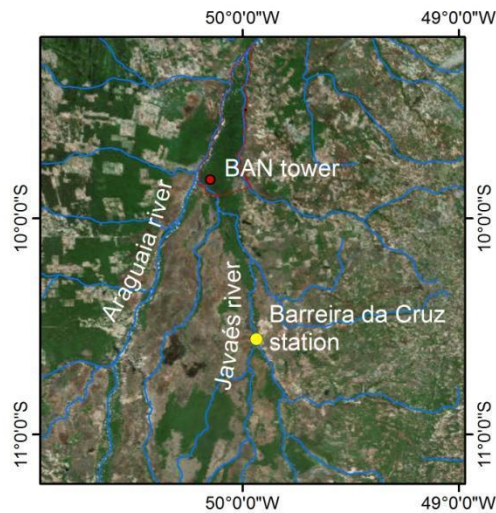
In the context of the FAPESP project described above, the study carried out by Tavares (2019) monitored the growth of 168 tree individuals distributed in the flooded (BAN1) and partially flooded (BAN2) plots using manual and automatic dendrometers, from May 2016 to October 2017. Surface water and groundwater levels were monitored through the three piezometers indicated in Figure 3.2.

Soil moisture measurements have been made using frequency domain reflectometers (FDR) near the micrometeorological tower installed at four depths 0.2, 0.4, 0.8, and 1.5 m from 2004 to 2006 and from 2006, two more sensors were added at 2.2 and 2.9 m depths. Soil moisture was estimated using a polynomial calibration of clay soils under forest area (BORMA et al., 2009; ROCHA et al., 2004).

The flood height was manually recorded by observations of hydrometric rulers at the tower every month, since January 2004. The dynamics of the flood height at the Cantão State Park are conditioned by the floods of the Araguaia, Coco and mainly the Javaés river (TOCANTINS, 2016). Therefore, the Javaés river level

record located upstream the BAN site was also analyzed from 1990 to 2017, extending the time series analysis. It was obtained at the Barreira da Cruz station from the National Water Agency (*Agência Nacional de Águas, ANA*) (ANA, 2019) (Figure 3.3).

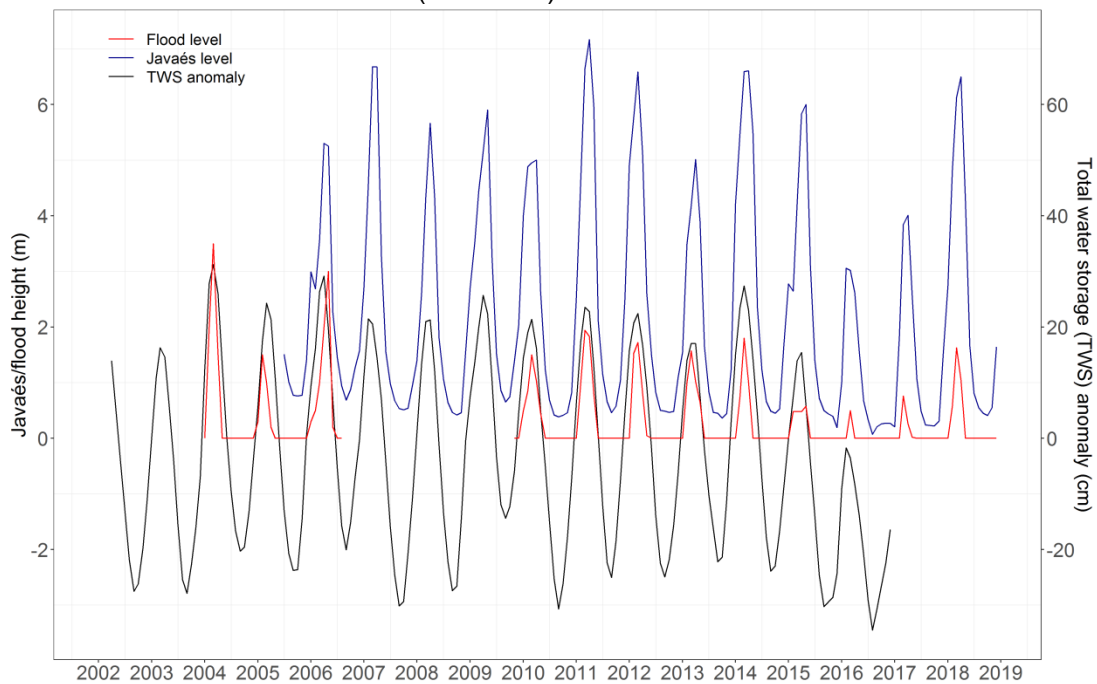
Figure 3.3 - Javaés river level station (Barreira da Cruz) location.



Source: Prepared by the author.

The total water storage product (TWS) from The Gravity Recovery and Climate Experiment (GRACE) satellite was also used to describe the flood pulse measured at the tower (Figure 3.4). The twin satellites of GRACE measured the Earth's gravity field anomalies from April 2002 to February 2017, detailing how water mass was distributed on the land surface and how it varied over time on a  $1^\circ \times 1^\circ$  grid (NASA, 2019). The google earth engine platform was used to extract these monthly changes in TWS from the point that contain the BAN tower, from March 2002 to December 2016.

Figure 3.4 - Seasonal pattern of flood height measured at the BAN Tower (red line), river level measured at ANA station (Blue line), and total water storage from satellite data (black line).



Source: Prepared by the author.

### 3.1.2 Micrometeorological tower

The site has a micrometeorological tower, which was installed in 2003 by researchers from the Biosphere and Climate laboratory of the University of São Paulo, in partnership with the team from the Federal University of Pará, Ecological Institute of the Federal University of Tocantins (UFT), and State University of Tocantins (UNITINS).

The Bananal flux tower has been recording 30 min average data of meteorological, turbulent exchange of water, carbon, and momentum at the ecosystem level from October 2003 to December 2016, however, with several periods of non-operation. More information about these instruments is described in Costa (2015) and Oliveira (2006). The variables used in this work were provided by the University of São Paulo (Table 3.1).

Table 3.1 - Equipments and measurements recorded on the flux tower.

Measurements	Equipments
<b>Surface fluxes</b>	
Eddy covariance: Turbulent latent heat fluxes ( $W m^{-2}$ ), sensible heat ( $W m^{-2}$ ) and CO <sub>2</sub> ( $\mu mol m^{-2} s^{-1}$ ) / 10Hz / 30 minutes	1 Campbell-SAT3 sonic anemometer; 1 Infrared gas analyzer Li-7500 Licor.
<b>Radiation fluxes</b>	
Incident and reflected global solar radiation ( $Wm^{-2}$ ) / 1 minute / 30 minutes	2 Piranometros Kipp-Zonen SP Lite.
Net radiation ( $Wm^{-2}$ ) / 1 minute/ 30 minutes	1 Balance radiometer Kipp-Zonen NR Lite.
<b>Climatologically variables</b>	
Temperature ( $^{\circ}C$ ) and relative humidity (g Kg <sup>-1</sup> ) / 30 minutes	1 termo-higrometer VAISALA HMP45C.
Precipitation (mm) / 1 minute/ 30 minutes	1 Hydrological Rain Gauge Services TB3.
Direction ( $^{\circ}$ ) and wind speed ( $ms^{-1}$ ) / 1 minute/30	1 Anemometer Met One 034B.
<b>Soil and hydrological variables</b>	
Soil heat flow ( $Wm^{-2}$ ) / 1 minute/ 30 minutes	5 Flowmeters REBS HFT3.
Water table (m)	5 piezometers
Volumetric soil moisture ( $m^3 m^{-3}$ )	5 FDR (Frequency Domain Reflectometry).

Source: Adapted from Costa (2015).

### 3.1.2.1 Net ecosystem exchange

The eddy covariance method was used to calculate the CO<sub>2</sub> turbulent flux between vertical wind velocity fluctuations ( $w'$ ) and the concentration of the scalar ( $c'$ , CO<sub>2</sub>), representing the first term of the equation 3.1, which is used to estimate the net ecosystem exchange (NEE). NEE describes the exchange between the surface and the atmosphere across all possible boundaries, vertical and/or horizontal (BALDOCCHI, 2003). The second term of the equation is the rate of change in the canopy storage, where  $z$  is the height above the ground surface,  $h$  is the flux measurement height,  $t$  is time, and the overbar denotes a time average.

$$NEE = \overline{w'c'} + \frac{\partial}{\partial t} \int_0^h \overline{c(z)} dz \quad (3.1)$$

NEE measurements were performed from 2011 to 2013 because of the vertical CO<sub>2</sub> profile data availability (COSTA, 2015). The description of the methods used in eddy covariance technique and the CO<sub>2</sub> ecosystem exchange are described below and more details are presented in RESTREPO-COUCPE et al. (2013) and COSTA (2015).

### 3.1.2.2 Gap filling of CO<sub>2</sub> estimates

In order to complete a continuous series of the NEE, gap filling on night and daily CO<sub>2</sub> estimates according to the method described in Restrepo-Coupe et al. (2013) were performed. There was an underestimation of night positive CO<sub>2</sub> fluxes due to insufficient turbulent mixing. We filled each missing nighttime value from an average of all valid nighttime values (from 6 pm to 5 am) within a 5-day window. The data was replaced by the average of this 5-day window, and when this was not possible, we applied windows varying 11–31 days. The correction performed in this study involved 35% of the total night data for a friction velocity ( $u^*$ ) threshold of 0.19 m s<sup>-1</sup> for the rainy season and 0.17 m s<sup>-1</sup> for the dry season. These data can be considered below the thresholds and percentage of gaps found in the literature for other sites in the Amazon region (RESTREPO-COUCPE ET AL., 2013).



The relationship between photosynthetically active radiation (PAR) and the observed data of NEE was used for filling daytime NEE (HUTYRA et al., 2007; CABRAL et al., 2011). The hyperbolic relationship pattern between these variables included coefficients which represented the maximum photosynthetic efficiency of the canopy (a2), its yield (a3) and the mean ecosystem nocturnal respiration (a1) (HUTYRA et al., 2007).

$$NEE = a1 + \frac{a2 * PAR}{a3 + PAR} \quad (3.2)$$

NEE values for PAR < 40  $\mu\text{mol CO}_2 \text{ m}^{-2} \text{ s}^{-1}$  were excluded from this analysis since this condition is generally associated with invalid turbulence and abrupt changes in light levels (HUTYRA et al., 2007). Further details are described in RESTREPO-COUCPE et al. 2013.

Measurements of NEE were separated into the component fluxes of ecosystem respiration (R) and gross primary production (GPP) (HUTYRA et al., 2007). R was estimated using the nighttime NEE and GPP was calculated from the equation, assuming NEE as a proxy for daytime turbulent flux.

$$NEE = R - GPP \quad (3.3)$$

### 3.1.2.3 Energy balance

The closure of energy balance is usually used for a quality check of measured fluxes, by comparing the sum of estimated atmospheric turbulent fluxes with the available energy as:

$$(\lambda E + H) \approx (R_n - G - S) \quad (3.4)$$

where  $R_n$  is the net radiation,  $G$  is the soil heat flux,  $S$  is the rate of change of heat storage in biomass and environment.

The energy balance of this site varied between 73% to 76%, which represents a low value compared to global means as reported in COSTA (2015). Apart from equipment failure, the possible explanation for this inconsistency is that during

the flood there is a mismatch of the footprints of the net radiation sensors and the measured turbulent fluxes. The fetch of the net radiation sensors is smaller and close to the tower (over a closed tall savanna) and the fetch of the turbulent fluxes is extensive and composed of large flooded areas (BORMA et al., 2009; COSTA, 2015). Considering this study aims to analyze the seasonal variation of evapotranspiration (calculated from the latent heat flux), this underestimation is not an issue. Nonetheless, these values are similar to other Amazonian *terra firme* sites, such as the studies conducted by ANDRADE et al. (2009), (70% a 85%); VON RANDOW et al. (2004), (74%), and OLIVEIRA (2006), (78%).

### 3.1.2.4 Evapotranspiration

In order to calculate the evapotranspiration (ET), a filter to eliminate noise data and other interferences from 30-min dataset of latent heat (LE) was applied by using a criterion of  $X(t) < (X_m - 4\sigma)$  or  $X(t) > (X_m + 4\sigma)$ , where  $X(t)$  denotes the variable (i.e., LE),  $X_m$  is the mean over the month interval and  $\sigma$  the standard deviation (BI et al., 2007; DIAZ; ROBERTI, 2015). After this procedure, ET was calculated from LE and air temperature ( $T_{ar}$ ) as a function of latent heat of water vaporization in a 30 minutes time step (Equation 3.5).

$$ET = LE / \lambda \quad (3.5)$$

where  $\lambda$  ( $J\ kg^{-1}$ ) =  $10^3 * (2,500 - 2.37 * T_a)$

Specific humidity and Vapour Pressure Deficit were calculated in a 30 min time step through Bolton (1980) equations using a script available freely for the R language (LEBAUER, 2018). Firstly, specific humidity ( $q$ ; equation 3.6) was calculated from the partial pressure of water vapor ( $e$ ; equation 3.7) and the atmospheric pressure ( $press$ ), where  $\epsilon$  (0.622) is a constant that expresses the ratio between the water and the dry air molecular weight. Vapour pressure deficit (VPD; equation 3.8) was calculated as a function of the saturated vapour pressure ( $e_s$ ; equation 3.9) and the relative humidity measured at the tower (RH).

Where  $q$  is the specific humidity ( $g/Kg$ ),  $press$  is the atmosphere pressure (mb) and  $tar$  is the air temperature ( $^{\circ}C$ ).

$$q = \epsilon e / \text{press} - e (1 - \epsilon) \quad (3.6)$$

$$e = q * \text{press} / (0.378 * q + 0.622) \quad (3.7)$$

$$e_s = 6.1078 e(2500000/461) * (1/273 - 1/(273 + t_a)) \quad (3.8)$$

$$\text{VPD} = (100 - \text{RH})/100 * e_s \quad (3.9)$$

## 4 PHENOLOGY AND SEASONAL ECOSYSTEM PRODUCTIVITY IN AN AMAZONIAN FLOODPLAIN FOREST<sup>1</sup>

### 4.1 Introduction

Tropical forests are known for their high productivity, accounting for 33% of terrestrial net primary production, which regulates carbon-climate feedbacks (BONAN, 2008). In this context, the Amazon forest represents a sink of 0.42 to 0.65 Pg C per year of total carbon assimilated, making it a significant carbon sink of tropical forests in the planet (PAN et al., 2011). However, extreme droughts have demonstrated the sensitivity of this ecosystem to environmental changes. Previous studies have reported aboveground biomass loss, increased tree mortality (PHILLIPS et al., 2009; ESPÍRITO-SANTO et al., 2014) and a long-term decreasing trend of carbon accumulation (BRIENEN et al., 2015), which could lead to the possible shift of forest functioning from a sink to a source of CO<sub>2</sub> during long-term droughts (GATTI et al., 2014; FELDPAUSCH et al., 2016).

Although detailed knowledge about the tropical forest carbon cycle is still lacking, previous studies have sought to understand the mechanisms of seasonal photosynthesis control, such as water and light availability (RESTREPO-COUBE et al., 2013b; WAGNER et al., 2017) and phenological cycles (HAVE et al., 2010; WU et al., 2016, 2018). To understand these seasonal patterns on a larger scale, several studies have correlated seasonal environmental drivers with remote sensing-based multispectral vegetation indices in the Amazon basin. Some of them have suggested the Amazon rainforest is resilient to seasonal droughts (HUETE et al., 2006) and extreme droughts (SALESKA et al., 2007). Other studies, however, reported that an apparent greening of the forest canopy could be attributed to abnormal leaf flushing or as an effect of sun position in relation to the sensor, increasing near infrared reflectance, and thus not reflecting

---

<sup>1</sup> This Chapter is an adapted version of the paper: Fonseca, L. D. M.; DALAGNOL, R.; MALHI, Y.; RIFAI, S.; COSTA, G. B.; SILVA, T. S. F.; DA ROCHA., H. R.; TAVARES, I. B.; BORMA, L. S. Phenology and seasonal ecosystem productivity in an Amazonian floodplain forest. **Remote Sensing**, v11, 1530, 2019.

a true resilience from the forest (ANDERSON et al., 2010; BRANDO et al., 2010; GALVÃO et al., 2011; XU et al., 2011; SOUDANI; FRANÇOIS, 2014; MORTON et al., 2016). Part of these uncertainties has been attributed to the high atmospheric contamination of the MODIS (Moderate Resolution Imaging Spectroradiometer) sensor surface reflectance data, the most commonly used sensor for phenological studies in the tropics (SAMANTA; GANGULY; MYNENI, 2011; HILKER et al., 2014).

Given the reported uncertainties related to sun-sensor geometry effects and atmospheric contamination, progress has been made towards the development of more robust atmospheric correction methods and data normalization procedures for MODIS data, such as the multi-angle implementation correction (MAIAC) algorithm (LYAPUSTIN et al., 2012) implementation of the bidirectional reflectance distribution function (BRDF). Enhanced vegetation index (EVI) values extracted from this improved MODIS product (MODIS-MAIAC) have shown a correlation between phenology and productivity of the Amazon forest occurring during the dry season, synchronized with mature leaf area index (MOURA et al., 2015; LOPES et al., 2016a; MAEDA et al., 2016; WU et al., 2016).

Apart from these advances, a remaining limitation is that the majority of studied forest plots in the Amazon are located in *terra firme* (upland) forests, even though c.a. 14% of the basin is covered by flooded forests (HESS et al., 2003), which remain understudied. These ecosystems are subjected to seasonal, long-lasting and monomodal flood pulses (JUNK et al., 2011), with studies reporting adaptation mechanisms developed by species in these environments in response to the excess or lack of water. During the flooded period, some species can increase root porosity, release biological volatile organic compounds into the atmosphere, enrich the rhizosphere with oxygen, reduce photosynthesis and exhibit anaerobic metabolism (DE SIMONE; JUNK; SCHMIDT, 2003; PAROLIN et al., 2004). During the dry season, decreases in leaf water potential, foliar surface, and xylem flow have been observed, which reduce water loss through transpiration (PAROLIN et al., 2010).

Floodplain areas are widely recognized for the ecosystem services they provide, playing an important role in water and climate regulation services (FINLAYSON et al., 2005; JUNK et al., 2011). Different studies have pointed to a higher resilience of Amazonian floodplain forests to seasonal droughts (SCHONGART et al., 2002, 2004; PAROLIN et al., 2004), as during the terrestrial phase, these forests had higher rates of stem growth (SCHONGART et al., 2002) and greater rates of CO<sub>2</sub> assimilation as a result of new leaves and soil aeration (TERESA FERNANDEZ PIEDADE; JUNK; PAROLIN, 2000; PAROLIN et al., 2010). Conversely, a period of dormancy has been suggested to be a survival strategy during the aquatic phase (SCHONGART et al., 2002).

According to the most recent IPCC report, floodplain forests are one of the most threatened ecosystems because of the undergoing "savannization" feedback to extreme drought events (NOBRE et al., 2016). In this scenario, the carbon and methane sink services they provide could be compromised (DALMAGRO et al., 2019). Furthermore, recent reports have demonstrated considerable tree mortality on central Amazonian floodplains due to changes in flooding quota by upstream dam construction (RESENDE et al., 2019). Although induced by indirect changes to the flood pulse, direct effects of extreme droughts also revealed the sensibility of this ecosystem. The droughts of 1997 and 2005 have also shown that fires have a stronger and longer-lasting impact on floodplain forest structure than in upland forests; moreover, these floodable areas are located at the core of the Amazon forest, threatening the resilience of the entire system (SCHEFFER et al., 2017).

Most Amazonian floodplain studies have been located in the central Amazon basin, surrounding the Solimões and Amazonas rivers. Nonetheless, a different pattern of climate change is expected to occur at the southern portions of the basin, with an increase in temperature and decrease of precipitation during wet seasons (MALHI; WRIGHT, 2004). In the southeast region, bordering the Amazon basin, there is an LBA (large-scale biosphere-atmosphere) eddy flux tower site (Bananal site) located on a seasonal floodplain forest, at the transition between the Amazon and Cerrado biomes. Previous studies have suggested that this

forest shows two periods of water stress—one due to excess of water in the peak of the rainy season—and another due to water deficit, at the end of the dry season (BORMA et al., 2009; COSTA, 2015; HOMEIER; KURZATKOWSKI; LEUSCHNER, 2017). During the El Niño drought of 2005, decreased rates of evapotranspiration (BORMA et al., 2009) and increasing rates of tree mortality were reported in this region (HOMEIER; KURZATKOWSKI; LEUSCHNER, 2017).

Given the uncertainties of floodplain environmental response to seasonal cycles of flood and dry periods, this study aims to evaluate the seasonal productivity of this floodplain forest located in the Amazon-Cerrado transition, as well as its environmental controls, based on field observations and on enhanced vegetation index (EVI) derived from MODIS (MAIAC) surface reflectance data. The following questions were assigned: (i) How does the Bananal seasonally flooded tropical forest respond to flood and drought cycles in terms of evaporative fluxes and gross primary productivity (GPP)? (ii) Do phenological patterns observed from field data agree with landscape-level remote observations (EVI from MODIS/MAIAC)? (iii) Does flooding affect the EVI signal of these forests?

## **4.2 Materials and methods**

### **4.2.1 Flux tower and field data**

Data from the flux tower used in this study include the following variables: GPP ( $\mu\text{mol CO}_2 \text{ m}^{-2} \text{ s}^{-1}$ ), air temperature ( $T_a$ , °C), rainfall (mm), net radiation ( $R_n$ , in  $\text{W m}^{-2}$ ), latent heat (LE, in  $\text{W m}^{-2}$ ), specific humidity ( $q$ ,  $\text{g Kg}^{-1}$ ), pressure (press, kPa), evapotranspiration (ET) and vapour pressure deficit (VPD, kPa). A detailed description of the methods used in eddy covariance technique the  $\text{CO}_2$  ecosystem exchange at this site are described in the section 3.2.1.1 and is reported in Restrepo-Coupe et al. (2013) and Costa (2015).

Soil moisture at six depths 0.2, 0.4, 0.8, 1.5, 2.0 and 2.9 m and the Javaes river level record was used to analyze the seasonal water availability.

#### 4.2.2 Litterfall collection

Litter was collected in traps installed along a transect of 200 × 800 m near the flux tower, spaced 25 m from each other. From April 2004 to May 2005, litterfall was collected every month from 30 litter traps, with 1 m<sup>2</sup> size. Litter was sorted into leaf material, reproductive material (flowers and fruits), woody material (twigs), and non-identifiable plant material. Following separation, the material was then dried to a constant mass in an oven and weighed to calculate biomass (MOREIRA et al., 2005).

#### 4.2.3 Remote-sensing data and products

The MODIS-MAIAC product EVI was acquired to access the forest phenology for the study area from the period of 2004 to 2017 (DALAGNOL et al., 2019). In this product, before EVI calculation, the surface reflectance data were normalized to nadir target and 45-degree solar zenith angle through the Bidirectional Reflectance Distribution function, at a spatial resolution of 1 km and aggregated to biweekly (16-day) composites using the median values. The EVI was calculated using equation 4.1 (HUETE et al., 2002). Further information on image processing and correction are described in Dalagnol et al. 2018. The composites were retrieved considering only cloud-free and low atmospheric turbidity according to MAIAC quality flags. For the MODIS-MAIAC pixel containing the flux tower, the mean number of samples per 16-day composite was 4.6 samples for the flooding period (February–May) and 12 samples for the non-flooding period. MODIS pixel values were extracted using raster and rgdal R packages.

$$EVI = 2.5 * \frac{\rho NIR - \rho Red}{\rho NIR + (6 * \rho Red - 7.5 * \rho Blue) + 1} \quad (4.1)$$

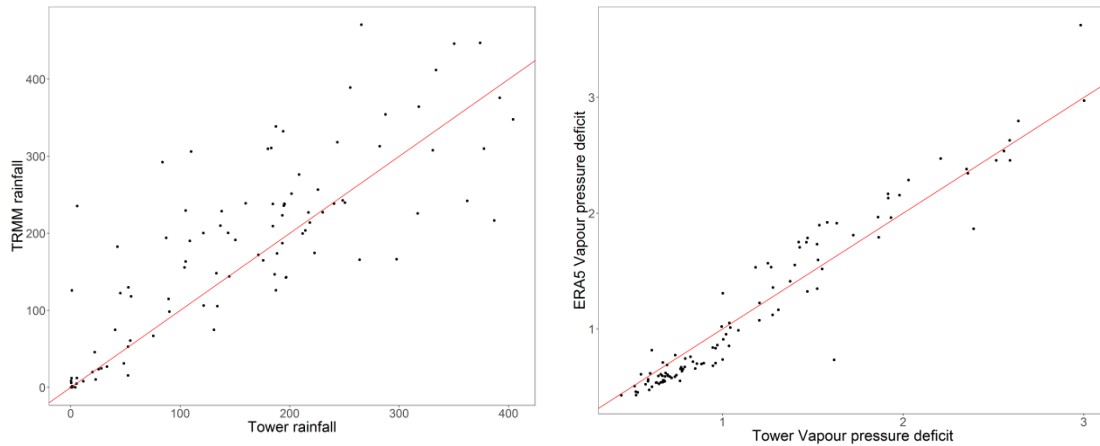
Where  $\rho NIR$  is infrared reflectance,  $\rho Red$  is red reflectance, and  $\rho Blue$  is blue reflectance. The constants (6, 7.5, 1, and 2.5) in the divisor represent the aerosol coefficient adjustment of the atmosphere for the red and blue band, the adjustment factor for the soil and the gain factor, respectively (HUETE et al., 2002).



However, there is a high density of water channels in the study area, therefore MODIS pixels composed of more than 10% of permanent water were excluded from the analysis, using the Global Forest Change product v1.4 mask (HANSEN et al., 2013). This procedure also eliminated areas that were disturbed from 2000 to 2016. The mask was resampled from 30 m to 1 km according to MODIS pixels resolution. Only pixels around the tower footprint (2 km) meeting these criteria were selected for analysis. To further check the presence of water channels in these pixels, we used the high resolution Bing Virtual Earth image on QGIS 2.18 to visual interpret and manually delineate permanent water bodies, and we found more than 94% of forest cover (Figure A1 and Table A1).

To explore rainfall variability over the time series, rainfall data were obtained from TRMM. The field measured rainfall data was not used directly due to gaps on records from 2014 to 2016 ( $r^2 = 0.62$ ,  $p < 0.001$ ) (Figure 4.1a). Air temperature and vapour pressure deficit data were also used from the ERA5 climate reanalysis (DEE et al., 2011) to build an inter-annual analysis, due to gaps in tower for these variables from 2010 to 2016 ( $r^2 = 0.83$ ,  $p < 0.001$ ) (Figure 4.1b).

Figure 4.1 - Monthly scatterplot of rainfall data from TRMM against flux tower data (a) and a monthly scatterplot of VPD from ERA5 against tower data (b). The fitted regression line (red).



Source: Prepared by the author.

The cumulative water deficit (CWD) was calculated to investigate negative monthly precipitation anomalies (ARAGÃO et al., 2007). Monthly average ET from the tower was calculated based on records with a good density of observations from 2004 to 2014, since there were gaps in measurements from 2010 to 2016. The CWD increases in magnitude when rainfall is lower than ET. The following rule was applied to the rainfall data (R) for each month (m) with evapotranspiration (E) being the mean from the period of tower measurements (120 mm).

$$CWD_m = CWD_{m-1} + R_m - E_m \quad (4.2)$$

$$\text{If } CWD_m > 0 \text{ then } CWD_m = 0$$

It was also performed a canopy gap analysis for the studied forest using airborne LiDAR data to assert the degree of expected interference of free standing water under the canopy during the flooded period on MODIS EVI values. The data was collected on 20 February 2016 along a 15 km transect with 500 m width, using a Riegl LMS-Q680i laser scanner at 500 m average flight altitude, 45° FFLMS of view, and 300 kHz scanning frequency. The data had a high pulse density of greater than 5 points per m<sup>2</sup>. Using the point cloud, we derived a canopy height model (CHM) utilizing the highest height of return within 1 x 1 m cells using

standard procedures, as described in (HUNTER et al., 2015). We detected canopy gaps following the procedures described in Hunter et al. 2015 and considering the traditional Brokaw's gap definition of a hole in the forest that extends to at least 2 meters above the ground. Lidar data from this study was obtained by the EBA project (Amazon biomass estimate, EBA). Regarding the canopy structure, as this transect is located 7 km away from the LBA tower, we compared tree heights of 170 individuals distributed in two experimental plots located 380 (BAN1) and 180 meters (BAN2) from the tower (Tavares, 2019) with LiDAR measurements. A forest inventory was performed in 2015 in these plots and tree heights were measured with a telescope pole of 15 m length.

#### **4.2.4 Statistical analysis**

The seasonal cycle of climatic drivers (rainfall, soil moisture, flood amplitude, evapotranspiration, net radiation, deficit vapour pressure, cumulative water deficit and air temperature) and phenology from EVI were based on monthly mean measurements from 2004 to 2016, while the GPP monthly average was based on measurements from 2011 to 2013 due to data availability (Figure A2). The analyzed EVI was based on the mean value of the seven pixels around the tower, considering the limits of the flux tower footprint and filtering of forest cover areas (>90%).

Since there are many parameters measured from different sources, data acquisition, availability and usage are summarized on Table 4.1.

Table 4.1 - Availability and usage description of tower, satellite and field data.

Parameter	Acquisitions	Start Year	End Year	Usage
LE	Tower	2004	2014	ET computation
PAR	Tower	2011	2013	NEE computation
Press	Tower	2004	2014	Relative humidity (RH) computation
q	Tower	2004	2016	RH and VPD computation
Rn	Tower	2004	2014	Correlation variable
GPP	Tower	2011	2013	Productivity estimate / Correlation variable
ET	Tower	2004	2014	Correlation variable
VPD	Tower/Satellite	2004	2016	Correlation variable
Ta	Tower/Satellite	2004	2016	VPD and ET computation / Correlation variable
Rainfall/TRMM	Tower/Satellite	2004	2014	Correlation variable
CWD	Tower/Satellite	2004	2016	Correlation variable
EVI	Satellite	2004	2016	Phenology and productivity proxy / Correlation variable
Soil moisture	Field	2014	2016	Correlation variable
Litterfall	Field	2004	2005	Phenology proxy / Correlation variable
Flood height	Tower	2004	2016	Define seasonal flooding

Seasonal analyses were divided into two distinct periods: Flooded (Feb to May) and non-flooded (Jun to Jan). The phenology pattern described by EVI was also analyzed with ground data (litterfall) from 2004 to 2005 (MOREIRA et al., 2005). In order to evaluate anomalies in relationships from year to year between monthly EVI and the climatological variables, an inter-annual analysis was also performed.

Correlation tests were performed using daily data from 2011 to 2013 (GPP data availability) to measure the degree of association between GPP and the climatic variables estimated for the significant models ( $p$ -value  $\leq 0.05$ ). Shapiro–Wilk test was used to analyze the normality of the distributions of all variables described in Table 4.1. The Pearson correlation test ( $r$ ) was performed between GPP, monthly EVI, and leaf litter mass (normally distributed variables). Other variables (rainfall, net radiation, evapotranspiration, soil moisture, CWD, temperature and vapour pressure deficit) were not normally distributed, thus we used the non-parametric Spearman's correlation ( $\rho$ ) to measure the degree of association between them with daily and monthly GPP.

### **4.3 Results**

#### **4.3.1 Seasonal meteorological, Gross Primary Productivity (GPP) and Enhanced Vegetation Index (EVI) patterns**

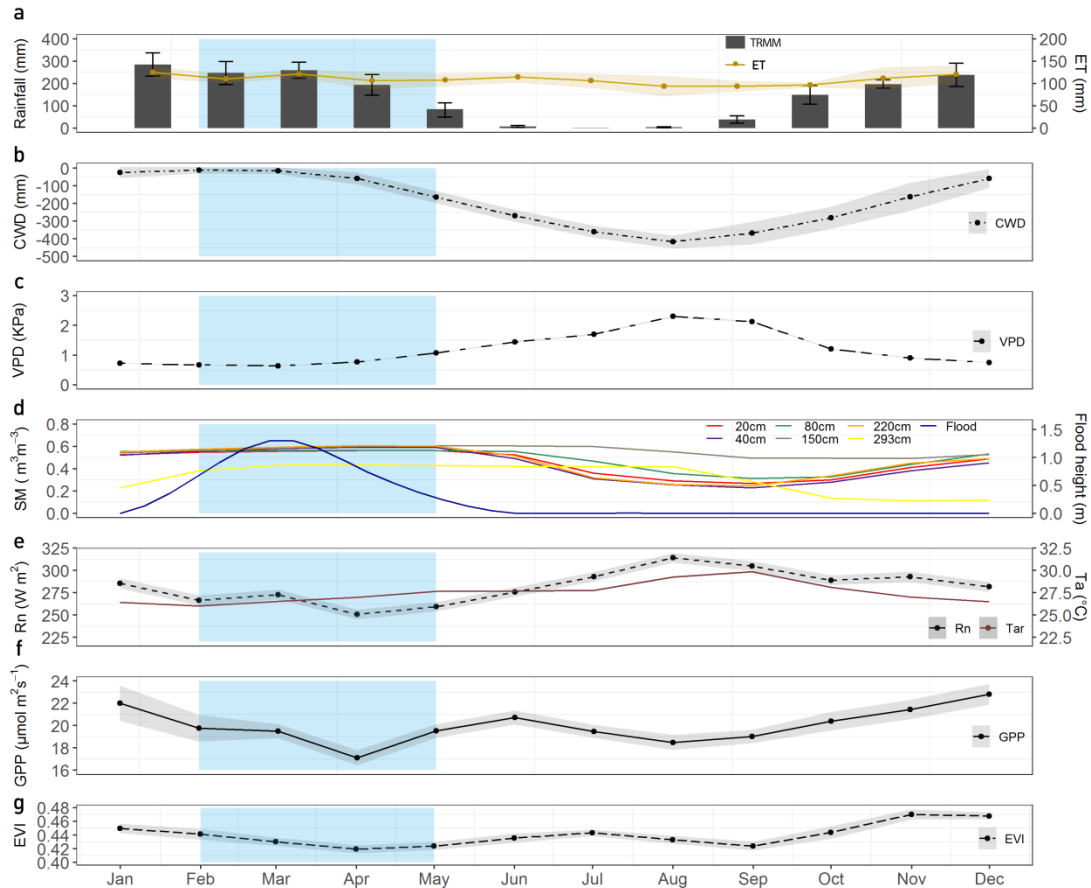
The seasonal variation of GPP and its interaction with environmental drivers (rainfall, evapotranspiration, cumulative water deficit, vapour pressure deficit, soil moisture, net radiation and temperature) and phenology (described through EVI), showed different patterns among periods of the year. An extended dry season was observed from May to September, when rainfall was below  $100 \text{ mm}\cdot\text{month}^{-1}$ , while ET remained high through all seasons (mean of  $110 \text{ mm}\cdot\text{month}^{-1}$ ), especially during the flooding (Figure 4.2a). This high ET values indicated that soil moisture was sufficient to attend the atmospheric demands, which were described by the increased VPD (Figure 4.2c) and decreased CWD from April to August (Figure 4.2b).

Although ET at this site exhibited a flat pattern, slight maximum values coincided with maximum GPP (Figure 4.2f), but the first and more pronounced peak occurred in March (123 mm), mid-flooding, in response to an increase of Rn at this month (Figure 4.2e). The second peak occurred in June/July (116 mm), mid-dry season, and a third in December, mid rainy season (122 mm), before the period of flooding.

Net radiation did not seem to be the main productivity driver on this site, since during the months of highest GPP values (June and December), Rn varied between 276 and 282 W.m<sup>2</sup>, respectively, and not close to the maximum value of 314 w.m<sup>2</sup> in August (Figure 4.2e).

Soil moisture seems to be the main productivity driver at this forest (Figure 4.2d). Soil water content remained relatively constant from March to June, especially for layers at 20 cm, 40 cm, 80 cm, and 200 cm depth, indicating that the soil was 100% saturated. Layers at both 150 cm and 293 cm depth remained saturated for a longer time, extending until July and August, respectively. During the months of maximum GPP (June and December), the mean soil moisture of layers at 20 cm, 40 cm, 80 cm, and 200 cm were 0.541 and 0.501 m<sup>3</sup> m<sup>-3</sup>. Conversely, in April and August (months of minimum GPP), the average volumetric soil moisture content was 0.585 and 0.344 m<sup>3</sup> m<sup>-3</sup>, respectively. Thus, both flooding and dry soil limited productivity at the BAN site.

Figure 4.2 - Average annual cycle of ET (2004 to 2014; black line) and rainfall from TRMM (2004 to 2016; dark grey bar) (a), cumulative water deficit (2004 to 2016; CWD) (b), vapour pressure deficit (2004 to 2014; VPD) (c), soil moisture (2004 to 2016; SM) and flood height (2004 to 2016; dark blue line) (d), net radiation (2004 to 2016; dashed black line) and air temperature (2004 to 2014; brown solid line) (e), GPP (2011 to 2013; black solid line) (f), and EVI (2004 to 2016; long dashed black line) (g). The shaded blue area corresponds to the flooded period. The standard deviation of the monthly variables is indicated by either shading or error bars.



Source: Adapted from Fonseca et al (2019).

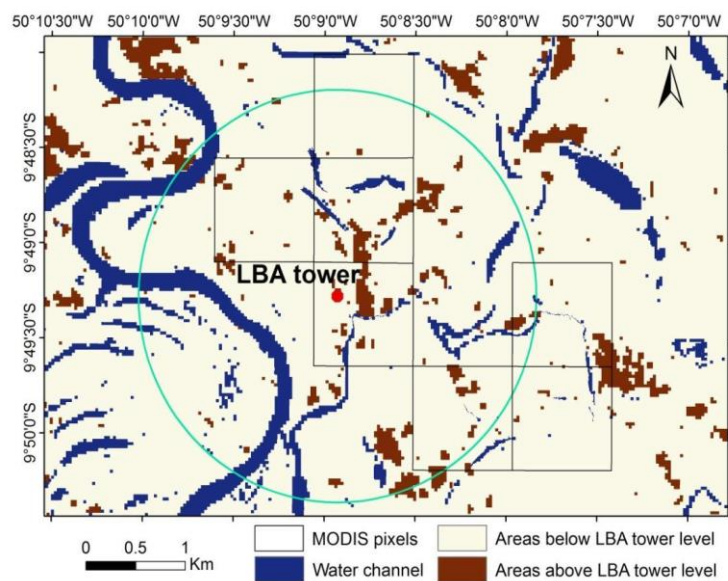
EVI values (Figure 4.2g) indicated a bimodal pattern of foliar production, with a peak in July (mid-dry season) and a more pronounced peak in December (mid-rainy season prior to flooding). These EVI peaks were in phase with GPP, which decreased at the peak of flooding (April) and at the peak of the dry season (September).

GPP remained high during the flooded period (Figure 4.2f) due to the shorter duration of soil saturation in higher terrain portions concentrated near the flux

tower (Figure 4.3). Therefore, the mean flood amplitude of 1.3 m (Figure 4.2d) could take longer to saturate the soil at the beginning of the flooded period. Similarly, these terrain portions would be aerated first at the end of flooding, enabling photosynthesis to recover after the anoxic conditions that occur during the flooded period, explaining the GPP increase in May, before the end of the flooded period (Figure 4.2f). Despite the SRTM data is representing the canopy height difference (digital elevation model), these assumptions are in agreement with local topography measurements, which exhibited high terrain portions close to the tower, and a height difference of 1.1 meters inside the plot (BAN1) (TAVARES, 2019).

However, the majority of the terrain around the tower footprint (89%) is at the same level or below the base tower level. This might be the reason why the landscape remained under anoxic conditions for a longer time, which was reflected on canopy response, suggesting a one-month lag between EVI and GPP during non-flooded months, from May to September (Figure 4.2f,g).

Figure 4.3 - Shuttle Radar Topographic Mission (SRTM) classified as areas below and above the tower level, which is located at 181 meters of altitude according to SRTM (red dot). Grey squares represent the Moderate Resolution Imaging Spectroradiometer (MODIS) pixels within the tower footprint (green circle, Borma et al. (2009)) selected to extract mean EVI and be analyzed.



Source: Adapted from Fonseca et al (2019).



### 4.3.2 Correlation between GPP, climatic variables and EVI

The relationship between GPP and Rn was positive during the flooded period ( $\rho = 0.2$ ,  $p < 0.05$ ) and negative but not significant during non-flooded months ( $\rho = -0.19$ ,  $p = 0.12$ ) (Figure 8a). GPP was positively associated with ET during both flooded ( $\rho = 0.25$ ,  $p < 0.05$ ) and non-flooded months ( $\rho = 0.38$ ,  $p < 0.05$ ) (Figure 4.4b).

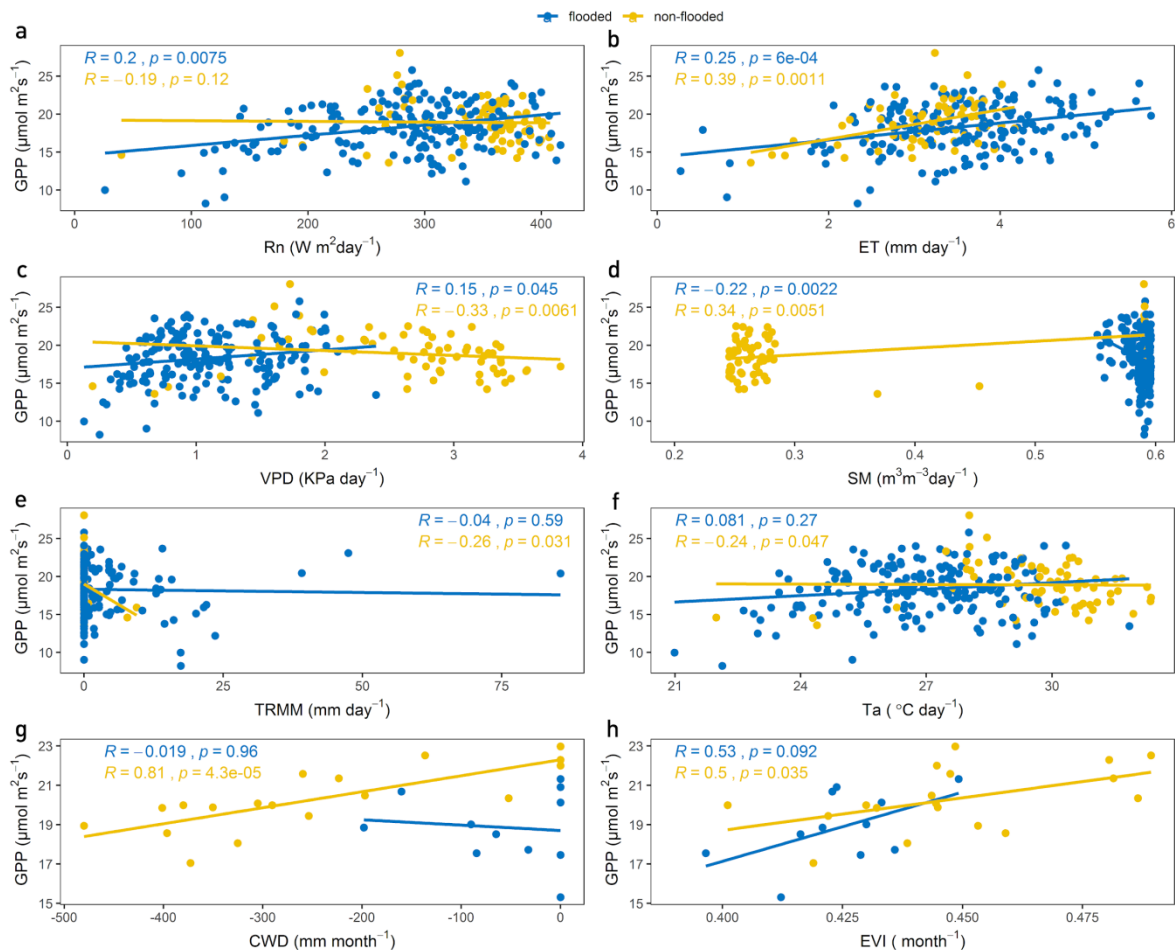
The analyses show that soil moisture and VPD are correlated with GPP in two contrasting ways. During the flooded period, soil moisture is negatively associated with GPP ( $\rho = -0.22$ ), while VPD is positively associated ( $\rho = 0.15$ ). However, during the non-flooded months, soil moisture is positively associated with GPP ( $\rho = 0.34$ ) and VPD negatively ( $\rho = -0.33$ ) (Figure 4.4c and 4.4d).

As GPP is in phase with soil moisture when the forest is not flooded, it decreases at the end of the dry season (September) and starts to increase in the onset of the rainy season (October). Nevertheless, a negative trend was observed between GPP and rainfall during non-flooded months ( $\rho = -0.26$ ,  $p < 0.05$ ) (Figure 4.1e). Air temperature was negatively associated with GPP during non-flooded months ( $\rho = -0.24$ ,  $p < 0.05$ ) and was not significant during the flooded months ( $\rho = 0.081$ ,  $p = 0.27$ ) (Figure 8f).

Monthly CWD had the strongest positive association with GPP during non-flooded months ( $\rho = 0.81$ ,  $p < 0.05$ ), to the extent that GPP increases when CWD gets less negative. No trend was observed during flooded months ( $\rho = 0.01$ ,  $p = 0.96$ ) (Figure 4.4g).

As a proxy of photosynthetic capacity, EVI was positively correlated with GPP during non-flooded months ( $r = 0.50$ ,  $p < 0.05$ ) and despite not being significant, a positive trend was also observed during flooded months ( $r = 0.53$ ,  $p = 0.09$ ) (Figure 4.4h).

Figure 4.4 - Scatterplots between the daily mean of eddy covariance GPP compared to climate drivers from 2011 to 2013: Net radiation (a), ET (b), VPD (c), Average soil moisture for layers up to 200 cm depth (d), Rainfall (e), Ta (f) and the monthly average of GPP compared to CWD (g) and EVI (h). Both lines represent the regression fit between variables during flooded (blue) and non-flooded (yellow) months.

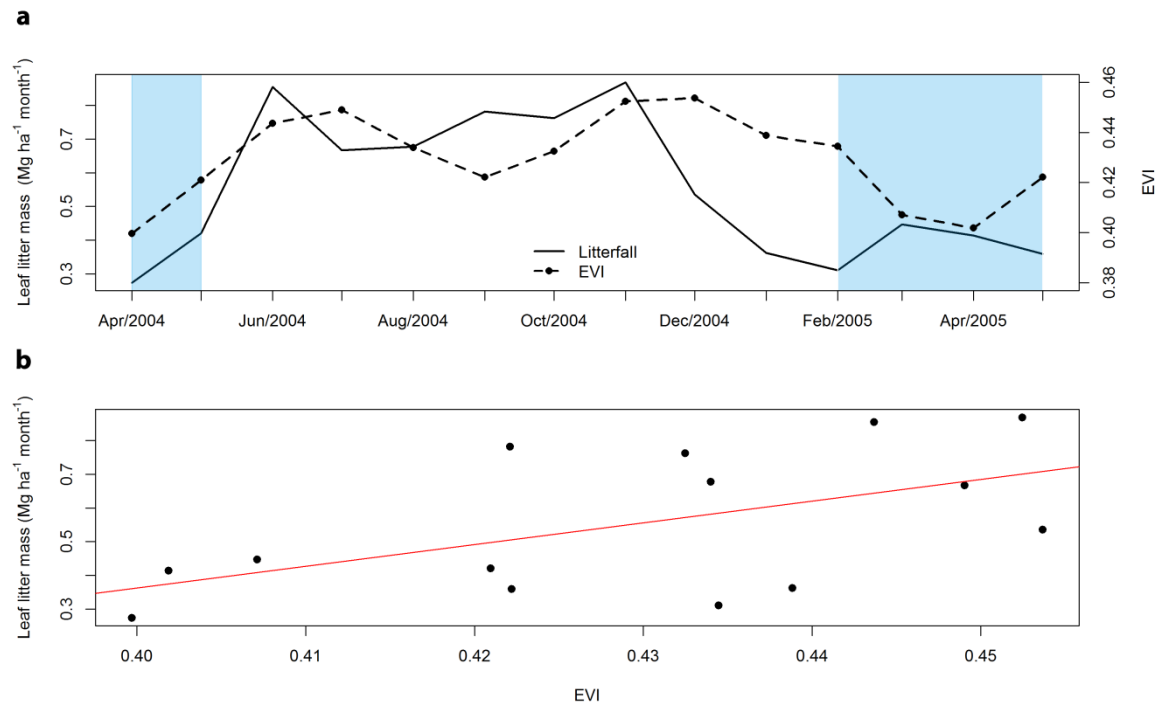


Source: Adapted from Fonseca et al (2019).

### 4.3.3 Seasonal phenology patterns and analysis of forest canopy gaps

Annual EVI was positively correlated to leaf litter mass ( $r = 0.55$ ;  $p < 0.05$ ). One month lag was observed between peaks in leaf litter mass (June and November) and EVI (July and December) (Figure 4.5). These observations suggest the months with greater leaf renewal would be June and November, which correspond to high peaks of seasonal GPP.

Figure 4.5 - Monthly average leaf litter mass rate (solid black line) collected at the surrounding area of the tower from April 2004 to May 2005 (Moreira et al., 2005), and monthly average EVI-multi-angle implementation correction (MAIAC) (black dashed line) for the same period. The flooded period is represented by the blue shading area (a). Scatterplot between EVI and leaf litter mass with the fitted regression line (red) (b).



Source: Adapted from Fonseca et al (2019).

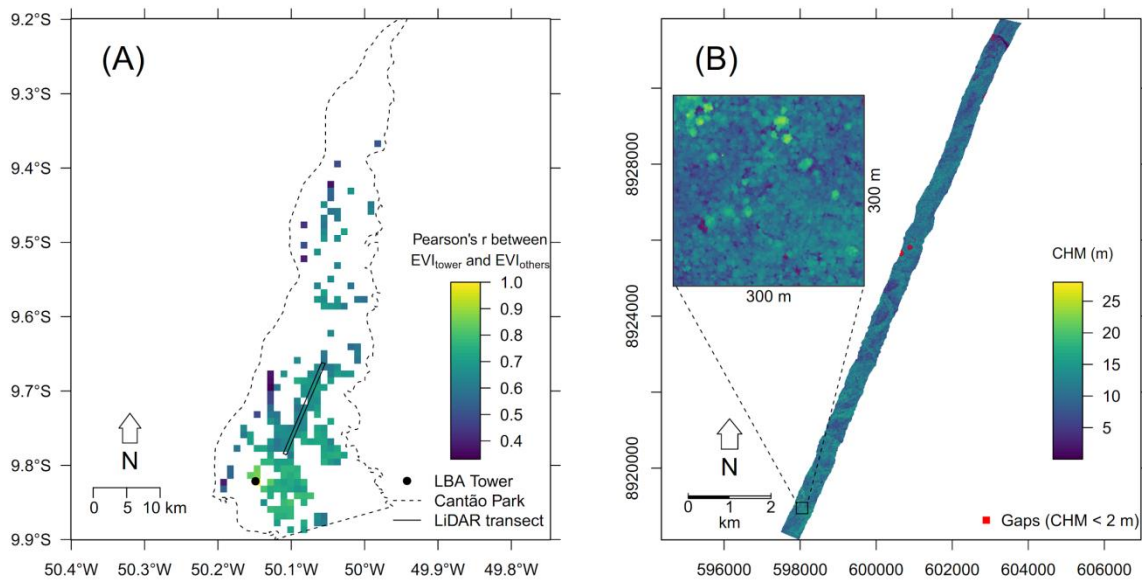
The canopy structure of the studied area according to Lidar had a mean height of 10.2 m (sd = 3.08), where most values from the canopy surface model are between the range of 4.8 and 14.9 m (5<sup>th</sup> and 95<sup>th</sup> percentile), and up to 38 m maximum height (Figure 4.6b). The canopy surface model shows the canopy is mostly closed with only 0.51% of the canopy area exhibiting gaps (height < 2 m), meaning that only a very small fraction of areas within the forest canopy would allow direct observation of the underlying understory. Although the LiDAR transect is 7 km away from the tower, field measurements of tree height support the assumptions that the forest structure around the tower is similar to those of the LiDAR transect, as described in Table 4.2.

Table 4.2 - Experimental plots and LiDAR statistics regarding tree height measurements.

Plots	Number of Individuals	Mean Tree Height (m)	5% Percentile (m)	95% Percentile (m)	Maximum (m)
BAN1	86	11.79	6.84	18.86	28.36
BAN2	84	12.48	4.5	19.77	38.89
LiDAR	-	10.2	4.8	14.9	38

The EVI spatial correlation also showed that pixels within this transect are positively correlated to the tower EVI response through the time series analysis ( $r \geq 0.6$ ,  $p < 0.01$ ). Hence, this result supports the hypotheses that there is no strong influence of free standing water on the EVI from MODIS-MAIAC observed during the flooded period, which could skew the observed phenological patterns.

Figure 4.6 - a) Spatial and temporal correlation between tower EVI and pixels with less than 10% of permanent water channels [52] inside the Cantão State Park. b) LiDAR canopy height model (CHM) transect and gaps ( $< 2\text{m}$  height) in red.

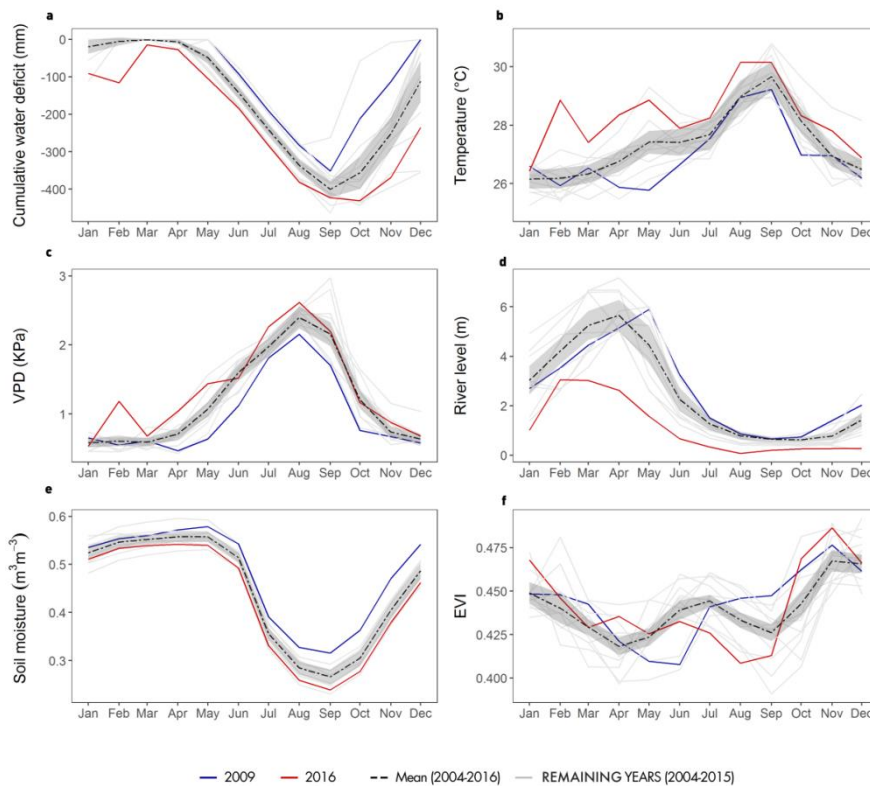


Source: Adapted from Fonseca et al (2019).

#### 4.3.4 Inter-annual variation of seasonal drivers and EVI-Multi-Angle Implementation Correction (MAIAC)

The inter-annual EVI analysis showed that during extreme wet (2009) or dry (2016) years, phenology patterns have changed due to both excess and lack of water (Figure 4.7). During 2009, soil moisture was higher compared to other years (Figure 4.7e). Lower cumulative water deficit (Figure 4.7a) and lower temperatures (Figure 4.7b) was also recorded. On the other hand, during 2016, the river level was well below the mean, which decreased soil moisture (Figure 4.7e) in association with high temperatures and high VPD (Figure 4.7c). These changes in water availability have produced an anomalous EVI seasonal trajectory between these two years (Figure 4.7d).

Figure 4.7 - Monthly variation of CWD (a), temperature (b), VPD (c), river level (d), soil moisture (e) and EVI (f). The dashed line represents the average value (2004–2016), the standard deviation of the monthly variables is indicated by the grey shading, the blue line represents the wettest year (2009), the red line the driest year (2016) and grey lines represent remaining years (2004–2015).



Source: Adapted from Fonseca et al (2019).

The period of leaf exchange in 2009 occurred from July to December, while in 2016, there were two peaks of EVI, a small peak from April to June and another from October to November. Thus, the bimodal patterns in 2009 was not observed, and in 2016 leaf renewal and photosynthetic capacity period have changed due to the decrease of flooding and increases in atmospheric demands, observed through VPD, CWD, and temperature.

#### **4.4 Discussion**

The annual average pattern of ET and GPP suggests that free water is exerting an influence on the evaporative processes during the flooded period since the peak of ET observed in March, matched the flooding peak. This analysis confirms the free water evaporation hypothesis reported by Borma et al. (2009) when observing higher values of ET during flood than during the dry season and lower GPP values (COSTA, 2015).

The unsynchronized pattern of ET and GPP on the rainy-flooded period describes the forest dormancy probably due to anoxic conditions along the flooded months, as reported for Amazon flooded forests (SCHONGART et al., 2002). However, remaining high levels of GPP was recorded until March (one month after the flood started) and at the end of the flooded period (May), due to the shorter duration of the flooded period (or soil saturation) in higher terrain portions near the flux tower.

Conversely, both ET and GPP decrease during the dry period as a result of soil moisture depletion, with the lowest values of ET occurring at the end of the dry season (September), and the lowest values of GPP recorded in August/September. ET and GPP recover during the early rainy season (October to January), with the highest seasonal carbon assimilation rates from 20.40 to 22.63  $\mu\text{mol CO}_2 \text{ m}^{-2} \text{ s}^{-2}$  (Costa, 2015). The same growth and carbon assimilation pattern were reported in the central Amazonian floodplain, which exhibited higher productivity during the terrestrial phase, reaching on average 20  $\mu\text{mol CO}_2 \text{ m}^{-2} \text{ s}^{-2}$  (PAROLIN et al., 2010) and the highest growth rates from September to November (SCHONGART et al., 2002). At other Amazonian sites, GPP is maximized during the early dry season as a result of increasing incident radiation and reduction of cloudiness, coupled with high levels of ET (DA ROCHA et al.,

2009; RESTREPO-COUBE et al., 2013), however, at the BAN site, GPP seasonality seems to be mainly governed by soil moisture which also regulates the canopy phenology.

The phenology pattern described by EVI suggests that the new leaves flush synchronized with senescence, which can be used as a proxy of canopy changes (WU et al., 2016). These peaks occur when GPP is maximized, suggesting the coupling between new leaves and phenology of photosynthetic capacity. Instead of light availability, EVI at this site seems to be strongly governed by soil moisture/aeration, differing from the *terra firme* forest (WAGNER et al., 2017). However, over the flooded forests across the Amazon basin, a similar pattern is expected to occur as observed in this study, which is important for modeling carbon seasonality since approximately 14% of the basin is composed of flooded forests (HESS et al., 2003). Nonetheless, phenology patterns obtained through satellite data in the central Amazon region should be interpreted carefully, since the flooding height is much higher than in this transitional area and assessments about the influence of flooding on vegetation indices should be considered. The EVI oscillation reflected the effect of soil moisture depletion at the end of the dry season, which reduced evapotranspiration and carbon assimilation rates, exhibiting the lowest peak in September.

Previous studies have suggested two or more months of lag between canopy greening and forest productivity at *terra firme* forests (MAEDA et al., 2016; WAGNER et al., 2017), which could be explained by leaf demography (WU et al., 2016). Although these results have shown one month of decoupling between EVI and GPP during the dry season (May–Sep), at a flooded site, this lag could be an effect of topography within the tower footprint where the early GPP response is from sub-footprint regions that are topographically higher and drier. The EVI is characterizing the larger landscape response, where most forest area remains in likely anoxic conditions due to a longer period of inundation.

The inter-annual analysis revealed a trend of increase in temperature and decrease of rainfall (Figure 4.7) as suggested by forecasts for this region (MALHI; WRIGHT, 2004; GLOOR et al., 2015), which is becoming drier over the last ten

years. The El Niño drought that significantly decreased rainfall and increased temperature in the Amazon basin during 2015/2016 (JIMÉNEZ-MUÑOZ et al., 2016) also affected this transition area, promoting a different vegetation response to environmental controls. The EVI suppression in 2009 reflected an extended dormant period due to soil saturation from January to June, while during these months in the ENSO year, EVI was slightly higher than the mean (Figure 4.7f), which was a result of the shorter flooded (eventually anoxic) period (Figure 4.7f). This seasonal EVI shift suggested that canopy changes are describing inter-annual water availability.

Hydroperiod has proven to be the main environmental control on above-ground biomass in central Amazonian floodplains (ASSIS et al., 2018) and according to these findings, the hydrological regime also plays an important role in the seasonal vegetation response and consequently on the ecosystem productivity in this study region, at the southeast of the Amazon basin. These results suggest that changes in flooding patterns, which increases the duration and/or intensity of the dry season, could directly impact these areas, increasing tree mortality (PIE DADE et al., 2013; RESENDE et al., 2019), wildfires (SCHEFFER et al., 2017) and CO<sub>2</sub> emissions (DALMAGRO et al., 2019), likewise reported for central Amazonian floodplain forests. Thus, it is essential to analyze the seasonality of flooded forests at landscape scales.

#### **4.5 Conclusions**

Cycles of ecosystem productivity and evapotranspiration are not synchronized in this southern Amazon flooded forest due to the dormancy period during flooded months, which influences the amount of free water evaporation and the decrease of productivity. The remaining high values of productivity at the beginning of the flooded period and before the flooding ends, in May, are explained by the shorter duration of soil saturation in higher terrain portions, concentrated near the flux tower. Although topographic differences in this floodplain forest only vary up to 2 meters in height, some terrain portions are not subject to the same flood pulse, given the mean flood height of 1.3 m. Flooding also determines the amount of soil moisture during the non-flooded months, which is positively associated with



productivity ( $\rho = 0.34$ ). To address the remote sensing challenges of detecting canopy phenology and productivity seasonality in this flooded area, tower measurements and leaf litter mass data were associated with the EVI from MODIS-MAIAC, and airborne LiDAR data was used to assess the density of canopy gaps. The results showed that EVI is positively associated with leaf litter mass ( $r = 0.55$ ) and with GPP ( $r = 0.5$ ), suggesting a coupling between new leaf production and phenology of photosynthetic capacity, with a bimodal productivity pattern of assimilating maximum carbon after the flooded period ends and during the rainy non-flooded season, under non-limiting soil water conditions. It was also found that this forest has a dense canopy, which means that free water exposed through gaps during the flooded period does not strongly influence EVI observations. Additionally, EVI described inter-annual variations of vegetation response to environmental drivers and revealed that water availability is the main phenological driver at this site, which can change vegetation phenology during extreme years, consequently affecting ecosystem productivity. The potential for accurate monitoring of phenology in floodplain forests using spaceborne remote sensing was assessed in this study.

## 5 ESTIMATION OF LONG-TERM EVAPOTRANSPIRATION OVER A TROPICAL FLOODPLAIN FOREST

### 5.1 Introduction

The Amazon forest plays an essential role in the global carbon, energy, and water cycles, absorbing CO<sub>2</sub> from the atmosphere locking it as biomass (PHILLIPS et al., 1998; MALHI et al., 2009; BRIENEN et al., 2015) and transferring large amounts of water from the land surface to the atmosphere through evapotranspiration (ET) (DA ROCHA et al., 2004; WRIGHT et al., 2017).

Some studies estimate that 25 to 35% of rainfall is recycled by evapotranspiration, which means that the forest and its climate are mutually dependent (ELTAHIR; BRAS, 1994; STAAL et al., 2018). Moreover, seasonal droughts are moderated by the rainforest, as indicated by the higher contribution of recycled moisture in the atmosphere during the dry season, which also influences on the onset of the rainy season (NEGRÓN JUÁREZ et al., 2007; WRIGHT et al., 2017). It means that any land use change at the forest boundary could impact the entire ecosystem.

In *terra firme* forest, ET is controlled by incident radiation, vapour pressure deficit, and water availability, which means that ET is in phase with radiation when water is non-limiting (e.g. k34, k67, k83 LBA sites) (DA ROCHA et al., 2009; FISHER et al., 2009; CHRISTOFFERSEN et al., 2014). Nonetheless, this pattern is not observed in regions that have an extended dry season or less water availability, thus, a dynamic shift between energy and water as drivers are exhibited across space and time in the Amazon basin (MAEDA et al., 2017; WAGNER et al., 2017).

Although some studies have contributed to the understanding of ET drivers and its variation across the Amazon basin (DA ROCHA et al., 2009; FISHER et al., 2009; RESTREPO-COUBE et al., 2013a; CHRISTOFFERSEN et al., 2014; MAEDA et al., 2017), some uncertainties remain due to the lack of data covering the full ecoregions, and the unclear interacting influence of climate drivers,

canopy transpiration and the hydrological cycle (GLOOR et al., 2013; CHRISTOFFERSEN et al., 2014).

The ET estimation over seasonally flooded forests in the Amazon is complex because of the influence of free water evaporation on ET rates (BORMA et al., 2009), associated with the unclear vegetation responses to annual flooding in terms of transpiration. Nonetheless, approximately 14% of the Amazon basin is composed of seasonally flooded forests (HESS et al., 2015), which presents variation in the extension and amplitude of annual flooding cycle, determined by topography and changes in river-water level (JUNK; BAYLEY; SPARKS, 1989; GLOOR et al., 2015). Regional variation in precipitation determines the lag time of 3 to 4 months between the peak rainy season and the peak of flooding height (JUNK; BAYLEY; SPARKS, 1989).

Many studies performed on flooded plots are located in the central Amazon forest, near the Amazon/Solimões rivers (SCHONGART et al., 2002; PAROLIN et al., 2010; PIEDADE et al., 2013; ASSIS et al., 2018), and they have pointed to different mechanisms in response to the excess or lack of water to supply plant physiology demand. During flooding, trees reduce photosynthesis and exhibit a period of dormancy, as a strategy to deal with anoxic conditions, whereas during the dry phase, trees present higher rates of stem growth (SCHONGART et al., 2002) and greater assimilation of CO<sub>2</sub>, as a result of soil re-aeration and the appearance of new leaves (PAROLIN et al., 2010).

Some studies reported that central Amazon floodplain forests presented an extended growth period during El Niño events, due to the prolonged vegetation period (SCHONGART et al., 2004). On the other hand, in the Bananal region, evapotranspiration rates decreased (BORMA et al., 2009), and increasing rates of tree mortality were reported during the El Niño of 2005 (HOMEIER; KURZATKOWSKI; LEUSCHNER, 2017). Moreover, the recent ENSO event of 2015/2016 (JIMÉNEZ-MUÑOZ et al., 2016) lead to a significant decrease in forest water volume (HUMPHREY et al., 2018; YANG et al., 2018), which in turn, diminished the Bananal forest biomass increment in 50% compared to a typical year (TAVARES, 2019).

In this context, although forest inventory plots within Amazonian flooded forests have provided some knowledge about phenology patterns, biomass increment, seasonal dormancy and growth period (SCHONGART et al., 2002; PAROLIN et al., 2010; ASSIS et al., 2018), there is no long-term eddy flux tower within these flooded sites. The only floodplain forest equipped with an eddy-covariance system from the LBA program is the Bananal site (BAN), located at the transition between the Amazon and Cerrado biomes. This site presents the unique opportunity to understand the interactions of the soil-plant-atmosphere continuum of a tropical seasonally flooded forest. Nonetheless, unlike central Amazonian forests, the southern periphery of the Amazon experiences strong precipitation seasonality (DA ROCHA et al., 2009).

Eddy flux towers from the Large Biosphere-Atmosphere (LBA) program have been one of the few sources of data to measure carbon and water fluxes of Amazonian forests. However, despite the valuable results provided by these towers, the eddy-covariance data usually present many gaps. Several gap-filling methods have been employed by the research community, such as linear interpolation, mean diurnal pattern, look-up tables, semi-parametric models, and artificial neural networks (FALGE ET AL., 2001; MOFFAT ET AL., 2007; PAPALE, ET AL. 2006).

The Generalized Additive Model – GAM (WOOD et al., 2017) is another method that also uses empirical data and does not have predetermined algorithms, which is suitable for very sparse data (PEDERSEN et al., 2018). GAMs are a robust tool to build nonlinear relationships between predictor variables and the response with flexible adjusts. Some recent studies performed at tropical forests used this method to fill gaps and identify drivers of phenological and carbon patterns of tropical forests (PAU et al., 2017, 2018; RIFAI et al., 2018).

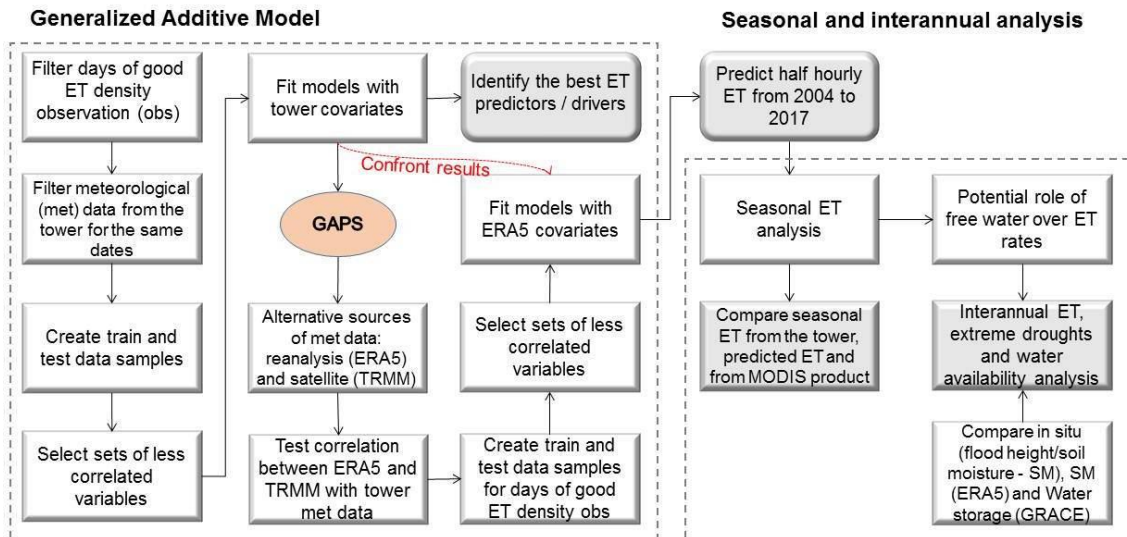
Given the uncertainties of these environments response to extreme events, and the sparse existing data of the flood pulse effect, we analyzed the evapotranspiration of a floodplain forest in the Amazon-Cerrado transition and its environmental controls. To overcome the gaps in the ET flux tower data, we developed statistical models (Generalized Additive Model) to fill gaps in the

observational record. Here we specifically ask: I) What are the main meteorological and hydrological drivers of ET, and how do these vary, seasonally and interannually? II) Do the evapotranspiration data obtained through the tower agree with landscape-level remote observations (ET product from MODIS16A2)? III) How did the Bananal flooded forest respond in terms of evaporative fluxes during the 2015/2016 drought year?

## **5.2 Methods**

Generalized Additive Models (GAMs) were constructed to fill gaps and estimate continuous evapotranspiration (ET) records for the Bananal island region, from January 2004 to December 2017. These models are calibrated by the response variable itself (ET) as a function of the predictor variables, which were the meteorological variables measured at the BAN tower. However, since tower records presented many gaps not only in ET but also in other hydrometeorological data, alternative sources of meteorological data (i.e., ERA5, TRMM) were used as model predictors. To use these alternative data, they were compared regarding the degree of association with observed variables from the flux tower. After validation, the best model was used to reconstruct the ET time series and to analyze the seasonal and interannual ET variability, identifying the main ET drivers over this flooded area. The reconstructed ET time series were compared with ET from MODIS (MOD16A2), to assess the reliability of this product. Finally, considering the potential role of the free water surface on ET rates, and the ENSO drought of 2015/2016, we compare in situ (flood height, soil moisture), reanalysis (soil moisture - ERA5) and satellite (total water storage - GRACE) data to test GRACE as a good predictor of the water status in this basin. The overview of this study is shown in Figure 5.1.

Figure 5.1 - Flow chart describing the overview of this study. The gray squares are representing the main results.



Source: Prepared by the author.

### 5.2.1 Gap filling and long-term ET prediction using the Generalized Additive Model (GAM)

Generalized Additive Models are statistical models that can fit nonlinear relationships between the response (y) and predictors (x, w, z) through several smoothing (aka spline) functions (s) that can capture non-linearities in the data, as described in equation 5.1 (WOOD, 2017). This flexible model structure has been used in some studies to access complex interactions in Earth System science, coupling field, and climate data (PAU et al., 2017, 2018; RIFAI et al., 2018).

$$y \sim s(x) + s(w) + s(z) \quad (5.1)$$

These models are calibrated by the response variable itself (y) as a function of the predictor variables (x,w,z), here, represented by the evapotranspiration and the meteorological data measured at the BAN tower, respectively. Only days with valid ET measurements for all daytime hours (7:00 to 17:00) from the BAN flux tower were used to generate GAM models, since the measured ET trains the model. This procedure also filtered the predictor variables from the tower for the

same dates as the ET observations. A random training dataset was created to train the model, and a test sample (excluding the ones used on the training sample) was used to validate it. Some meteorological variables are highly correlated, therefore, to avoid multicollinear covariates, only less correlated variables were selected to construct models, and many combinations between them were tested to find the best ET predictors.

The GAM model constructed with locally measured meteorological drivers as covariates should be as accurate as possible. However, the lack of data from the tower covering the entire time series prevents filling gaps and estimating long-term ET. Therefore, GAMs using tower predictors were constructed to identify the main ET drivers and to validate the accuracy of this method.

Therefore, due to gaps in the flux tower measurements, predictor variables were obtained from reanalysis (the fifth generation of reanalysis data - ERA5) and satellite-based remote sensing data (TRMM) to reconstruct the time series from 2004 to 2017. Meteorological variables (global radiation, net radiation, vapour pressure deficit, soil moisture, temperature, rainfall) from ERA5 were extracted for the pixel that includes the BAN tower from the period from 2000 to 2017, at a spatial resolution of  $0.25^\circ \times 0.25^\circ$  (Copernicus Climate Change Service, 2017), adjusted to the same time zone, and interpolated to half-hourly time step to match the temporal resolution of the ET from the eddy flux dataset. The data were downloaded in a netCDF file and processed using the “ncdf4” R package (PIERCE, 2013). The relative humidity and vapor pressure deficit are not diagnostic outputs of ERA5, so they were calculated using Bolton (1980) equations, described in section 2, through a freely available script on R language (LEBAUER, 2018).

The Tropical Rainfall Measuring Mission (TRMM) data were extracted for the pixel that contains the BAN tower in a three hourly time step, using the Google Earth Engine platform, from January 2004 to December 2017. The data were interpolated to half-hourly time step to match the eddy flux dataset and adjusted to the same time zone.

The same procedure described to build the GAM model with tower covariates was performed with ERA5 data to estimate continuous records of ET from 2004 to 2017. Finally, the coefficients of determination obtained from the tower and ERA5 models were compared to evaluate the accuracy of ERA5 drivers.

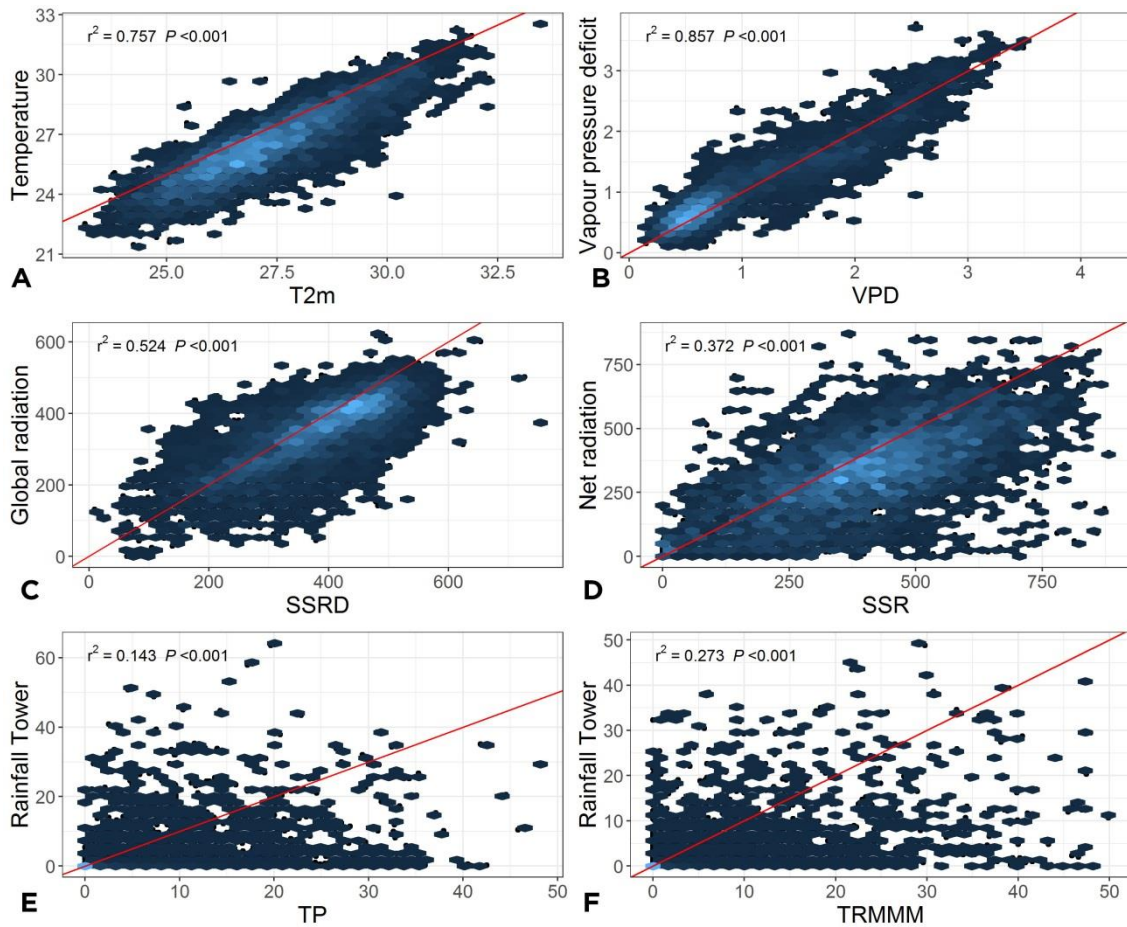
The entire analysis was performed on R using different packages (eg. tidyverse, lubridate, ggplot2, RcppRoll). The mgcv R package was specifically used to build the GAM models (PEDERSEN et al., 2018).

### **5.2.2 Association between flux tower, reanalysis and remote sensing data**

Daily meteorological variables from ERA5 and rainfall from TRMM were compared to tower records to test the coefficient of determination (calculated as the square of the Pearson correlation coefficient) between them (Figure 5.2). VPD and temperature from ERA5 – T2m (Figure 5.2a and b) were highly correlated with daily tower measurements ( $r^2 = 0.85$  and  $r^2 = 0.75$ , respectively), along with global radiation - SSRD ( $r^2 = 0.52$ ; Figure 5.2c) and net radiation - SSR ( $r^2 = 0.37$ ; Figure 5.2d). However, rainfall in a daily scale was poorly described by both ERA5 - TP and TRMM data.



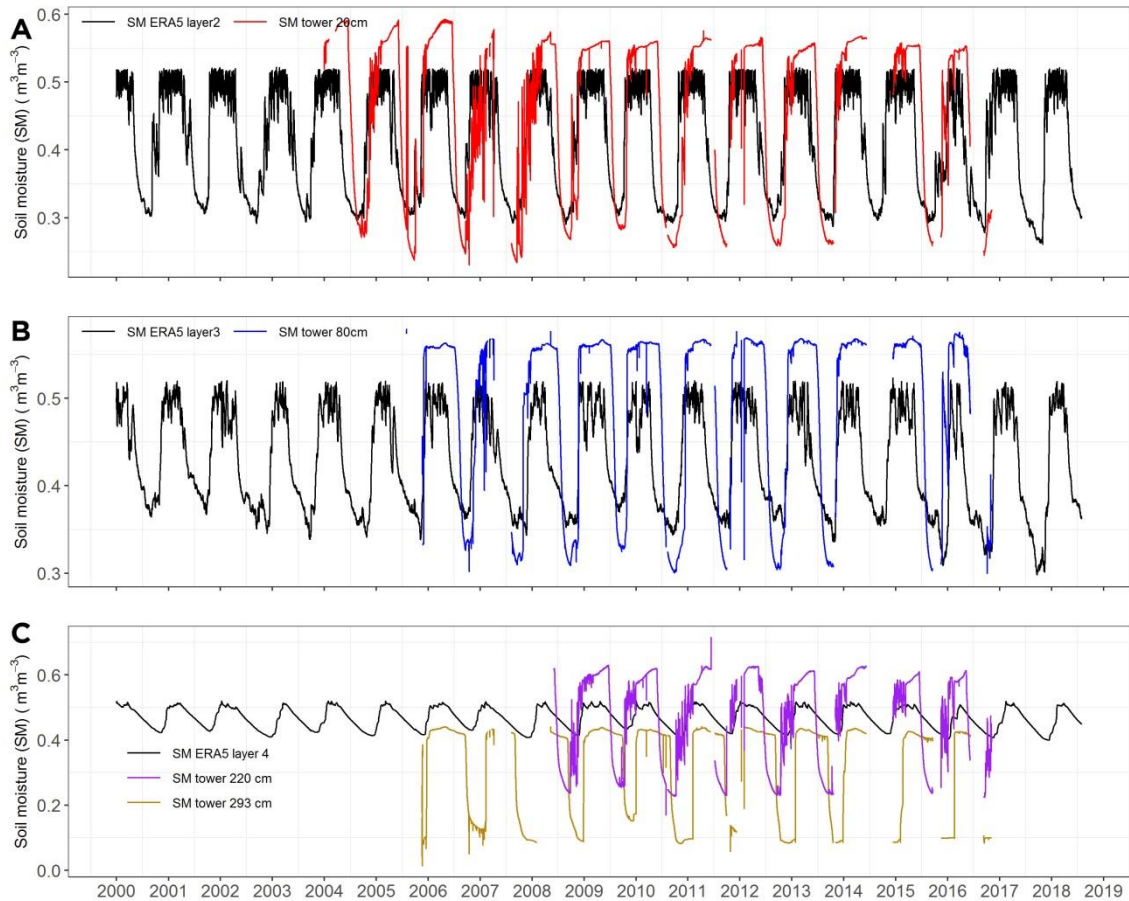
Figure 5.2 - Daily scatterplot between tower (ordinate), and its correspondent variable from ERA5 and TRMM data (abscissa). The red line represents the fitted regression line.



Source: Prepared by the author.

The seasonal soil moisture at the base of the BAN tower and ERA5 data is presented on Figure 5.3. The daily soil water volume of layer two from ERA5 refers to the soil moisture estimate from 0-20 cm depth at the base of the BAN tower (Figure 5.3a), and layer three from ERA5 refers to the soil moisture content at 40-80 cm depth (Figure 5.3b). The soil moisture measured from 0.73 - 1.89 cm (swvl4) presented the seasonal variation in agreement with both soil moisture measured from 150 - 220 and 220 - 293 cm depth from the BAN flux tower (Figure 5.3c).

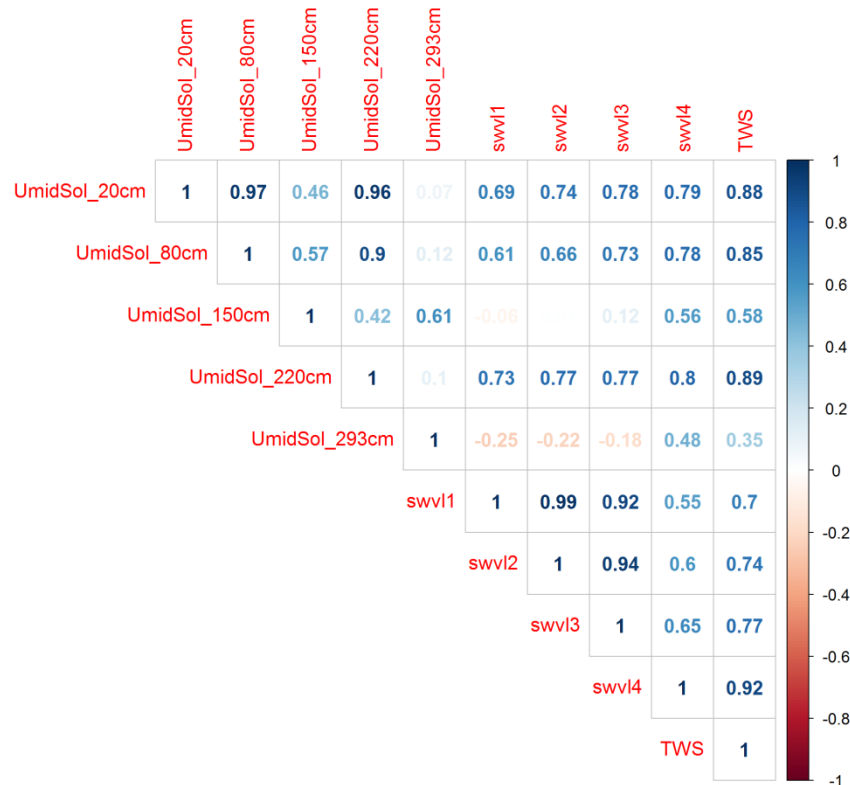
Figure 5.3 - Interannual relationship between soil moisture measured at different depths from the BAN flux tower and soil moisture measurements from ERA5 products. The black line represents volumetric soil moisture layers from ERA5, and the tower (FDR) lines are varying according to the depth, 20 cm is red, 80cm is blue, 220cm is purple and 293 cm is the dark yellow line.



Source: Prepared by the author.

The correlations between soil moisture measured close to the tower with ERA5 data, and with the total water storage (TWS) from GRACE are presented in Figure 5.4. It is possible to observe that layers referring to the same depth are highly correlated, for example, the soil moisture measured at 20cm depth with swvl2 ( $r^2 = 0.77$ ,  $p < 0.001$ ), and also the TWS with soil water volume layer 4 from ERA5 ( $r^2 = 0.92$ ,  $p < 0.001$ ).

Figure 5.4 – Correlation between soil moisture measured close to the BAN tower (UmidSol\_20cm, UmidSol\_80cm, UmidSol\_150cm, UmidSol\_220cm, UmidSol\_293cm), ERA5 reanalysis data (swvl1, swvl2, swvl3, swvl4) and GRACE product (TWS).



Source: Prepared by the author.

### 5.2.3 Seasonal analysis

A linear relationship between ET and the hydrological drivers measured at the tower from 2004 to 2010 were tested and analyzed through the months to identify the main drivers and if they change over the year. The coefficient of determination (calculated as the square of the Pearson correlation coefficient) was applied to measure the degree of association between them.

Seasonal ET was analyzed based on daily observed ET (tower), modeled ET (from GAM with ERA5 predictors) and MODIS product ET (MOD16A2). The coefficient of determination (calculated as the square of the Pearson correlation coefficient) was applied to test the linear relationship between the tower ET with the predicted and the MODIS product.

The evapotranspiration from MODIS16A2 was acquired to access the reliability of this product, describing ET seasonality over a flooded forest. The earth engine platform was used to extract the data for the pixel that include the BAN tower, from January 2004 to December 2017. This product is based on the modified Penman-Monteith method (MU; ZHAO; RUNNING, 2011) as described in equation 5.2.

$$ET = \frac{\Delta(R_n - G) + \rho C_p(e_s - e_a)/r_a}{\Delta + \gamma(1 + \frac{r_s}{r_a})} \quad (5.2)$$

where  $R_n$  is the available energy,  $G$  is the soil heat flux,  $\rho$  is the air density,  $c_p$  is the specific heat of air,  $e_s$  is the saturated vapor pressure,  $e_a$  is the actual vapor pressure,  $\Delta$  is the slope of vapor pressure curve,  $\gamma$  is the psychrometric constant,  $r_a$  is the aerodynamic resistance, and  $r_s$  is the surface resistance. The MOD16 algorithm needs input information derived from reanalysis (e.g., solar radiation and air temperature) and remote sensing (e.g., albedo and LAI) datasets from the Modern Era Retrospective Analysis for Research and Applications (MERRA; RIENECKER et al., 2011).

#### **5.2.4 Interannual ET analysis and the influence of extreme droughts over the Bananal forest**

The interannual cycle of predicted ET was based on monthly mean measurements and compared with climatic drivers from ERA5 (soil moisture, net radiation, deficit vapour pressure, cumulative water deficit and air temperature), rainfall from TRMM, which presented a significant coefficient of determination with tower records in a monthly scale (Figure A2;  $r^2 = 0.62$ ,  $p < 0.001$ ) and tower flood height from January 2004 to December 2017. During this period, extreme droughts took place in this region. Therefore, given the fundamental role of soil moisture on ET predictions, the total water storage (TWS) from The Gravity Recovery and Climate Experiment (GRACE) satellite was used to analyze the long term change on the hydrological pattern and its influence on ET rates.

A standard anomaly of total water storage was calculated to highlight anomalies during this period:

$$(X_t - X_m) / X\sigma \quad (5.3)$$

where  $X(t)$  denotes the measurement (i.e., TWS),  $X_m$  is the mean over the month interval and  $\sigma$  the standard deviation over the month interval.

Since many variables were used from different sources and purposes, they are summarized in table 5.1, specifying the tower data and its availability with ERA5 correspondent data.

Table 5.1 - Tower data and availability, ERA5 and satellite correspondent variables and usage description.

Environmental covariates				
Tower		ERA5 / satellite		Usage
Variable	Period			
ET		-		Response variable / interannual analysis
Air temperature (Tar)	2004 2016	-	2 metre dewpoint temperature (d2m)	VPD and ET computation / Predict ET / interannual analysis
Global radiation (Ki)	2004 2014	-	Surface solar radiation downwards (ssrd)	Predict ET / interannual analysis
Net radiation (Net)	2004 2014	-	Surface solar net radiation (ssr)	Predict ET / interannual analysis
Precipitation (precip)	2004 2016	-	Total precipitation (tp)	Predict ET
-			TRMM precipitation – (TRMM)	Interannual analysis

To be continued

Table 5.1 - Conclusion.

Vapour pressure deficit (vpd_tow)	2004 - 2016	Vapour pressure deficit (VPD)	Predict ET / interannual analysis
Soil moisture 10 cm (UmidSol_10cm)	2004 - 2016	Soil water volume layer 1 (0.7 cm) (swvl1)	- Predict ET / interannual analysis
Soil moisture 20 cm (UmidSol_20cm)	2004 - 2016	Soil water volume layer 2 - 0.21 cm (swvl2)	Predict ET / interannual analysis
Soil moisture 80 cm (UmidSol_80cm)	2004 - 2016	Soil water volume layer 3 -0.72 cm (swvl3)	- Predict ET / interannual analysis
Soil moisture 220 cm (UmidSol_220cm) / Soil moisture 293 cm (UmidSol_293cm)	2004 - 2016	Soil water volume layer 4 -1.89 cm (swvl4)	Predict ET / interannual analysis
Flood pulse	2004 - 2016	≅ Total water storage -cm- (TWS)	Interannual analysis

\* soil moisture is given in volumetric water content ( $\text{cm}^3 \text{cm}^{-3}$ )

## 5.3 Results

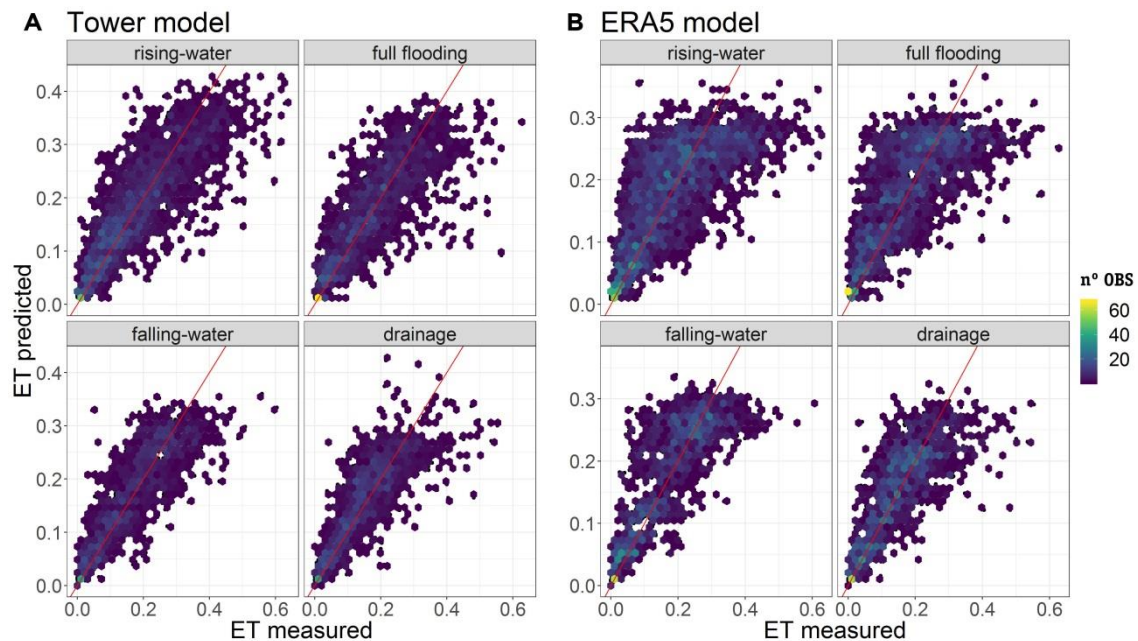
### 5.3.1 Reconstructing ET measurements using GAMs

The best predicted ET obtained from the GAM model used vapour pressure deficit, global solar radiation downwards and both soil moisture from layer 2 and 4 as ERA5 covariates. The predicted ET from this model well described the hourly ET from 9 pm to 4 pm, peaking at 2 pm ( $r^2 = 0.54$ ) (Figure B2). However, the

model poorly fitted periods of low turbulence time (7 am to 9 am and 4 pm to 7 pm).

Regarding the accuracy of ET estimations using ERA5 drivers, daily tower and ERA5 models were constructed using the same meteorological predictors, plotted using the test sample data against the observed ET, and compared by periods of the year. It is possible to observe that both of them best represented the falling-water and drainage periods (Figure 5.5 a and b). The rising water period (early rainy season) was the hardest one to fit along with full flooding. Nonetheless, the overall coefficient of determination between the tower and fitted daily ET from the ERA5 GAM model ( $r^2 = 0.54$ ) did not greatly differ from the one using only tower data ( $r^2 = 0.66$ ), and the pattern was similar between them.

Figure 5.5 - Seasonal quarters of predicted and observed half-hourly ET with tower covariates (A) and with ERA5 covariates (B). Periods are divided into Rising-water (NOV-DEC-JAN), full flooding (FEB-MAR-APR), falling water (MAY-JUN-JUL) and drainage (AGO-SEP-OCT). The color ramp represent the number of observations ( $n^{\circ}$  OBS).

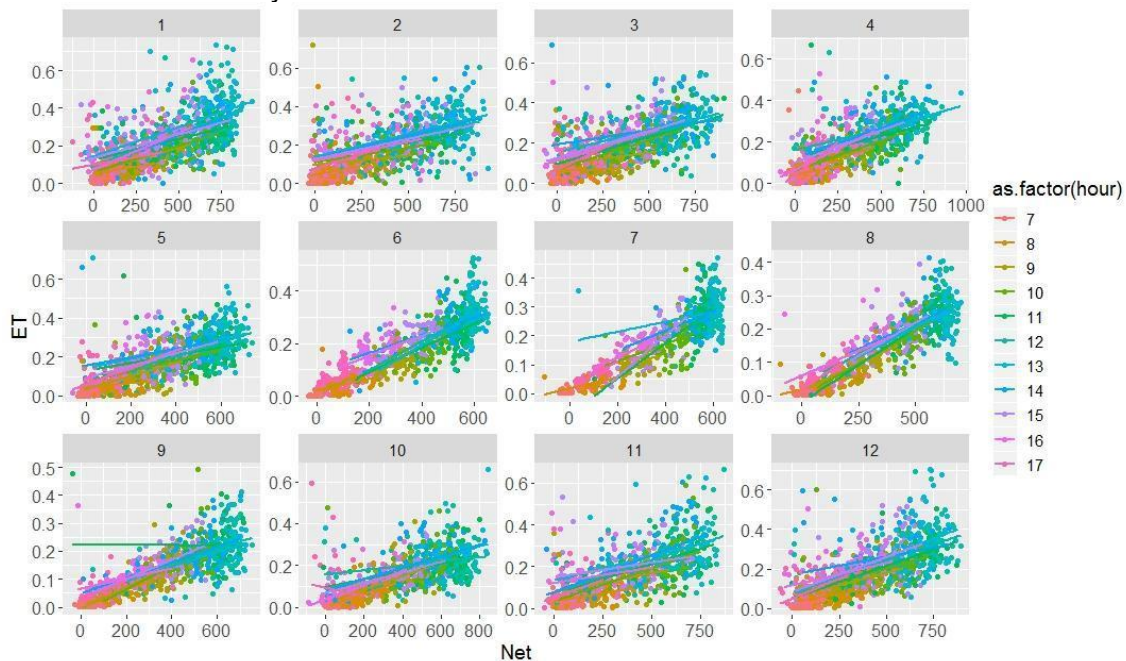


Source: Prepared by the author.

### 5.3.2 Do the meteorological and hydrological drivers of ET change throughout the year?

Diurnal observations of global and net radiation from the tower showed a positive linear relationship with daily ET along the whole year ( $r^2 = 0.56$ ,  $p < 0.001$ ) (Figure 5.6 and 5.7). Despite high VPD occurring from July (middle of the dry season) to October (early rainy season), ET diminished during these months ( $r^2 = 0.11$ ,  $p < 0.001$ ) (Figure 5.7). During the same period, although it was not statistically significant, soil moisture at 20 cm, 80 cm, and 220 cm depth exhibited a positive relationship with ET, indicating that ET is dependent on water availability during these months (Figure 5.9, 5.10, 5.11). Therefore, these results showed that ET is mainly governed by radiation and VPD, but may be limited by soil moisture.

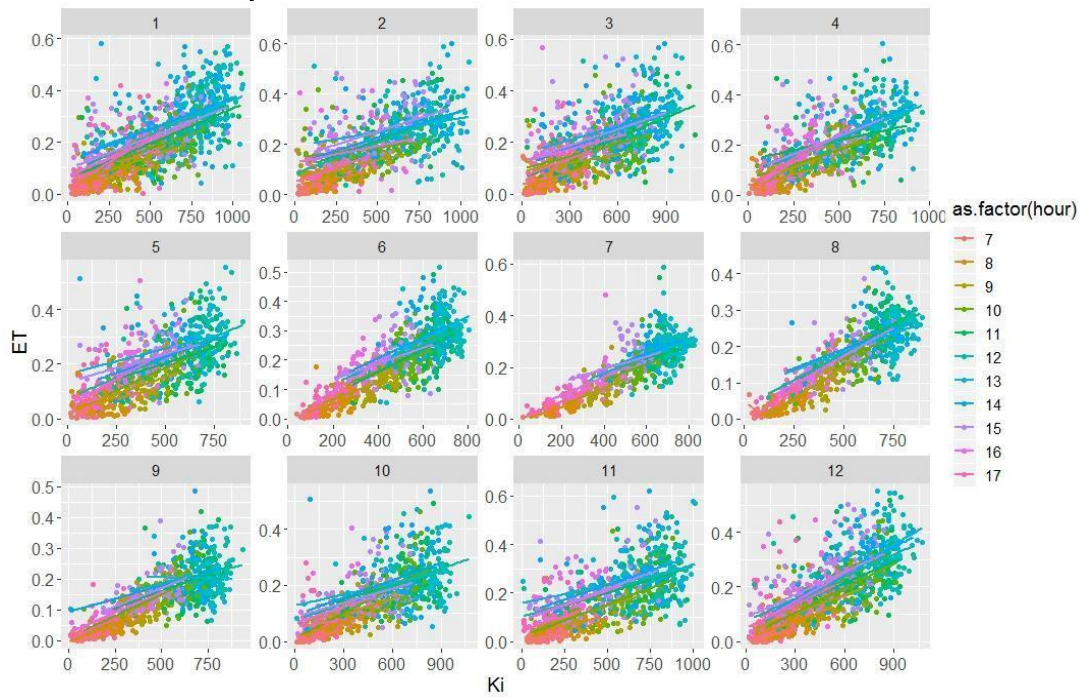
Figure 5.6 - Scatterplot between ET and Net radiation in an hourly time step (colour ramp), divided in months (1 to 12) for the periods of good ET observation density from the BAN flux tower.



Source: Prepared by the author.

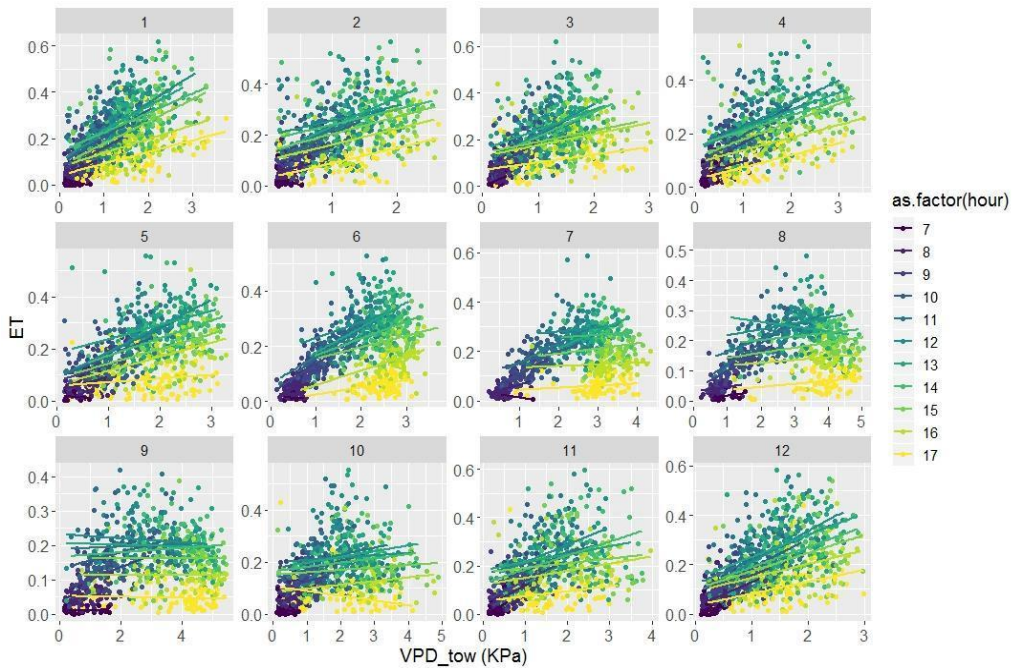


Figure 5.7 - Scatterplot between ET and global radiation in an hourly time step (colour ramp), divided in months (1 to 12) for the periods of good ET observation density from the BAN flux tower.



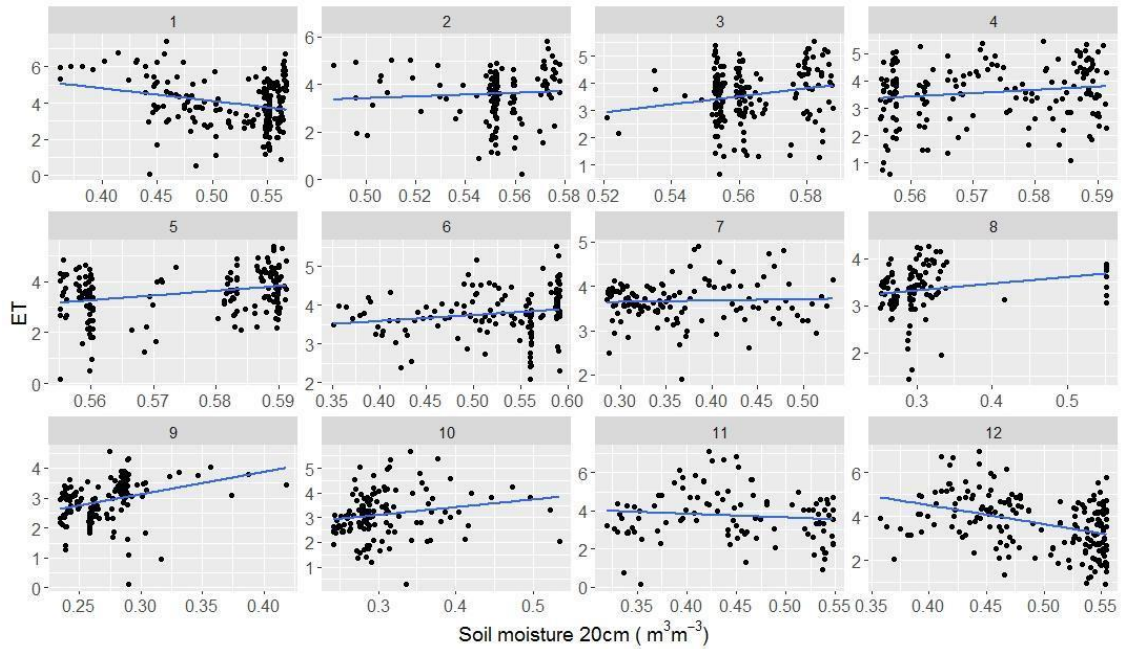
Source: Prepared by the author.

Figure 5.8 - Scatterplot between ET and VPD in an hourly time step (colour ramp), divided in months (1 to 12) for the periods of good ET observation density from the BAN flux tower.



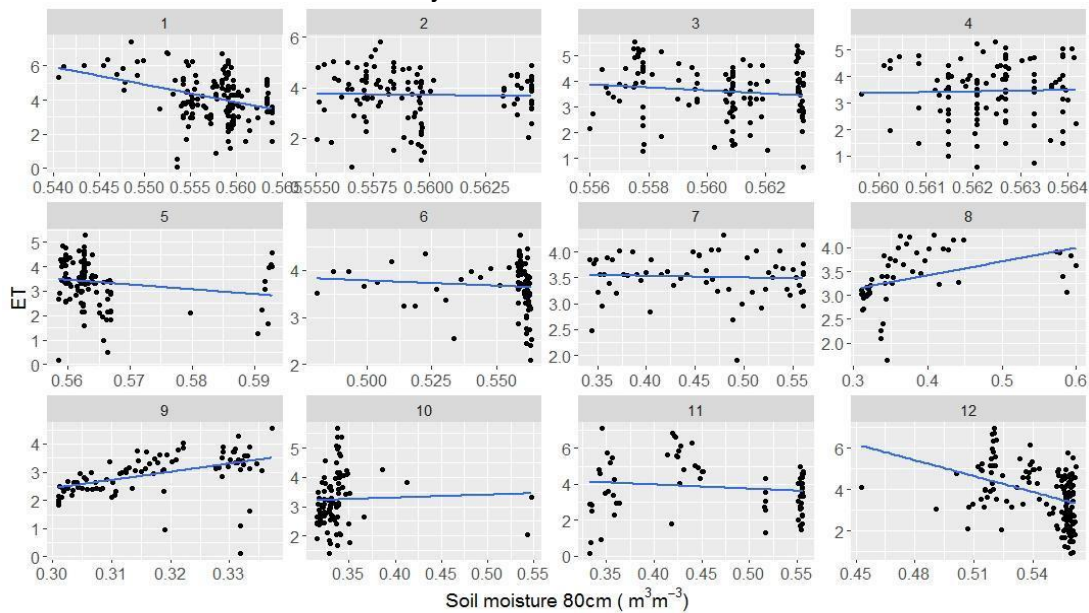
Source: Prepared by the author.

Figure 5.9 - Scatterplot between ET and soil moisture content at 20 cm depth in a daily time step divided by months (1 to 12) for the periods of good ET observation density from the BAN flux tower.



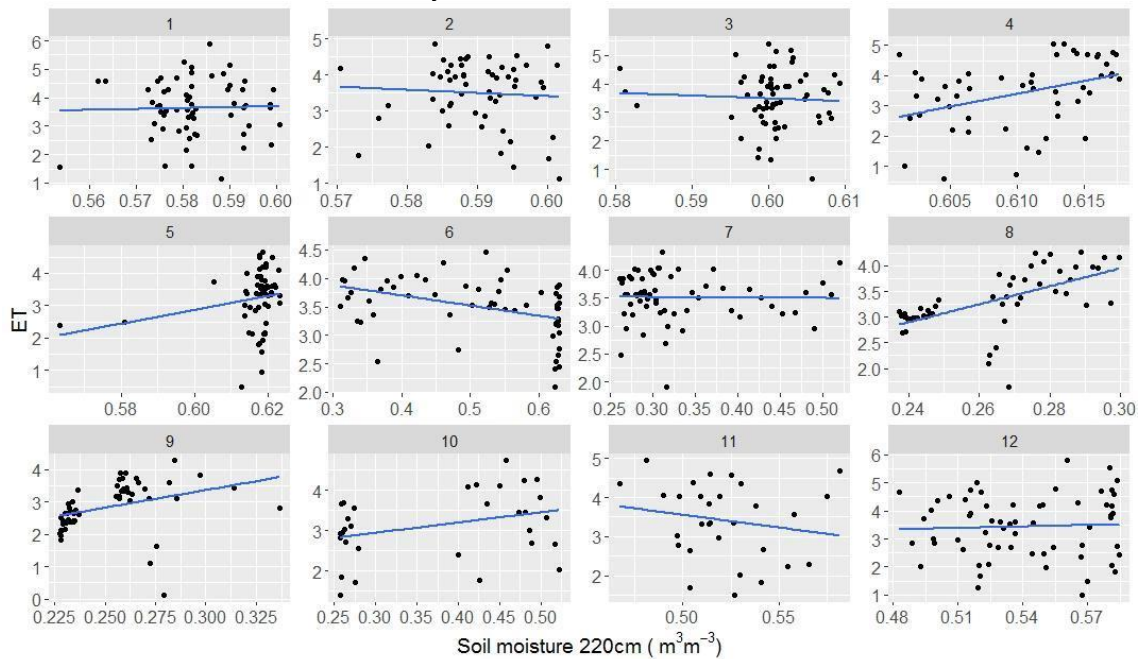
Source: Prepared by the author.

Figure 5.10 - Scatterplot between ET and soil moisture content at 80 cm depth in a daily time step divided by months (1 to 12) for the periods of good ET observation density from the BAN flux tower.



Source: Prepared by the author.

Figure 5.11 - Scatterplot between ET and soil moisture content at 220 cm depth in a daily time step divided by months (1 to 12) for the periods of good ET observation density from the BAN flux tower.

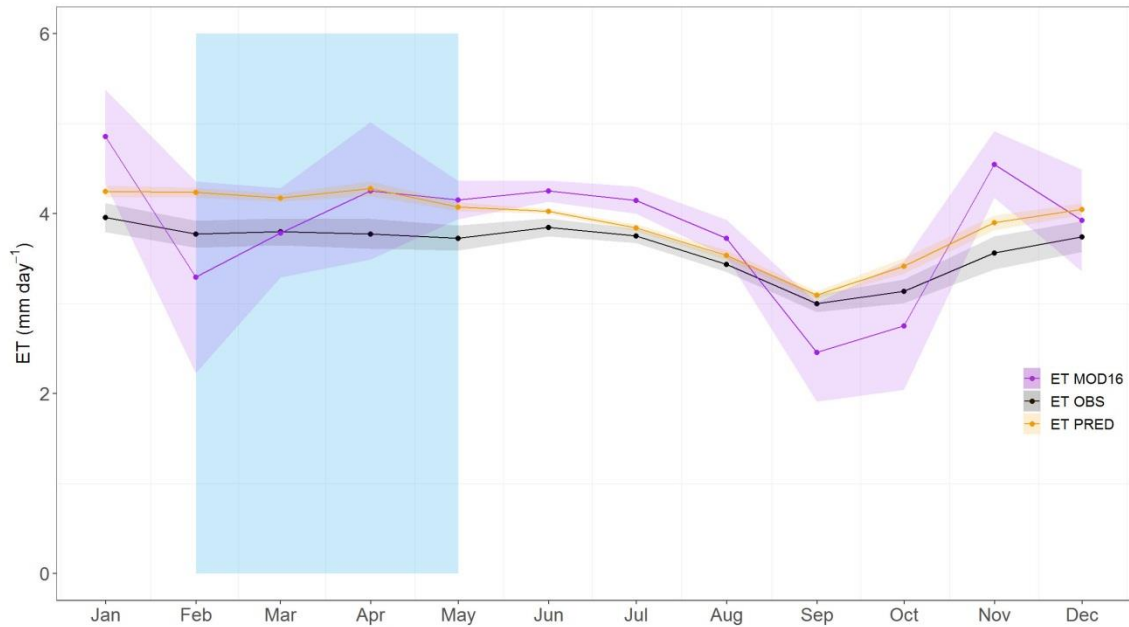


Source: Prepared by the author.

### 5.3.3 Seasonal ET variation

Predicted daily ET has described the observed ET pattern with a slightly super estimation from January to June, but well described the dry and early rainy season (Figure 5.12), as previously discussed in Figure 5.4. The annual mean observed ET is 3.61 mm/day while predicted ET is 3.90 mm/day, and MODIS is 3.87 mm/day. MODIS ET presented a high variation around the mean both during the flooded period (super estimating) and at the late dry season, underestimating ET.

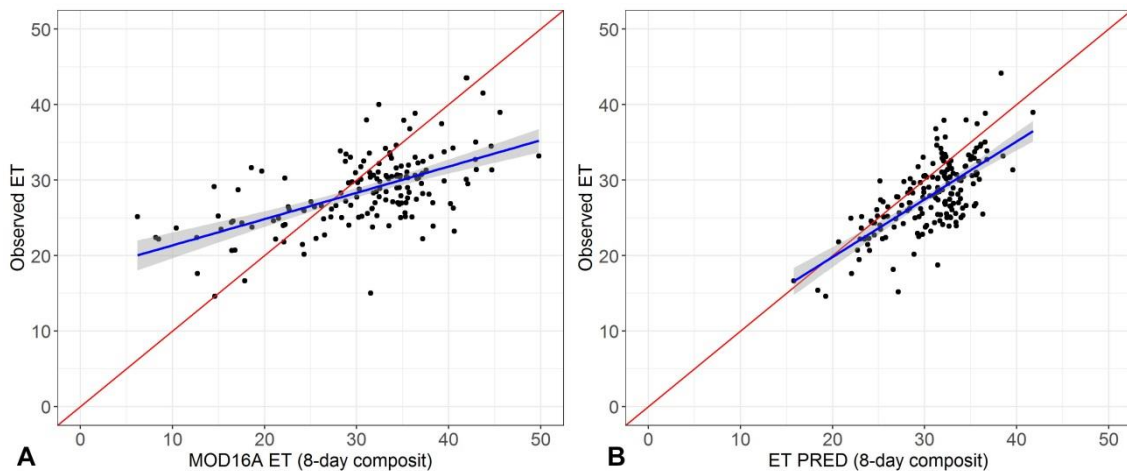
Figure 5.12 - Seasonal daily observed (black line), predicted (yellow line) and MODIS product ET (purple line) from 2004 to 2010 (considering days of good ET observed records). The standard deviation of the monthly variables is indicated by the corresponding shading color.



Source: Prepared by the author.

This difference between MODIS and observed (tower measured) ET is highlighted by the coefficient of determination between them, summarized in a 8 day time step, meeting MODIS composite measurements (Figure 5.13). The relationship between predicted ET and observed ET is higher ( $r^2 = 0.47$ ,  $p < 0.001$ ) and the slope is better adjusted compared to MODIS product ( $r^2 = 0.34$ ,  $p < 0.001$ ). Besides, a great year-to-year variation in ET was found within these 6 years (2004-2010). The mean monthly observed ET varied 8.29%, while the predicted one varied 4.55%, and MODIS 24.58%, presenting the higher variability.

Figure 5.13 - Scatterplot between observed ET from the tower and MODIS (a) and scatterplot between predicted ET from GAM using ERA5 data and observed ET (tower data) in a 8 day time scale.



Source: Prepared by the author.

#### 5.3.4 Interannual evapotranspiration variability and the ENSO drought

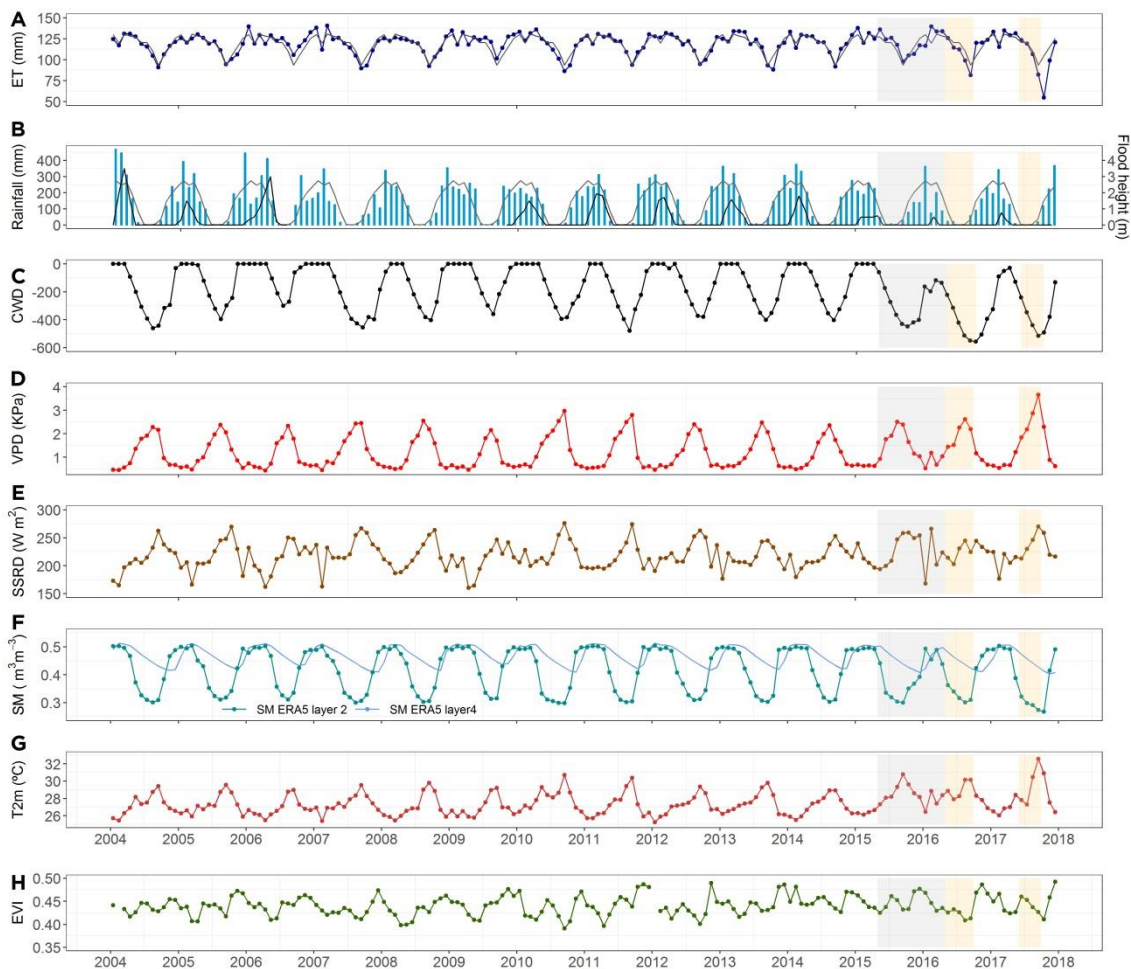
In general, ET was higher during the flooded period (127mm), decreasing through the dry season (111 mm), reaching minimum rates on September (peak of the dry season, 92 mm, in average), and recovering on the rainy non-flooded period (119 mm) (Figure 5.14a). The slightly seasonal ET decline every year from January to February (-11 mm) is related to higher rainfall amounts, approximately 27 mm (Figure 5.14b), which could be limiting ET by increasing cloudiness, therefore reducing global radiation ( $-3 \text{ W m}^2$ ) (Figure 5.14e).

During the rainy season, from September 2015 to May 2016, it is possible to observe small amounts of rainfall compared to the mean (grey line, Figure 5.14b), low flood height (up to 0.5 m, Figure 5.14b), higher CWD (Figure 5.14c) and a shrinkage flooded period (From Jan to Mar; Figure 5.14f). Besides, higher global radiation during all these months (except for January, 2016) was also recorded (Figure 5.14e), probably due to less cloud cover.

The effect of these changes over ET was the maintenance of high ET amounts (133 mm) during the flooded period, and a decreasing trend during the dry

season, which was 8.5% lower than the mean (99.8 mm), reaching the minimum value on September (81.9 mm, 12.7% below the mean).

Figure 5.14 - Interannual ET (a), meteorological drivers (b,c,d,e,g), soil moisture (f) and the phenology pattern (h) represented by the EVI. The grey shaded area corresponds to the ENSO period (May 2015 to May 2016), and the yellow ones correspond to the annual dry season (June to September). Gray lines represent the ET (a) and the rainfall (b) seasonal average.



Source: Prepared by the author.

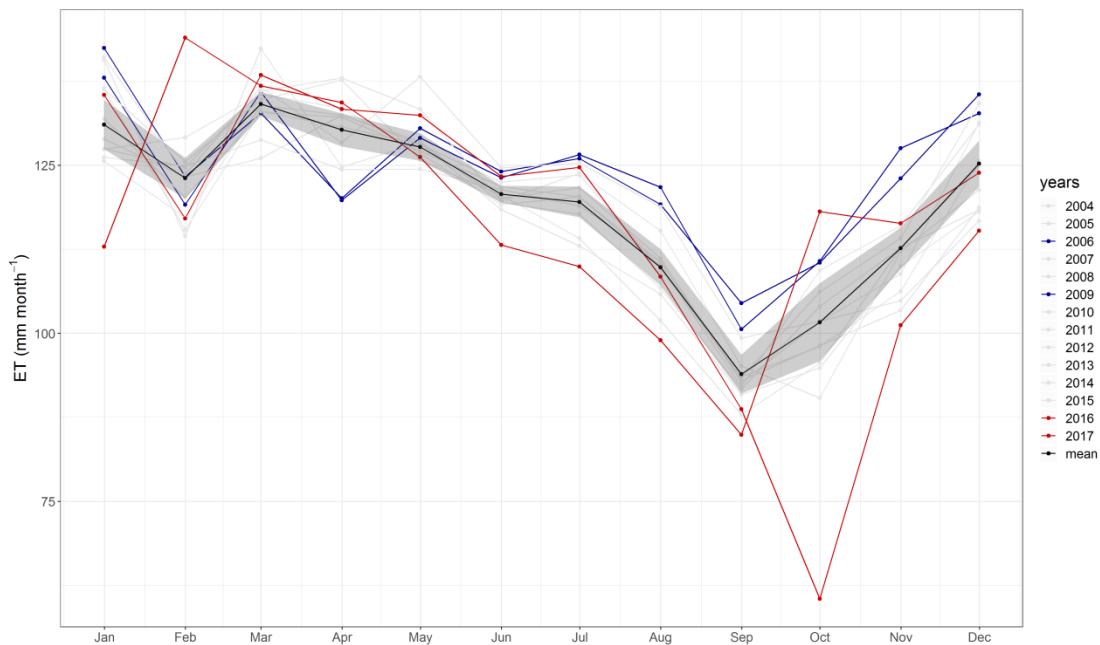
The phenology pattern represented by the EVI also exhibited a decreased pattern during 2016, recovering in the rainy season of 2017 (5.14h).

Although the rainy season from September 2016 to May 2017 presented slightly higher rainfall amounts compared to the wet season of 2016 (Fig 5.14b), and soil

moisture remained saturated for an extended period (From Jan to Apr), a higher impact over ET was observed on the following early rainy season, from September/2017 to December/2017. During these months, ET was 22.8% below the average, reaching the minimum value on October, 53% lower than the mean, associated with an extremely high VPD (2.29 KPa, 99% higher than the mean) and low soil moisture.

Therefore, the interannual analyze is suggesting the ENSO 2015/2016 effect over the forest extended for more than two years (May 2015 to September 2017), since the rainfall remained below the mean, and both shallow and deep soil moisture decreased, which did not recharge the unsaturated zone at the onset of the wet season. This ENSO effect is clearly showed in the Figure 5.15; the red lines represent the years 2016 and 2017, which are well below the mean, while the blue lines represent wetter years (2006 and 2009).

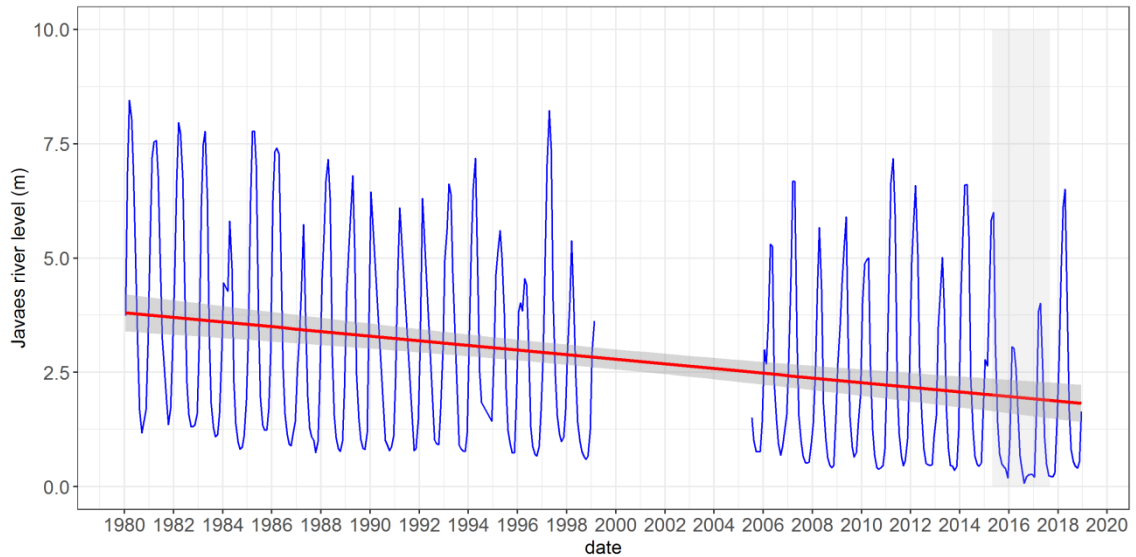
Figure 5.15 - Monthly variation of ET from 2004 to 2017. The standard deviation of the monthly variables is indicated by the grey shading.



Source: Prepared by the author.

From the hydrological record (ANA, 2019), it is possible to observe a decreasing trend of the Javaés river level over the last 40 years (Figure 5.16). It is also highlighted the ENSO (grey shaded area) effect over the river level during 2016 and 2017, which consequently decreased the flood height at the BAN site.

Figure 5.16 - Javaés river level from 1980 to 2018 at Barreira da Cruz station.

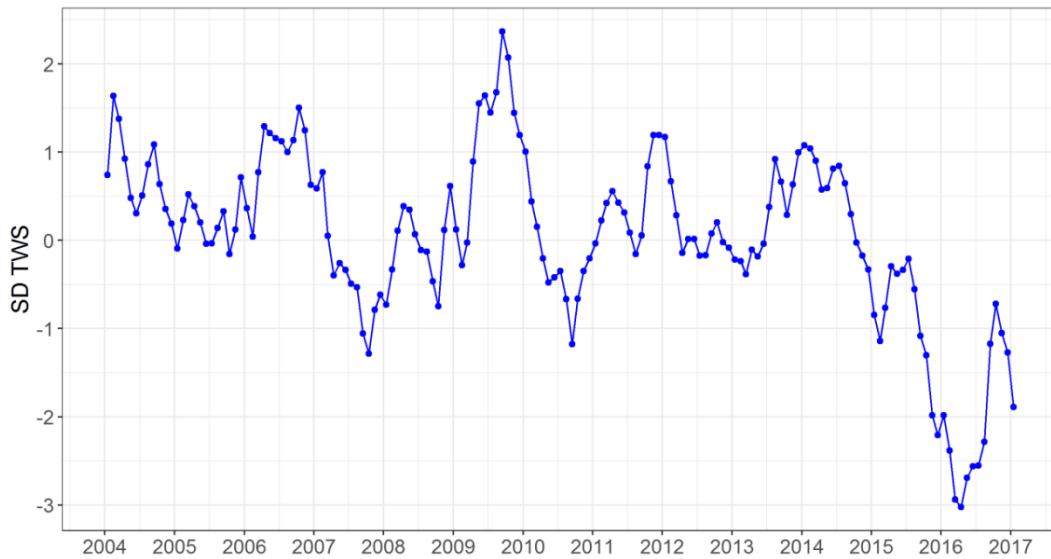


Source: Prepared by the author.

The satellite data from GRACE is supporting the ENSO effect on the hydrological regime, showing the negative standard anomaly values of TWS during 2016 (Figure 5.17). It is also possible to observe the variation of total water storage since 2004, highlighting wetter years (2006 and 2009).



Figure 5.17 - The standard anomaly of total water storage from GRACE product from January 2004 to December 2016.



Source: Prepared by the author.

#### 5.4 Discussion

The Generalized Additive model was able to fill gaps and reconstruct daily ET for the periods of BAN flux tower operation, until 2017. The reliability of soil moisture data from the ERA5 reanalysis product was an important ET driver and has proven to be an accurate record compared to *in situ* soil moisture measurements and with GRACE product (TWS). Previous studies have suggested improving ET estimations over the Amazon forest using both leaf phenology and belowground hydrology (CHRISTOFFERSEN et al., 2014; WAGNER et al., 2017). It was possible to fill gaps and build a consistent time series of this forest functioning in terms of evapotranspiration, since the predictions were performed using eddy-covariance measurements (ET) coupled with meteorological and hydrological drivers. Besides, the model accurately represented the dry season, allowing the analysis of the ENSO effect over this flooded forest.

The monthly seasonal variation of ET obtained from the observed and the predicted measurements are consistent with the 5%–10% variations previously observed in Amazon forest sites (NEGRÓN JUÁREZ et al., 2007; AGUILOS et al., 2018) and previous studies conducted at the BAN site (BORMA et al., 2009),

while MODIS showed a very high monthly variation 24.5%, given the variability around the mean during both flooded (super estimated) and dry seasons (overestimated). Previous studies validating MOD16A2 product against *in situ* flux data at tropical forests reported the challenge of using MODIS ET (XU et al., 2019). For K67 site (*terra firme* forest) the correlation between this product and the tower data (XU et al., 2019) was even lower ( $r^2 = 0.16$ ) than the one reported in this study ( $r^2 = 0.34$ ). This finding indicates that remote sensing-based ET models need to be further assessed to represent the ecosystem function seasonality in wet tropical forests.

Previous ET estimations performed well at LBA equatorial sites (k34,k67,k83) (*terra firme*) but poorly at transitional southern forests (RJA, BAN), due to less seasonality in available light or water limitation (RESTREPO-COUCPE et al., 2013a; CHRISTOFFERSEN et al., 2014). However, these analyses comprised three years of eddy-covariance data, while the flood pulse at BAN site was high enough to recharge the soil moisture during the dry season (2004 to 2006). Here, on the other hand, it was possible to access the drivers changing over seasons and the role of flooding in forest functioning.

VPD presented a high linear correlation with ET, while soil moisture was not significant. However, from the modeled ET it is possible to observe that high global radiation and high VPD diminished ET associated with low soil moisture during the dry season, highlighting the complexity of these drivers, which are not linear associated to determine ET. The high amplitude on soil moisture content is associated with shallow clay layers (up to 2m) and an abrupt texture transition to sand at around 2.2 m (Figure B3) (TAVARES, 2019). Despite the prevailing atmospheric conditions on ET estimation (VPD and Incident radiation), the amount of water input during the flooded period determines both the free water evaporation and the water availability during the following dry season. Moreover, the water table elevation at the onset of the wet season also contributes to the soil moisture recharge at the unsaturated zone. Therefore, soil moisture is a significant predictor to analyze seasonal ET variation at this site, as also reported by other studies (BORMA et al., 2009; CHRISTOFFERSEN et al., 2014).

Given the main role of soil moisture/flooding as an ET driver, it is possible to observe that ET is higher during the flooded period (Feb to May; 130 mm) compared to the dry (109 mm) and rainy non-flooded season (120 mm), which associated to the dormant period (TAVARES, 2019) possibly describes the free water evaporation, supporting a previous study performed at this site (BORMA et al., 2009).

Another evidence of the free water evaporation is the decreased carbon assimilation (RESTREPO-COUBE et al., 2013; COSTA, 2015) and the canopy photosynthetic capacity (described by the Enhanced Vegetation Index - EVI) during the flooded period. ET is negatively associated with EVI during the flooded period (Figure B3). However, during non-flooded months, EVI and ET exhibited a positive correlation ( $r^2 = 0.27$ ;  $p < 0.001$ ), which means ET increases as the canopy photosynthetic capacity increases, following the GPP pattern when the soil is not saturated.

Unlike flooded forests located at the central Amazon region that grow during seasonal droughts, taking advantage from the shrinkage flooded period (SCHONGART et al., 2004), trees at the BAN site exhibited trunk dormancy even during extreme dry years - 2016 and 2017 (TAVARES, 2019), which means that higher ET amounts observed during these years (133 mm and 128 mm, respectively) are likely to be associated to free water evaporation, due to less cloudiness and high incident global radiation.

The lower ET rates during non-flooded months in 2016 (June to December) are in agreement with low water availability for plants and the reduction of biomass increment in 50% reported by Tavares (2019). Besides, the phenological pattern during this period has changed (FONSECA et al., 2019), diminishing the photosynthetic capacity of the canopy through the entire dry season, which could be associated to a drought-avoidance mechanism adopted by the forest (DA COSTA et al., 2018; TAVARES, 2019). However, the strongest ET decreasing pattern was observed on 2017, since rainfall remained below the mean and flood height remained very low, which associated to high evaporative demands (VPD)

and net radiation probably lead to stomatal regulation, restricting transpiration (DA COSTA et al., 2018; TAVARES, 2019).

The ENSO drought strongly affected the forest functioning in 2016 and 2017 considering the growth period is likely to occur from August to January (TAVARES, 2019). Therefore, given the hydrological trend of decreasing water availability and storage in this ecosystem, associated with an increasing temperature (MALHI; WRIGHT, 2004), these results highlight the drought vulnerability of this floodplain forest, also suggested by previous studies (BORMA et al., 2009; COSTA, 2015; HOMEIER; KURZATKOWSKI; LEUSCHNER, 2017; FONSECA et al., 2019; TAVARES, 2019).

## **5.5 Conclusion**

The statistical model used here was able to fill gaps and predict ET from eddy-covariance measurements. This method could be used to fill gaps of other environmental variables, being applied in other sites equipped with micrometeorological towers. Furthermore, the reanalysis ERA5 product was able to describe in situ measurements and be used as another source of meteorological data.

The flood pulse of this forest was identified as an important ET driver through the model calibration process, represented by the saturated soil moisture period and also from the seasonal analysis. This finding also highlighted the vulnerability of the BAN forest facing extreme dry years, given the decreased flood pulse trend reported here, which consequently might diminish the water availability for trees during non-flooded months, as reported in 2016.

## 6 GENERAL CONCLUSIONS

The bimodal carbon cycle synchronized with phenological patterns obtained in situ and from satellite data (Enhanced Vegetation Index - EVI) provided the first analysis about the seasonality of the ecosystem productivity in a floodplain forest at a broader scale.

The challenging of using optical images to analyze phenological patterns in a flooded plot was sorted out coupling a range of different sources of data, such as I) The LiDAR airborne data, which was used to process gaps between canopies and identify if the free water exposed through canopies during the flooded period influenced EVI observations. This airborne data was validated using measurements of tree heights from a forestry inventory performed at both plots around the tower; II) The Bing Virtual Earth image, a free high-resolution image provided on QGIS, which was used to calculate the percentage of water channels inside pixels around the tower; III) and The Digital Elevation Model from SRTM data used to analyze the homogeneity of the terrain around the tower. These independent satellite data provided more information about the accuracy of using the enhanced vegetation index to access the phenological pattern of this flooded plot.

Although it was found a significant relationship between GPP, leaf litter mass, and EVI computed from the moderate resolution images (MODIS), the forest seasonality analysis could be investigated combining other remote sensing data with finer spatial resolution. In this context, the new products from the GEDI (Global Ecosystem Dynamics Investigation) and ECOSTRESS (ECOsysteM Spaceborne Thermal Radiometer Experiment on Space Station) are an alternative to obtain Earth Observation data at a very high spatial and temporal resolution to investigate the carbon and water cycle in this forest.

The seasonal ecosystem productivity and Evapotranspiration (ET) are not synchronized in this Southern Amazon forest, because the free water evaporation mainly drives ET during the flooded period while the forest is dormant, and by forest transpiration during non-flooded months, as indicated by the association with phenology and climate seasonal patterns.

Generalized Additive Models were suitable to fill gaps and analyze the complex interaction between climate data and the flood cycle to describe ET seasonality of this flooded forest. The correlation between meteorological variables from the tower with ERA5 data has proven the reliability of this reanalysis data. Moreover, it was reported the similarity between the models build with variables from the tower and with ERA5 to estimate ET.

The meteorological data obtained from the tower, satellite (TRMM) and reanalysis (ERA5) data have shown the long-term drying of this region, presenting an increasing air temperature and vapour pressure deficit trend, coupled with lowering river level, which consequently diminished the soil water volume in recently years, especially during the ENSO drought of 2016.

## REFERENCES

- AGUILOS, M. et al. Interannual and seasonal variations in ecosystem transpiration and water use efficiency in a tropical rainforest. **Forests**, v. 10, n. 1, p. 14, 2018.
- AGÊNCIA NACIONAL DE ÁGUAS - ANA. **Séries históricas**. Available from: <http://www.snirh.gov.br/hidroweb/apresentacao>. Access in: 30 Mar. 2018.
- ANDERSON, L. O. et al. Remote sensing detection of droughts in Amazonian forest canopies. **New Phytologist**, v. 187, n. 3, p. 733–750, 2010.
- ANDRADE, N.L.R. de; AGUIAR, R.G.; SANCHES, L.; ALVES, E.C.R. de F.; NOGUEIRA, J. de S. Partição do saldo de radiação em áreas de floresta amazônica e floresta de transição amazônia- cerrado. **Revista Brasileira de Meteorologia**, São José dos Campos, v.24, n.3, 346-355, 2009.
- AQUINO, S.; LATRUBESSE, E. M.; SOUZA-FILHO, E. E. de. Relações entre o regime hidrológico e os ecossistemas aquáticos da planície aluvial do Rio Araguaia. **Acta Scientiarum - Biological Sciences**, v. 30, n. 4, p. 361–369, 2008.
- ARAGÃO, L. E. O. C. et al. Spatial patterns and fire response of recent Amazonian droughts. **Geophysical Research Letters**, v. 34, n. 7, p. 1–5, 2007.
- ARNESEN, A. S. et al. Monitoring flood extent in the lower Amazon River floodplain using ALOS/PALSAR ScanSAR images. **Remote Sensing of Environment**, v. 130, p. 51–61, 2013.
- ASSIS, J. et al. Above-ground woody biomass distribution in Amazonian floodplain forests: effects of hydroperiod and substrate properties. **Forest Ecology and Management**, v. 432, p. 365–375, 2018.
- BALDOCCHI, D.D. Assessing the eddy covariance technique for evaluating carbon dioxide exchange rates of ecosystems; past, present and future. **Global Change Biology**, Oxford, v.9, p. 479-492, 2003.
- BARROS, F. DE V. et al. Hydraulic traits explain differential responses of Amazonian forests to the 2015 El Niño-induced drought. **New Phytologist**, v. 223, n. 3, p. 1253–1266, 2019.
- BECERRA, J. A. B.; SHIMABUKURO, Y. E.; ALVALÁ, R. C. DOS S. Relação do padrão sazonal da vegetação com a precipitação na região de cerrado da Amazônia Legal, usando índices espectrais de vegetação. **Revista Brasileira de Meteorologia**, v. 24, n. 2, p. 125–134, 2009.

BI, X. et al. Seasonal and diurnal variations in moisture, heat, and CO<sub>2</sub> fluxes over grassland in the tropical monsoon region of southern China. **Journal of Geophysical Research Atmospheres**, v. 112, n. 10, p. 1–14, 2007.

BOLTON, D. The computation of equivalent potential temperature. **Atmospheric Physics group**, v. 180, p. 1046-1053, 1980.

BONAN, G. B. Forests and climate change: forcings, feedbacks, and the climate benefits of forests. **Science**, v. 320, n. 5882, p. 1444–1449, 2008.

BORMA, L. S. et al. Atmosphere and hydrological controls of the evapotranspiration over a floodplain forest in the Bananal Island region, Amazonia. **Journal of Geophysical Research: Biogeosciences**, v. 114, n. 1, p. 1–12, 2009.

BRANDO, P. M. et al. Seasonal and interannual variability of climate and vegetation indices across the Amazon. **Proceedings of the National Academy of Sciences**, v. 107, n. 33, p. 14685–14690, 2010.

BRIENEN, R. J. W. et al. Long-term decline of the Amazon carbon sink. **Nature**, v. 519, n. 7543, p. 344–348, 2015.

BRUM, M. et al. Hydrological niche segregation defines forest structure and drought tolerance strategies in a seasonal Amazon forest. **Journal of Ecology**, v. 107, n. 1, p. 318–333, 2019.

CABRAL, O. M. R. et al. Fluxes of CO<sub>2</sub> above a plantation of Eucalyptus in southeast Brazil. **Agricultural and Forest Meteorology**, v. 151, n. 1, p. 49–59, 2011.

CHAVE, J. et al. Regional and seasonal patterns of litterfall in tropical South America. **Biogeosciences**, v. 7, n. 1, p. 43–55, 2010.

CHRISTOFFERSEN, B. O. et al. Mechanisms of water supply and vegetation demand govern the seasonality and magnitude of evapotranspiration in Amazonia and Cerrado. **Agricultural and Forest Meteorology**, v. 191, n. March, p. 33–50, 2014.

COPERNICUS CLIMATE CHANGE SERVICE. **ERA5**: fifth generation of ECMWF atmospheric reanalyses of the global climate. Copernicus Climate Change Service Climate Data Store (CDS), 2017. Available from: <https://cds.climate.copernicus.eu/cdsapp#!/home>. Access in: 20 Oct. 2018.

COSTA, G.P. **Fluxos de energia, CO<sub>2</sub> e CH<sub>4</sub> Sobre a Floresta em Planície de Inundação da Ilha do Bananal**. 2015. Tese (Doutorado em Ecologia Aplicada) - Universidade de São Paulo, Escola Superior de Agricultura “Luiz de Queiroz”, Piracicaba, 2015.



DA COSTA, A. C. L. et al. Stand dynamics modulate water cycling and mortality risk in droughted tropical forest. **Global Change Biology**, v. 24, n. 1, p. 249–258, 2018.

DA ROCHA, H. R. et al. Patterns of water and heat flux across a biome gradient from tropical forest to savanna in Brazil. **Journal of Geophysical Research: Biogeosciences**, v. 114, n. 1, p. 1–8, 2009.

DA ROCHA, H. R. et al. Seasonality of water and heat fluxes over a tropical forest in eastern Amazonia. **Ecological Applications**, v. 14, n. June 2000, p. 22–32, 2004.

DALAGNOL, R. et al. Life cycle of bamboo in southwestern Amazon and its relation to fire events. **Biogeosciences**, n. 5, p. 1–28, 2018.

DALMAGRO, H. J. et al. Radiative forcing of methane fluxes offsets net carbon dioxide uptake for a tropical flooded forest. **Global Change Biology**, v. 4, n. October 2018, p. 1967–1981, 2019.

DALAGNOL, R. WAGNER, F. H. ARAGÃO, L. E. O. C. (2019). **"MODIS (MAIAC) satellite BRDF-corrected C6 vegetation indices (EVI and NDVI) for South America at 1 km and 16 days composite"**. (Version v1) [Data set]. Zenodo. Available from: <https://doi.org/10.5281/zenodo.3159488>. Access in: 20 Jan. 2017.

DAVID PIERCE. **ncdf4**: interface to unidata netCDF (version 4 or earlier) format data files. R package version 1.16.1. 2019. Available from: <https://CRAN.R-project.org/package=ncdf4>. Access in: 12 Nov. 2018.

DE ALMEIDA, T. I. R. et al. Principal component analysis applied to a time series of MODIS images: the spatio-temporal variability of the Pantanal wetland, Brazil. **Wetlands Ecology and Management**, v. 23, n. 4, p. 737–748, 2015.

DE SIMONE, O.; JUNK, W. J.; SCHMIDT, W. Central Amazon floodplain forests: root adaptations to prolonged flooding. **Russian Journal of Plant Physiology**, v. 50, n. 6, p. 848–855, 2003.

DE SIMONE, O.; MÜLLER, E.; JUNK, W. J.; SCHMIDT, W. Adaptations of Central Amazon tree species to prolonged flooding: root morphology and leaf longevity. **Plant Biology**, v. 4, n. 4, p. 515–522, 2002.

DEE, D. P. et al. The ERA-Interim reanalysis: configuration and performance of the data assimilation system. **Quarterly Journal of the Royal Meteorological Society**, v. 137, n. 656, p. 553–597, 2011.

DIAZ, M.; ROBERTI, D. R. Cálculo das trocas de carbono num agroecossistema de arroz com aplicação de técnicas de preenchimento de falhas. **Ciência e Natura**, v. 37, n. 0, p. 27–31, 2015.

- ESPÍRITO-SANTO, F. D. B. et al. Size and frequency of natural forest disturbances and the Amazon forest carbon balance. **Nature Communications**, v. 5, p. 1–6, 2014.
- ELTAHIR, E.A.B.; BRAS, R.L. Precipitation recycling in the Amazon basin. **Quarterly Journal of the Royal Meteorological Society**, v. 120, n.518, p. 861–880, 1994.
- EUROPEAN SPACE AGENCY - ESA. **Sentinel-2**. Available from: <https://sentinel.esa.int/web/sentinel/home>. Access in: 10 Oct. 2016.
- FALGE, E. et al. Seasonality of ecosystem respiration and gross primary production as derived from FLUXNET measurements. **Agricultural and Forest Meteorology**, v. 113, n.1-4, p. 53-74, 2002.
- FELDPAUSCH, T. R. et al. Amazon forest response to repeated droughts. **Global Biogeochemical Cycles**, v. 30, n. 7, p. 964–982, 2016.
- FISHER, J. B. et al. The land-atmosphere water flux in the tropics. **Global Change Biology**, v. 15, n. 11, p. 2694–2714, 2009.
- FONSECA, L. D. M. et al. Phenology and seasonal ecosystem productivity in an Amazonian floodplain forest. **Remote Sensing**, v. 11, n. 13, p. 1–17, 2019.
- FURTADO, L. F. et al. Dual-season and full-polarimetric C band SAR assessment for vegetation mapping in the Amazon várzea wetlands. **Remote Sensing of Environment**, v. 174, p. 212–222, 2016.
- GALVÃO, L. S. et al. On intra-annual EVI variability in the dry season of tropical forest: A case study with MODIS and hyperspectral data. **Remote Sensing of Environment**, v. 115, n. 9, p. 2350–2359, 2011.
- GATTI, L. V. et al. Drought sensitivity of Amazonian carbon balance revealed by atmospheric measurements. **Nature**, v. 506, n. 7486, p. 76–80, 2014.
- GLOOR, M. et al. Recent Amazon climate as background for possible ongoing Special Section : **Global Biogeochemical Cycles**, v. 29, n. 9, p. 1384–1399, 2015.
- GLOOR, M. et al. Intensification of the Amazon hydrological cycle over the last two decades. **Geophysical Research Letters**, v. 40, n. 9, p. 1729–1733, 2013.
- GOLTZ, E. et al. Utilização de índices espectrais de vegetação do sensor MODIS na determinação de áreas suscetíveis a alagamento no Pantanak Sulmatogrossense. **Revista Brasileira de Cartografia**, v. 59, n. 1, p. 35–44, 2007.

HANSEN, M. C. et al. High-resolution global maps of 21st-century forest cover change. **Science**, v. 850, p. 2011–2014, 2013.

HERRERA, A. Responses to flooding of plant water relations and leaf gas exchange in tropical tolerant trees of a black-water wetland. **Frontiers in Plant Science**, v. 4, p. 1–12, 2013.

HESS, L. et al. 2015. **LBA-ECO LC-07 wetland extent, vegetation, and inundation: lowland Amazon basin**. ORNL DAAC, Oak Ridge, Tennessee, USA. Available from: <https://doi.org/10.3334/ORNLDAAAC/1284>. Access in: 10 Jan. 2018.

HESS, L. et al. Remote sensing of wetland types: tropical flooded forests. In: HESS, L.; COSTA, M.; EVANS, T.; SILVA, T. S.; CHAPMAN, B.; MILNE, T. **The wetland book: remote sensing of wetland types: tropical flooded forests**. Berlin: Springer, 2016. Available from: [https://link.springer.com/referenceworkentry/10.1007%2F978-90-481-9659-3\\_303](https://link.springer.com/referenceworkentry/10.1007%2F978-90-481-9659-3_303). Access in: 15 Jan. 2018.

HESS, L. et al. Dual-season mapping of wetland inundation and vegetation for the central Amazon basin. **Remote Sensing of Environment**, v. 87, n. 4, p. 404–428, 2003.

HESS, L. et al. Use of MODIS enhanced vegetation index to detect seasonal patterns of leaf phenology in central Amazon várzea forest. **International Geoscience and Remote Sensing Symposium (IGARSS)**, v. 4, p. 1007–1010, 2009.

HILKER, T. et al. Vegetation dynamics and rainfall sensitivity of the Amazon. **Proceedings of the National Academy of Sciences**, v. 111, n. 45, p. 16041–16046, 2014.

HOMEIER, J.; KURZATKOWSKI, D.; LEUSCHNER, C. Stand dynamics of the drought-affected floodplain forests of Araguaia River, Brazilian Amazon. **Forest Ecosystems**, v. 4, n. 1, p. 10, 2017.

HUETE, A. et al. Overview of the radiometric and biophysical performance of the MODIS vegetation indices. **Remote Sensing of Environment**, v. 83, n. 1, p. 195–213, 2002.

HUETE, A. R. et al. Amazon rainforests green-up with sunlight in dry season. **Geophysical Research Letters**, v. 33, n. 6, p. 2–5, 2006.

HUMPHREY, V. et al. Sensitivity of atmospheric CO<sub>2</sub> growth rate to observed changes in terrestrial water storage. **Nature**, v. 560, n. 7720, p. 628–631, 2018.

HUNTER, M. O. et al. Structural dynamics of tropical moist forest gaps. **PLoS ONE**, v. 10, n. 7, p. 1–19, 2015.

HUTYRA, L. R. et al. Seasonal controls on the exchange of carbon and water in an Amazonian rain forest. **Journal of Geophysical Research: Biogeosciences**, v. 112, n. 3, 2007.

JENSEN, J. R. **Sensoriamento remoto do ambiente: uma perspectiva em recursos terrestres**. São José dos Campos: Parêntese, 2009. 598 p.

JIMÉNEZ-MUÑOZ, J. C. et al. Record-breaking warming and extreme drought in the Amazon rainforest during the course of El Niño 2015-2016. **Scientific Reports**, v. 6, n. August, p. 1–7, 2016.

JUNK, W.; BAYLEY, P.; SPARKS, R. The flood pulse concept in river - floodplain systems. **Canadian Journal of Fisheries and Aquatic Sciences**, v. 106, p. 110–127, 1989.

KURZATKOWSKI, D.; LEUSCHNER, C.; HOMEIER, J. Effects of flooding on trees in the semi-deciduous transition forests of the Araguaia floodplain, Brazil. **Acta Oecologica**, v. 69, p. 21–30, 2015.

LEBAUER, D. The Predictive Ecosystem Analyzer (PEcAn) is an integrated ecological bioinformatics toolbox. 2018. Available from: <https://github.com/PecanProject/pecan/blob/master/modules/data.atmosphere/R/metutils.R>.

LEIVAS, J. F.; ANDRADE, R. G.; BOLFE, É. L. Padronização do índice de vegetação do Pantanal a partir de imagens do SPOT Vegetation. In: SIMPÓSIO DE GEOTECNOLOGIAS NO PANTANAL, 4., 2012, Bonito, MS. **Anais....** 2012, p. 798–805.

LOPES, A. et al. R. Remote sensing of environment leaf flush drives dry season green-up of the Central Amazon. **Remote Sensing of Environment**, v. 182, p. 90–98, 2016.

LYAPUSTIN, A. I. et al. Multi-angle implementation of atmospheric correction for MODIS (MAIAC): 3. atmospheric correction. **Remote Sensing of Environment**, v. 127, p. 385–393, 2012.

MAEDA, E. E. et al. Evapotranspiration seasonality across the Amazon Basin. **Earth System Dynamics**, v. 8, n. 2, p. 439–454, 2017.

MAEDA, E. E. et al. Consistency of vegetation index seasonality across the Amazon rainforest. **International Journal of Applied Earth Observation and Geoinformation**, v. 52, p. 42–53, 2016.

MALHI, Y.; WRIGHT, J. Spatial patterns and recent trends in the climate of tropical rainforest regions. **Philosophical Transactions of the Royal Society B: Biological Sciences**, v. 359, n. 1443, p. 311–329, 2004.

- MALHI, Y. et al. Comprehensive assessment of carbon productivity, allocation and storage in three Amazonian forests. **Global Change Biology**, v.15, p.1255–1274, 2009.
- MARENGO, J. A. Characteristics and spatio-temporal variability of the Amazon river basin water budget. **Climate Dynamics**, v. 24, n. 1, p. 11–22, 2005.
- MARENGO, J. A. et al. The drought of 2010 in the context of historical droughts in the Amazon region. **Geophysical Research Letters**, v. 38, n. 12, p. 1–5, 2011.
- MARKEWITZ, D. et al. Soil moisture depletion under simulated drought in the Amazon: Impacts on deep root uptake. **New Phytologist**, v. 187, n. 3, p. 592–607, 2010.
- MELACK, J. M.; HESS, L. L. Remote sensing of the distribution and extent of wetlands in the Amazon Basin. In: JUNK, W. J. et al. (Org.). **Amazonian floodplain forests: ecophysiology, biodiversity and sustainable management**. New York: Springer, 2010.
- MILLENNIUM ECOSYSTEM ASSESSMENT. **Ecosystems and human well-being: wetlands and water synthesis**. Washington: World Resources Institute, 2005.
- MOFATT A. M. et al. Comprehensive comparison of gap-filling techniques for eddy covariance net carbon fluxes. **Agriculture and Forest Meteorology** v. 14, n.3–4, p.209–232, 2007.
- MOREIRA, K. S. et al. Avaliação na queda de liteira em ecótonos no entorno da Ilha do Bananal. In: CONGRESSO CIENTÍFICO DA UFT, 1., 2005, Palmas TO. **Anais...** 2005.
- MORTON, D. C. et al. Amazon forest structure generates diurnal and seasonal variability in light utilization. **Biogeosciences Discussions**, v. 12, n. 23, p. 19043–19072, 2016.
- MOURA, Y. M. et al. Seasonality and drought effects of Amazonian forests observed from multi-angle satellite data. **Remote Sensing of Environment**, v. 171, p. 278–290, 2015.
- MOURA, Y. et al. Spectral analysis of amazon canopy phenology during the dry season using a tower hyperspectral camera and MODIS observations. **ISPRS Journal of Photogrammetry and Remote Sensing**, v.131, p.52–64, 2017.
- MU, Q.; ZHAO, M.; RUNNING, S. W. Improvements to a MODIS global terrestrial evapotranspiration algorithm. **Remote Sensing of Environment**, v. 115, n. 8, p. 1781–1800, 2011.

NEGRÓN JUÁREZ, R. I. et al. Control of dry season evapotranspiration over the Amazonian forest as inferred from observation at a Southern Amazon forest site. **Journal of Climate**, v. 20, n. 12, p. 2827–2839, 2007.

NOBRE, C. A. et al. Land-use and climate change risks in the Amazon and the need of a novel sustainable development paradigm. **Proceedings of the National Academy of Sciences**, v. 113, n. 39, p. 10759–10768, 2016.

OLIVEIRA, L. D. S. **Fluxos atmosféricos de superfície sobre uma área de ecótono na Ilha do Bananal**. 114 p. Tese (Doutorado em Meteorologia) — Universidade de São Paulo, Piracicaba, 2006.

PAN, Y. et al. A large and persistent carbon sink in the world's forests. **Science**, v. 333, n. 6045, p. 988–993, 2011.

PAPALE, D. et al. Towards a standardized processing of net ecosystem exchange measured with eddy covariance technique: algorithms and uncertainty estimation, **Biogeosciences**, v. 3, n.4, p.571-583, 2006.

PAROLIN, P. et al. Drought responses of flood-tolerant trees in Amazonian floodplains. **Annals of Botany**, v. 105, n. 1, p. 129–139, 2010.

PAROLIN, P.; MULLER, E.; JUNK, W. J. Water relations of amazonian várzea trees. **International Journal of Ecology and Environmental Sciences**, v. 31, n. 4, p. 361–364, 2005.

PAROLIN, P. et al. Central Amazonian floodplain forests: tree adaptations in a pulsing system. **The Botanical**, v. 70, n.3, p.357-380, 2004.

PAU, S. et al. Tropical forest temperature thresholds for gross primary productivity. **Ecosphere**, v. 9, n. 7, p. 1–12, 2018.

PAU, S. et al. Long-term increases in tropical flowering activity across growth forms in response to rising CO<sub>2</sub> and climate change. **Global Change Biology**, v. 24, n. 5, p. 2105–2116, 2017.

PEDERSEN, E. J. et al. **Hierarchical generalized additive models: an introduction with mgcv**. 2018. Available from: <https://doi.org/10.7287/peerj.preprints.27320v1>. Access in: 10 Sept. 2018.

PEREIRA, L. O. et al. Multifrequency and full-polarimetric SAR assessment for estimating above ground biomass and leaf area index in the Amazon Várzea Wetlands. **Remote Sensing**, v. 10, n. 9, 2018.

PHILLIPS, O. L. et al. Changes in the carbon balance of tropical forests: evidence from long-term plots. **Science**, v. 282, p. 439–442, 1998.

PHILLIPS, O. L. et al. Drought sensitivity of the Amazon rainforest. **Science**, v. 1344, p. 1344–1348, 2009.

PIEDADE, M. T. F. et al. Impactos ecológicos da inundação e seca na vegetação de áreas alagáveis amazônicas. In: BORMA, L. S.; NOBRE, C. A. (Org.). **Secas na Amazônia: causas e conseqüências**. São Paulo: Oficina de Textos, 2014. p. 268–304.

PIEDADE, M.T.F; JUNK, W. J.; PAROLIN, P. The flood pulse and photosynthetic response of trees in a white water floodplain (várzea) of the Central Amazon, Brazil. **SIL Proceedings**, v. 27, n. 4, p. 1734–1739, 2000.

PIERCE, D. **A netcdf package for R**. 2013. Available from: <http://cirrus.ucsd.edu/~pierce/ncdf/>. Access in: 3 Nov. 2018.

QUESADA, C. A. et al. Regional and large-scale patterns in Amazon forest structure and function are mediated by variations in soil physical and chemical properties. **Biogeosciences Discussions**, v. 6, p. 3993–4057, 2009.

R Core Team. **R: a language and environment for statistical computing**. Vienna, Austria: R Foundation for Statistical Computing, 2013. Available from: <http://www.R-project.org/>. Access in: 15 Jan. 2018.

RESENDE, A. F. et al. Massive tree mortality from flood pulse disturbances in Amazonian floodplain forests: the collateral effects of hydropower production. **Science of the Total Environment**, v. 659, p. 587–598, 2019.

RESTREPO-COUBE, N. et al. What drives the seasonality of photosynthesis across the Amazon basin? a cross-site analysis of eddy flux tower measurements from the Brasil flux network. **Agricultural and Forest Meteorology**, v. 182–183, p. 128–144, 2013.

RIENECKER, M. M. et al. MERRA: NASA's Modern-era retrospective analysis for research and applications. **Journal of Climate**, v. 24, n.14, p. 3624–3648, 2011.

RIFAI, S. W. et al. ENSO Drives interannual variation of forest woody growth across the tropics. **Philosophical transactions of the Royal Society of London. Series B, Biological sciences**, v. 373, n. 1760, 2018.

SALESKA, S. R. et al. Amazon Forests green-up during 2005 drought. **Science**, v. 318, p. 2007–2007, 2007.

SAMANTA, A.; GANGULY, S.; MYNENI, R. B. MODIS enhanced vegetation index data do not show greening of amazon forests during the 2005 drought. **New Phytologist**, v. 189, n. 1, p. 11–15, 2011.

SCHEFFER, M. et al. Floodplains as an Achilles' heel of Amazonian forest resilience. **Proceedings of the National Academy of Sciences**, v. 114, n. 17, p. 4442–4446, 2017.

SCHONGART, J. et al. Teleconnection between tree growth in the Amazonian floodplains and the El Niño -Southern Oscillation effect. **Global Change Biology**, v. 10, n. 5, p. 683–692, 2004.

SCHONGART, J. et al. Phenology and stem-growth periodicity of tree species in Amazonian floodplain forests. **Journal of Tropical Ecology**, v.18, n.4, p. 581–597, 2002.

SOMBROEK, W. Spatial and temporal patterns of Amazon rainfall. **Journal of the Human Environment**, v. 30, n. 7, p. 388–396, 2001.

SOUDANI, K.; FRANÇOIS, C. Remote sensing: a green illusion. **Nature**, v. 506, p. 165–166, 2014.

STAAL, A. et al. Forest-rainfall cascades buffer against drought across the Amazon. **Nature Climate Change**, v. 8, n. 6, p. 539–543, 2018.

TANNUS, R. N. **Funcionalidade e sazonalidade sobre Cerrado e sobre ecótono Floresta-Cerrado** : uma investigação com dados micrometeorológicos de energia e CO<sub>2</sub>. 112p. 2004. Dissertação (Mestrado em Ecologia de Agroecossistemas) - Universidade de São Paulo, Piracicaba, 2004.

TAVARES, I. B. **Resposta ecohidrológica da floresta inundável à seca de 2015/2016 na região da Ilha do Bananal**. 123 p.Tese (Doutorado em Ciência do Sistema Terrestre) - Instituto Nacional de Pesquisas Espaciais, São José dos Campos, 2019.

UNITED STATES GEOLOGICAL SURVEY - USGS.- **Serviço de levantamento geológico americano**. Available from: <http://earthexplorer.usgs.gov/>. EUA, 2016. Access in: 20 Feb. 2017.

VALENTE, C. R.; LATRUBESSE, E. M.; FERREIRA, L. G. Relationships among vegetation, geomorphology and hydrology in the Bananal Island tropical wetlands, Araguaia River basin, Central Brazil. **Journal of South American Earth Sciences**, v. 46, p. 150–160, 2013.

VIANA, D. R.; CÉLIA, R. Vegetation index performance for the Pantanal region during both dry and rainy seasons. **Geografia**, v. 36, p. 143–158, 2011.

VON RANDOWN, C. et al. Comparative measurements and seasonal variations in energy and carbon exchange over forest and pasture in South West Amazonia. **Theoretical and Applied Climatology**, v.78, p.5-26. 2004.



WAGNER, F. H. et al. Climate drivers of the Amazon forest greening. **PLoS ONE**, v. 12, n. 7, p. 1–15, 2017.

WITTMANN, F.; ANHUF, D.; FUNK, W. J. Tree species distribution and community structure of central Amazonian várzea forests by remote-sensing techniques. **Journal of Tropical Ecology**, v. 18, n. 2002, p. 805–820, 2002.

WITTMANN, F. et al. Phytogeography, species diversity, community structure and dynamics of central Amazonian floodplain forests. In: JUNK W. J. et al. (Ed.). **Central Amazonian floodplain forests: ecophysiology, biodiversity and sustainable management**. New York: Springer, 2010.

WRIGHT, J. S. et al. Rainforest-initiated wet season onset over the southern Amazon. **Proceedings of the National Academy of Sciences**, v. 114, n. 32, p. 8481–8486, 2017.

WU, J. et al. Leaf development and demography explain photosynthetic seasonality in Amazon evergreen forests. **Science**, v. 351, n. 6276, p. 972–976, 2016.

WU, J. et al. Biological processes dominate seasonality of remotely sensed canopy greenness in an Amazon evergreen forest. **New Phytologist**, v. 217, n. 4, p. 1507–1520, 2018.

XU, D.; AGEE, E.; WANG, J.; IVANOV, V. Y. Estimation of evapotranspiration of Amazon rainforest using the maximum entropy production method. **Geophysical Research Letters**, v. 46, n. 3, p. 1402–1412, 2019.

XU, L. et al. Widespread decline in greenness of Amazonian vegetation due to the 2010 drought. **Geophysical Research Letters**, v. 38, n. 7, p. 2–5, 2011.

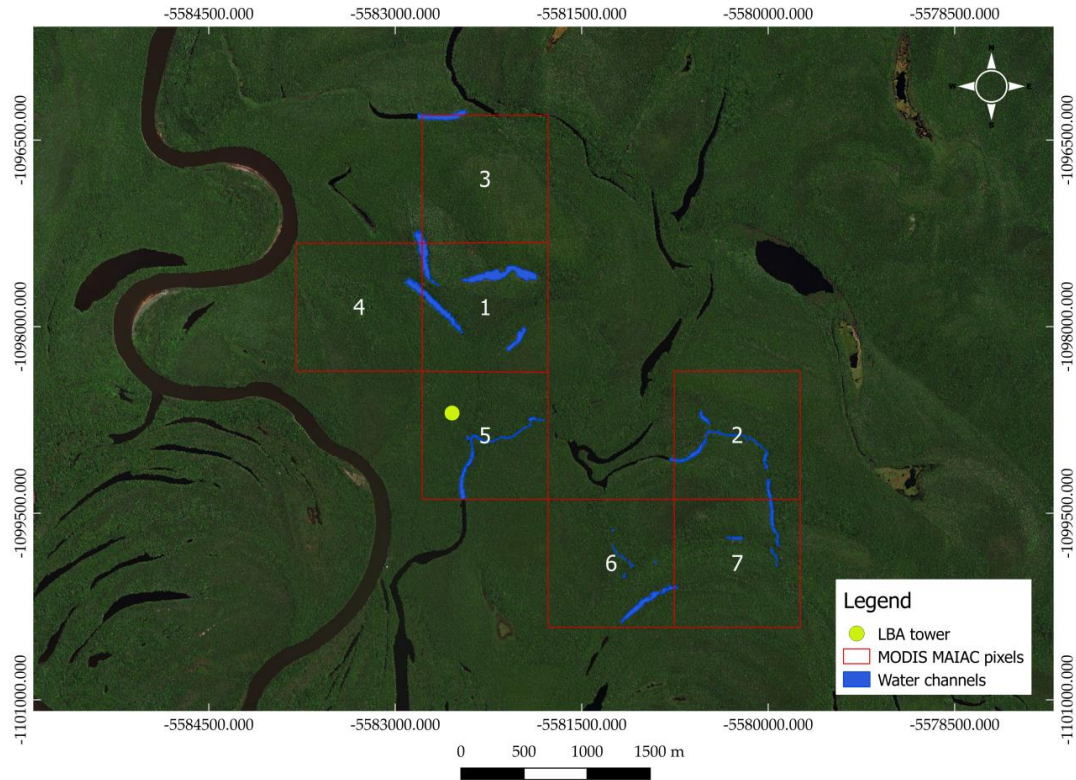
YANG, J. et al. Amazon droughts and forest responses: largely reduced forest photosynthesis but slightly increased canopy greenness during the extreme drought of 2015/2016. **Global Change Biology**, n. August 2017, 2018.

WOOD, S. N. **Generalized additive models: an Introduction with R**. 2.ed. Boca Raton, FL: CRC Press, 2017.

WORBES, M. et al. On the dynamics, floristic subdivision and geographical distribution of várzea forest in central Amazonia. **Journal of Vegetable Science**, v. 3, p. 553-564, 1992.

## APPENDIX A – COMPLEMENTARY MATERIAL OF CHAPTER 4

Figure A. 1 - Bing Virtual Earth image. MODIS MAIAC pixels (red squares) around the LBA tower (Yellow dot) and mapped water channels.



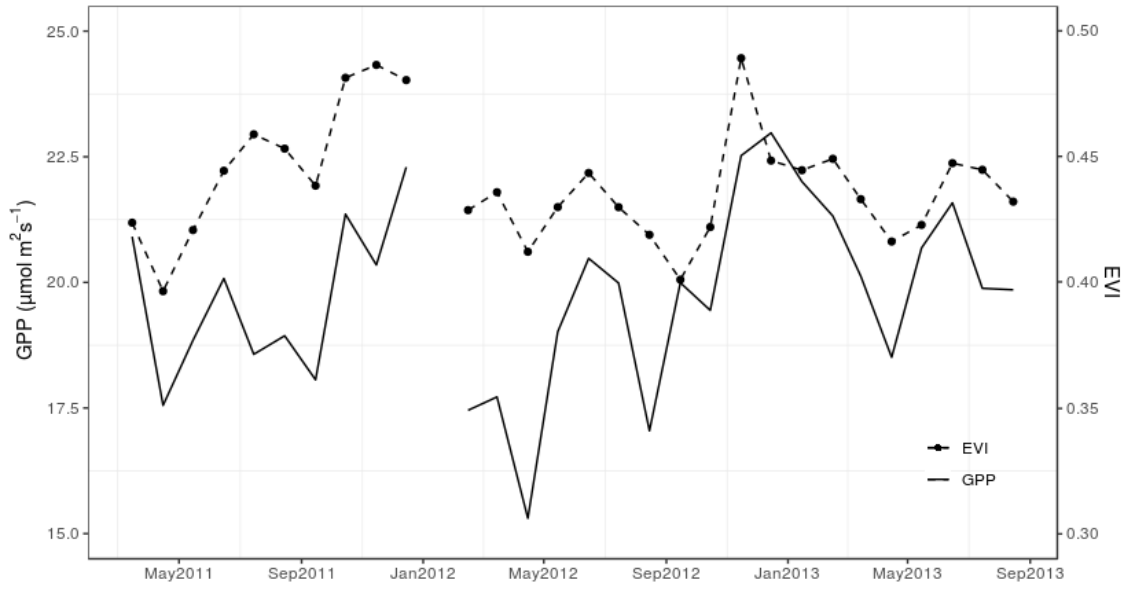
Source: Prepared by the author.

Table A.1 - Percentage of permanent water channels and forest cover in MODIS pixels as delineated with high-resolution Bing Virtual Earth image on QGIS.

<b>Pixel ID</b>	<b>Water channels (km<sup>2</sup>)</b>	<b>Modis pixel area (km<sup>2</sup>)</b>	<b>Water channels (%)</b>	<b>Forest cover (%)</b>
1	0.07	1.01	6.42	94.88
2	0.02	1.01	1.65	98.95
3	0.01	1.00	1.03	99.27
4	0.01	1.01	0.96	99.54
5	0.02	1.00	1.61	98.39
6	0.02	1.01	1.54	99.06
7	0.01	1.00	0.92	99.48

Source: Prepared by the author.

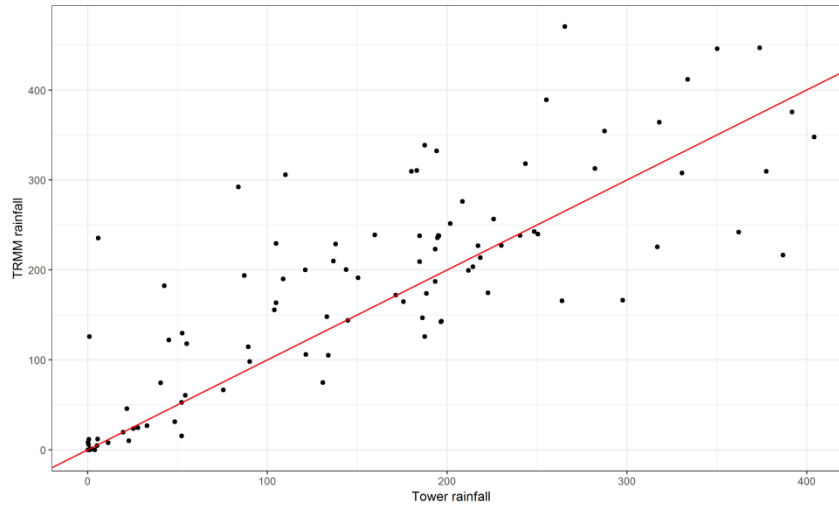
Figure A. 2 - Monthly GPP and EVI from May 2011 to September 2013.



Source: Prepared by the author.

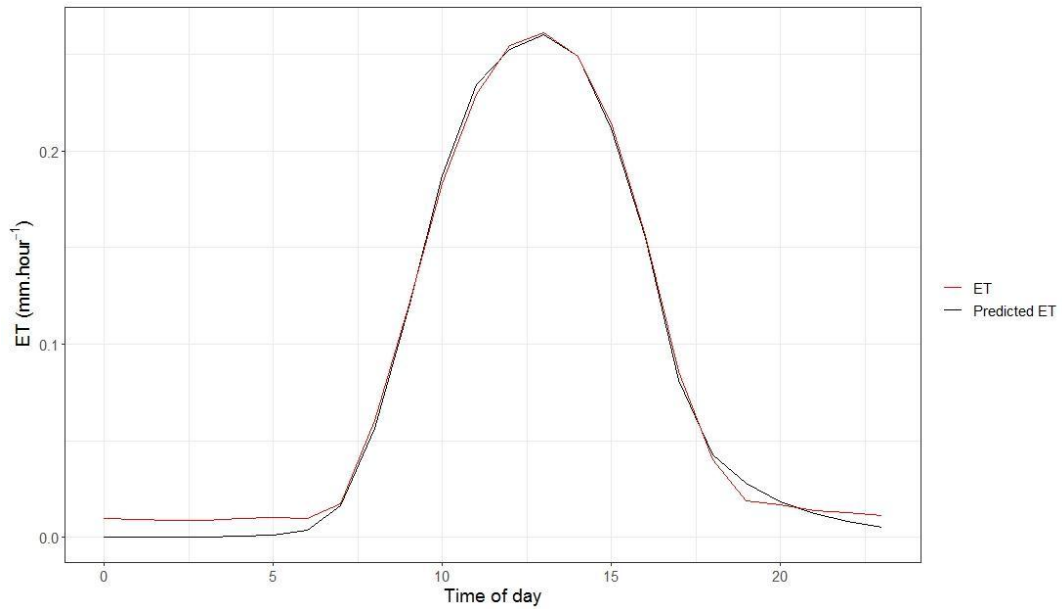
## APPENDIX B - COMPLEMENTARY MATERIAL OF CHAPTER 5

Figure B.1 - Monthly scatterplot of rainfall data from TRMM against flux tower data. The fitted regression line (red).



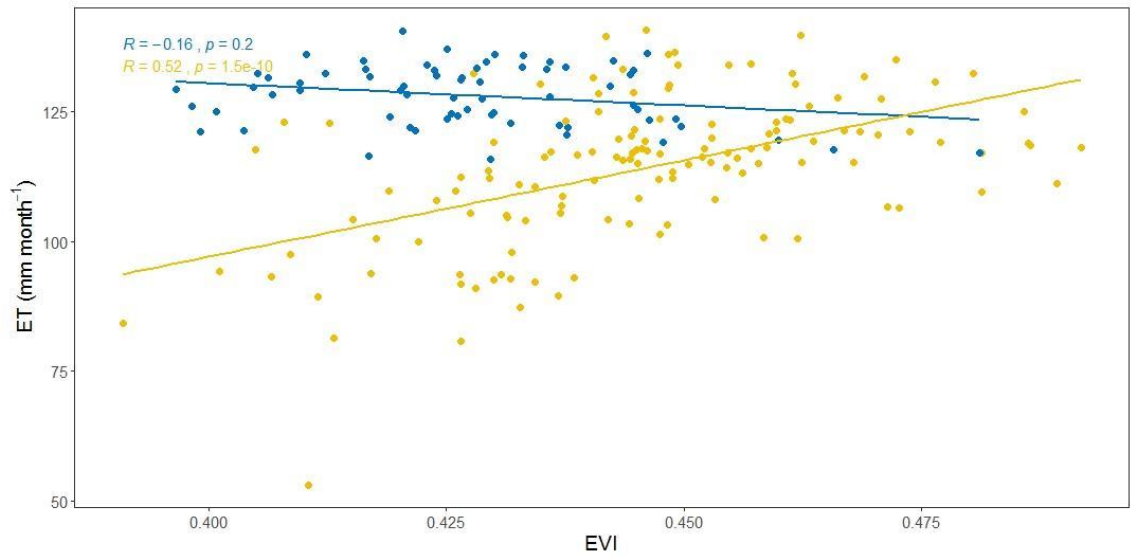
Source: Prepared by the author.

Figure B. 2 - Hourly observed (red) and predicted (black) ET.



Source: Prepared by the author.

Figure B.3 - Scatterplots between monthly EVI and ET from 2004 to 2017. Both lines represent the regression fit between variables during flooded (blue) and non-flooded (yellow) months.



Source: Prepared by the author.